

SOME CHARACTERISTICS OF TWO-PHASE FLOW
IN MONOLITH CATALYST STRUCTURES

by

Fahri Özel

B.S., M.S. Ankara University, Turkey
(1970)

S.M., Massachusetts Institute of Technology
(1973)

SUBMITTED IN PARTIAL FULFILLMENT
OF THE REQUIREMENTS FOR THE
DEGREE OF DOCTOR OF PHILOSOPHY
at the
MASSACHUSETTS INSTITUTE OF TECHNOLOGY
April, 1976

Signature of Author.....
Chemical Engineering Department, April, 1976

Certified by.....
Charles N. Satterfield, Thesis Supervisor

Approved by.....
Glenn C. Williams, Chairman
Departmental Committee on Graduate Studies



ABSTRACT

SOME CHARACTERISTICS OF TWO-PHASE FLOW
IN MONOLITH CATALYST STRUCTURES

by

Fahri Özel

Submitted to the Department of Chemical Engineering
on April 30, 1976 in partial fulfillment of the
requirements for the degree of Doctor of Philosophy

The possible use of monolith catalyst structures as the packing in trickle bed reactors or other gas-liquid contactors was explored. Measurements were made of pressure drop during two-phase downwards flow through a vertical 1" diameter column of monolith sections comprising a total length of 4 feet. Individual sections were either 3" or 6" long and contained either 200 passageways (cells) per square inch or 360 passageways per square inch cross section. The 200 cell/in² material is commercially manufactured for use in automobile exhaust catalyst units. The fluids studied were water and air or cyclohexane and air. These studies were supplemented with observations of the flow pattern and pressure drop in a single vertical capillary tube.

In stacked monoliths the pressure drop is sensitive to the degree of uniformity of initial distribution of liquid. Over wide ranges of gas and liquid flow rates a lower pressure drop occurs with poor than with good initial liquid distribution because of the existence of open channels in the former case.

Results obtained are interpreted in terms of the conditions under which slug-type flow occurs in contrast to annular flow and in terms of the relative contributions of constriction (orifice) effects, hydrodynamic friction, and gravity head to the pressure drop.

Thesis Supervisor: Professor Charles N. Satterfield

Title: Professor of Chemical Engineering

Dedicated to my Late Father
Yahya Öze1

ACKNOWLEDGEMENTS

The author wishes to thank Professor Charles N. Satterfield for initiation and support of this investigation. Also, I would like to thank the Scientific and Technical Research Council of Turkey for its financial support in the form of a NATO scholarship.

TABLE OF CONTENTS

		Page
1	Summary	1
	1-1 Introduction	1
	1-2 Experimental Apparatus	3
	1-3 Liquid Distributor	7
	1-4 Effect of Distributor	11
	1-5 Cyclohexane-Air System	27
	1-6 Single Tube Studies	27
	1-7 Correlation of Results	37
2	Introduction	39
3	Objectives	48
4	Background and Review of Related Studies	50
5	Experimental Studies	54
	5-1 Single Capillary Studies	54
	5-2 Monolith Columns	59
	5-3 Flow Circuits	67
6	Results and Discussion	71
	6-I Studies with Monolith	71
	6-II Studies with Monolith	81
	6-II-1 Effect of Liquid Distributor	81
	6-II-2 Comparison of Pressure Drop in Capillary Tube and Monolith	91
	6-II-3 Cyclohexane-Air System	99
	6-II-4 Comparison with Study by Kiser	102
	6-II-5 Streamlines in Monolith Two-Phase Flow	104
7	Correlation of Results	108
	7-I Calculation of Frictional Pressure Drop From Data	108
	7-I-1 Orifice Effect	108
	7-I-2 Static Head and Frictional Pressure Drop	109
	7-II Theoretical Analysis of Data	112
	7-III Dimensional Analysis	117
8	Conclusion	127
9	Recommendations	129

TABLE OF CONTENTS (Cont'd)

	Page
10 Appendixes	
10-1 Appendix A	130
10-2 Appendix B	132
10-3 Appendix C	139
10-4 Appendix D	153
Nomenclature	157
Literature Citations	159
Biography of Author	162

TABLE OF FIGURES

<u>Figure No.</u>		<u>Page</u>
1.1	Effectiveness Factor with First Order Kinetics	6
1.2	Distributors	8
1.3	Distributor 3	10
1.4	Flow Circuit for Water Studies in Monoliths	12
1.5	Comparison of Pressure Drop Data for Distributor 1 and 3	14
1.6	Comparison of Pressure Drop Data for Distributor 1 and 3	15
1.7	Comparison of Pressure Drop Data for Distributor 1 and 3	16
1.8	Comparison of Pressure Drop Data for Distributor 1 and 3	17
1.9	Pressure Drop	20
1.10	Pressure Drop	21
1.11	Pressure Drop	22
1.12	Pressure Drop	23
1.13	Comparison of Pressure Drop in Monoliths with those in Packed Beds.	25
1.14	Comparison of Present Results and those of Kiser	26
1.15	Pressure Drop	28
1.16	Pressure Drop	29
1.17	Flow in a Single Capillary - Regions of Annular vs. Slug Flow	30
1.18	Pressure Drop in a Capillary Tube for Annular Flow	32
1.19	Pressure Drop in a Capillary Tube with Distributor B	34
1.20	Comparison of Pressure Drop for Slug and Annular Flow in Capillary Tubes	35
1.21	Comparison of Pressure Drop for Capillary Slug Flow and Monoliths	36

TABLE OF FIGURES (Cont'd)

		Page
1	Effectiveness Factor with First Order Kinetics	47
2	Bolus Flow	51
3.	Distributor A	56
4.	Distributor B	57
5.	Flow Circuit for Capillary Studies	58
6.	Cross-Section of the Monolith Column	62
7.	Distributor 1	63
8.	Distributor 2	65
9.	Distributor 3	66
10.	Flow Circuit for Water Studies in Monolith	68
11.	Flow Circuit for Cyclohexane Studies in Monoliths	69
12.	Flow in a Single Capillary -- Regions of Annular vs. Slug Flow	72
13.	Recirculation Pattern in Capillary Slug Flow	73
14.	Pressure Drop in a Capillary Tube for Annular Flow	75
15.	Pressure Drop in a Capillary Tube with Distributor B.	77
16.	Comparison of Pressure Drop for Slug and Annular Flow in Capillary Tubes	78
17.	Fraction of Capillary Tube Length Occupied by Liquid Slugs in a Capillary Tube	79
18.	Comparison of Pressure Drop Data for Distributor 1 and 3	84
19.	Comparison of Pressure Drop Data for Distributor 1 and 3	85
20.	Comparison of Pressure Drop Data for Distributor 1 and 3	86
21.	Comparison of Pressure Drop Data for Distributor 1 and 3	87
22.	Pressure Drop for Distributor 1	89
23.	Pressure Drop for Distributor 1	90
24.	Comparison of Pressure Drop for Capillary Slug Flow and Monoliths	92

TABLE OF FIGURES (Cont'd)

	Page
25. Pressure Drop vs. Liquid Velocity	93
26. Pressure Drop	94
27. Pressure Drop	95
28. Pressure Drop	96
29. Pressure Drop	97
30. Pressure Drop	100
31. Pressure Drop	101
32. Comparison of Present Results and those of KISER	103
33. Comparison of Pressure Drop in Monoliths with those in Packed Beds	105
34. Streamlines in Monoliths Two Phase Flow	106
35. Control Volume	110
36. Stress Tensor	115

LIST OF TABLES

<u>TABLE</u>	<u>Page</u>
1.1 Surface Areas and Void Fractions	4
1.2 Comparison of Thiele Modulus	5
1. Surface Areas and Void Fractions	45
2. Comparison of Thiele Modulus	46
3. Some Values of Measured, Orifice and Static Pressure Drops	113
4. Mathematics of Flow	118
5. Results of Regression Analysis	120
6. Results of Regression Analysis	124
7. Results of Regression Analysis	125

1 -SUMMARY

Some Characteristics of Two-Phase Flow in Monolithic Catalyst Structures
1-1Introduction

The large scale manufacture of monolithic "honeycomb" catalyst supports for use in automotive catalytic convertors is making available for the first time in large quantity a new form of catalyst structure which may have a number of potential advantages for use in reactors for the chemical and petroleum industry. Of particular interest here is their possible use in trickle bed reactors in which a gas and liquid flow co-currently downwards through a bed of solid catalyst. Some of the possible advantages of monoliths for this purpose are:

1. Low pressure drop relative to conventional packed beds
2. The high compressive strength may permit deep beds to be constructed without the necessity of using intermediate supports and gas-liquid redistributors, which greatly increase capital costs.
3. The "controlled channelling" that they provide may give better contacting and better liquid distribution than that obtained in conventional trickle bed reactors, especially at low liquid flow rates.
4. The uniformity of passageways may minimize axial dispersion
5. With liquids containing fine solids, such as those derived from liquefaction of coal, bed plugging may be minimized, or avoided.

6. The high superficial area can allow a higher effectiveness factor to be achieved under diffusion-limiting conditions.

As a first step in evaluating their potential, this study focussed on the hydrodynamic and two-phase flow characteristics of these supports. Particular emphasis was on the effect of gas and liquid flow rate on pressure drop. This is of interest of itself but in addition pressure drop studies give valuable information on type of flow and flow distribution.

As used on automobiles, a monolith catalyst support comprises a web of solid containing within it an array of parallel, uniform, straight, non-connecting channels. They are currently manufactured by several companies and by more than one process, so that a variety of cross-sectional shapes, sizes and wall (web) thicknesses are or can be readily formed. This study utilized monoliths supplied by the Corning Glass Works which are manufactured by extrusion of a thick dough, followed by drying and firing. Most of the work was done with monoliths having a square cross-section channel, nominally 200 channels per square inch of cross section and with a nominal wall thickness of 10 mills. As measured, our samples had about 200 channels/in², probably reflecting a slight shrinkage on drying, and a wall thickness of from 0.25 to 0.33 mm, these slightly thicker than nominal values probably reflecting some die wear. This catalyst support is that currently used in the automobile manufacturing industry. A few studies were also made with monoliths having a nominal 300 channels/in². Actual count was 360 channels/in² and measured wall thickness was 10 mills. Table 1.1 presents equations

for the superficial (outside) area per unit gross volume and void fraction for monoliths with square channels as a function of wall thickness and channel density. Values for representative dimensions are also given. For comparison the area/volume ratio and representative values are also given for packing of spheres. In general monoliths have a substantially higher void fraction and higher surface/volume ratio than conventional reactor catalyst packing.

In Figure 1.1 effectiveness factors for spheres and monoliths are given as a function of the Thiele modulus (Satterfield, 1970). Here monolith webs are treated as flat plates of the same thickness as the web, exposed from both sides. The effectiveness factor as used here is defined as the ratio of actual reaction rate to that which would occur if all of the surface throughout the inside of the catalyst were exposed to reactant of the same concentration and temperature as that existing at the outside surface of the particle. The definitions of the Thiele modulus are given in the Table 1.2 For comparison of spheres and flat plates, one compares ϕ_s to $3\phi_L$ as in Figure 1.1 The ratios of Thiele modulus for spheres to 3 times the Thiele modulus for monoliths are given in the same table. Since typical monoliths have much lower $3\phi_L$ values than ϕ_s values for typical spherical packing, they have higher effectiveness factors.

1-2

Experimental Apparatus

Monolith blocks were carefully core-drilled into sections exactly 1" in diameter and then cut to provide 3" or 6" lengths. These sections were then stacked on top of one another so as to constitute a column 4 feet long (with the 210 cell/in² material)

TABLE 1.1
COMPARISON OF SUPERFICIAL AREAS AND
VOID FRACTION FOR MONOLITHS AND SPHERES

PACKING TYPE	SPECIFICATIONS	SUPERFICIAL AREA (CM ² /CM ³)	VOID FRACTION
SPHERICAL	d = DIAMETER (CM)	$\frac{3.75}{d}$	0.375*
MONOLITH WITH SQUARE HOLES	a = WALL THICKNESS (CM) M = $\frac{\text{HOLES}}{\text{UNIT AREA}}$ $\frac{1}{(\text{CM}^2)}$	$4\sqrt{M(1-2a\sqrt{M})}$	$(1-2a\sqrt{M})$

CALCULATED VALUES FOR MONOLITHS AND SPHERES

	200 CELLS/IN ²		360 CELLS/IN ²	1/4"	1/8"	1/16"	1/32"	cm ² /cm ³
	a=.0270 cm	a=.054 cm	a=.027 cm	Dia.	Dia.	Dia.	Dia.	
AREA Superfi.	18.625	14.68	23.08	5.91	11.81	23.61	47.24	
VOID FRAC.	.70	.43	.60	.375	.375	.375	.375	

* McGreary (1961)

TABLE 1.2

THIELE MODULUS FOR FIRST ORDER REACTIONS

$$\text{MONOLITHS} \quad \phi_L = \frac{a}{2} \sqrt{\frac{k_v}{D_{\text{eff}}}}$$

$$\text{SPHERES} \quad \phi_S = R \sqrt{\frac{k_v}{D_{\text{eff}}}}$$

 RATIO OF THIELE MODULUS FOR SPHERES
 AND MONOLITHS ($\phi_S/3\phi_L$)

Monolith with a=	Spheres with Diameter of			
	2R=1/4"	2R=1/8"	2R=1/16"	2R=1/32"
a=0.027 cm	7.84	3.92	1.96	.98
a=0.054 cm	3.92	1.96	.98	.49

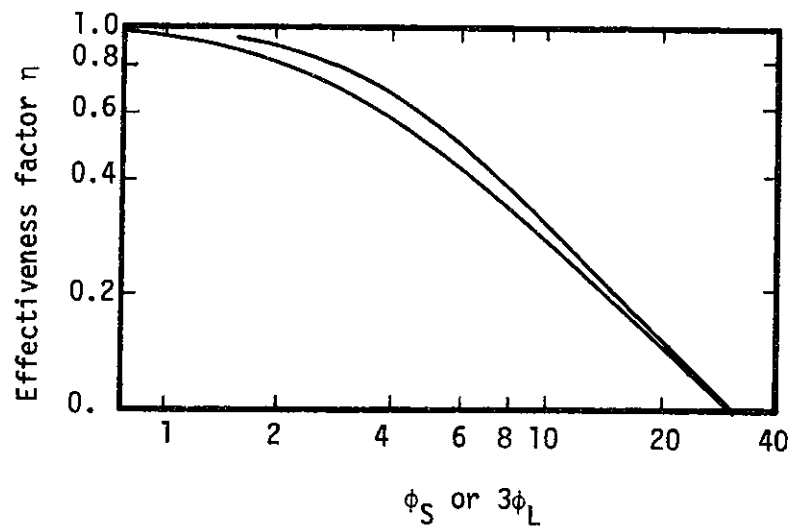


FIGURE 1.1
EFFECTIVENESS FACTOR WITH FIRST ORDER KINETICS

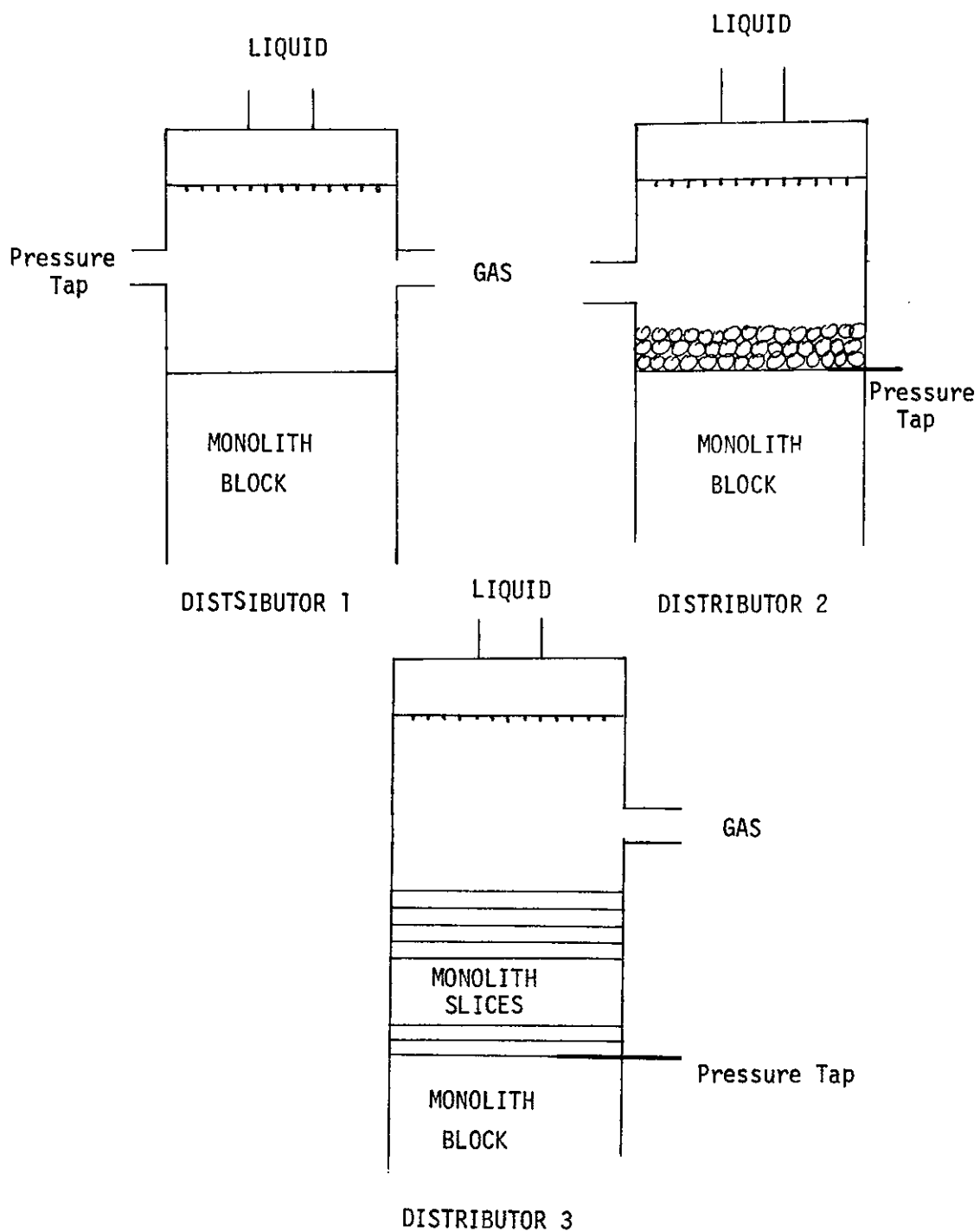
or 4 ft long with 360 cell/in² material.

In one configuration the outside of the column was first sealed with a special rubber type adhesive and this was surrounded by a silicone rubber. In a second configuration the monolith sections were fitted into 1" i.d. Teflon tubing, after first heating the Teflon to 250°C to cause it to expand and then allowing it to shrink so as to hold the sections in tightly. In all cases the monolith ends were cut precisely perpendicular to the channels so that adjacent sections were in contact with one another across the entire cross-section. This precaution is necessary since liquid will easily move radially (horizontally) across an exposed end of a vertically arranged monolith. Sections were stacked randomly so some offset would be expected between the array of cells in one monolith section and in that immediately below it. For the structures used here the void fraction is much greater than the solid fraction (Table 1.1) so a channel would never be completely blocked off from flow by the solid web of the section immediately above it.

1-3

Liquid Distributors

The initial liquid distribution will presumably maintain itself with little change as it flows through successive sections, so it is vitally important to obtain uniform distribution initially. Several types of distributors investigated were found wanting. Figure 1.2 illustrates three, the third of which was chosen for all subsequent studies. The first comprised a flat shower head with 37 small pipes which dripped liquid uniformly over the cross section. However, there are about 157 cells in a 1" diameter section and liquid did not



DISTRIBUTORS
FIGURE 1.2

distribute itself uniformly through all these cells, as shown by the fact that the pressure drop was irreproducible and changed significantly with a slight rotation of the shower head, i.e. the scale of uniformity provided by the pipe distributor was considerably larger than the cross-section of the cells. In the second distributor configuration a layer of 4 mm spheres was placed on the top of the monoliths and the pipe distributor was retained as a predistributor. Reproducibility improved but some flooding above the layer of spheres occurred at high liquid flow rates; some channel entrances were probably effectively plugged by the spheres. None of the data obtained with distributor no. 2 were retained since they were of dubious value.

The best reproducibility and minimum pressure fluctuations were obtained by placing a sandwich of thin monolith slices (27 slices each about 1/8" thick) above the monolith array. The detailed design is shown in Figure 1.3. A 1/16" tube, used as a pressure tap, was placed between the stack of monolith slices and the monoliths. A 4" long Plexiglas (polymethyl methacrylate) tube which had a larger I.D. than the column O.D. was placed over the top of the column. The annular space between the Plexiglas tube and the column was sealed at the lower end. The liquid predistributor (shower head) was fitted and sealed to the other end of the 4" tube. Gas was introduced to the top of the column through a side tube on the 4" Plexiglas tube and moved upward through an annulus. This design minimizes disturbances of the liquid predistribution by the gas.

Most of the studies were performed with water and air although some studies were made with cyclohexane and air. The flow circuit

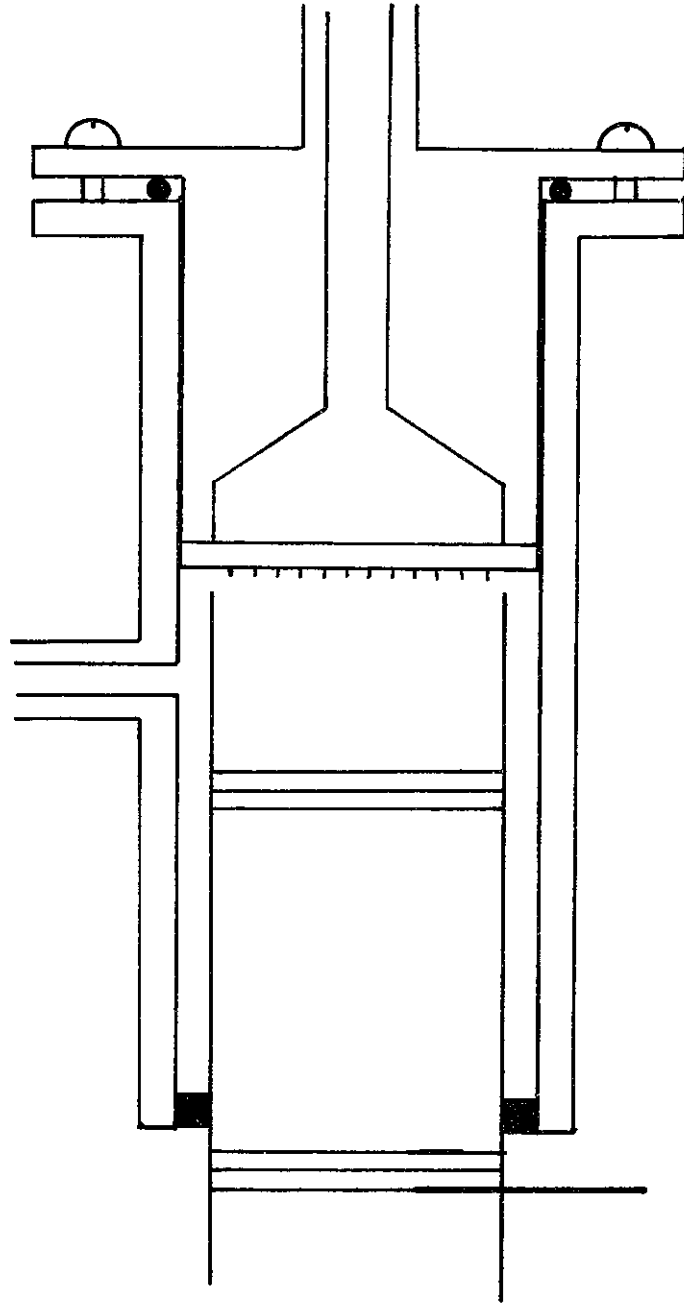


FIGURE 1.3 DISTRIBUTOR 3

used for the water-air system is given in Figure 1.4. In the case of cyclohexane, basically the same diagram was used except some additions were made to recirculate the cyclohexane.

The pressure drop and presumably, the degree of axial dispersion and mixing, is affected by the type of flow achieved in the monolith channels, specifically by whether the liquid passes downward as an annular film or as slugs. To obtain some idea of the hydrodynamic flow pattern as a function of gas and liquid flow rates in a single channel, some observations were made of water-air flow in a piece of precision bore capillary tubing, 0.0791"(0.200 cm) in inside diameter and 102 cm long. This is slightly larger than the hydraulic diameter of the 200 cell monolith channels (0.1528 cm).

EXPERIMENTAL RESULTS

1-4

Effect of Distributor

The marked effect of the nature of the distributor is demonstrated on Figures 1.5 through 1.8 which show the observed pressure drop (cm of water per meter length of monolith stack) as a function of superficial air flow rate (cm/s at room temperature and atmospheric pressure) for each of two representative values of the superficial liquid flow rate of water and for a stack of 3" monoliths as compared to 6" monoliths. As noted above, with distributor no. 1 the pressure drop varied substantially with a slight degree of rotation which presumably altered the degree of uniformity of distribution. The values shown are the highest observed, which occur with the most uniform distribution (see below). Regardless of the type of distributor, a negative measured pressure drop is encountered at low gas

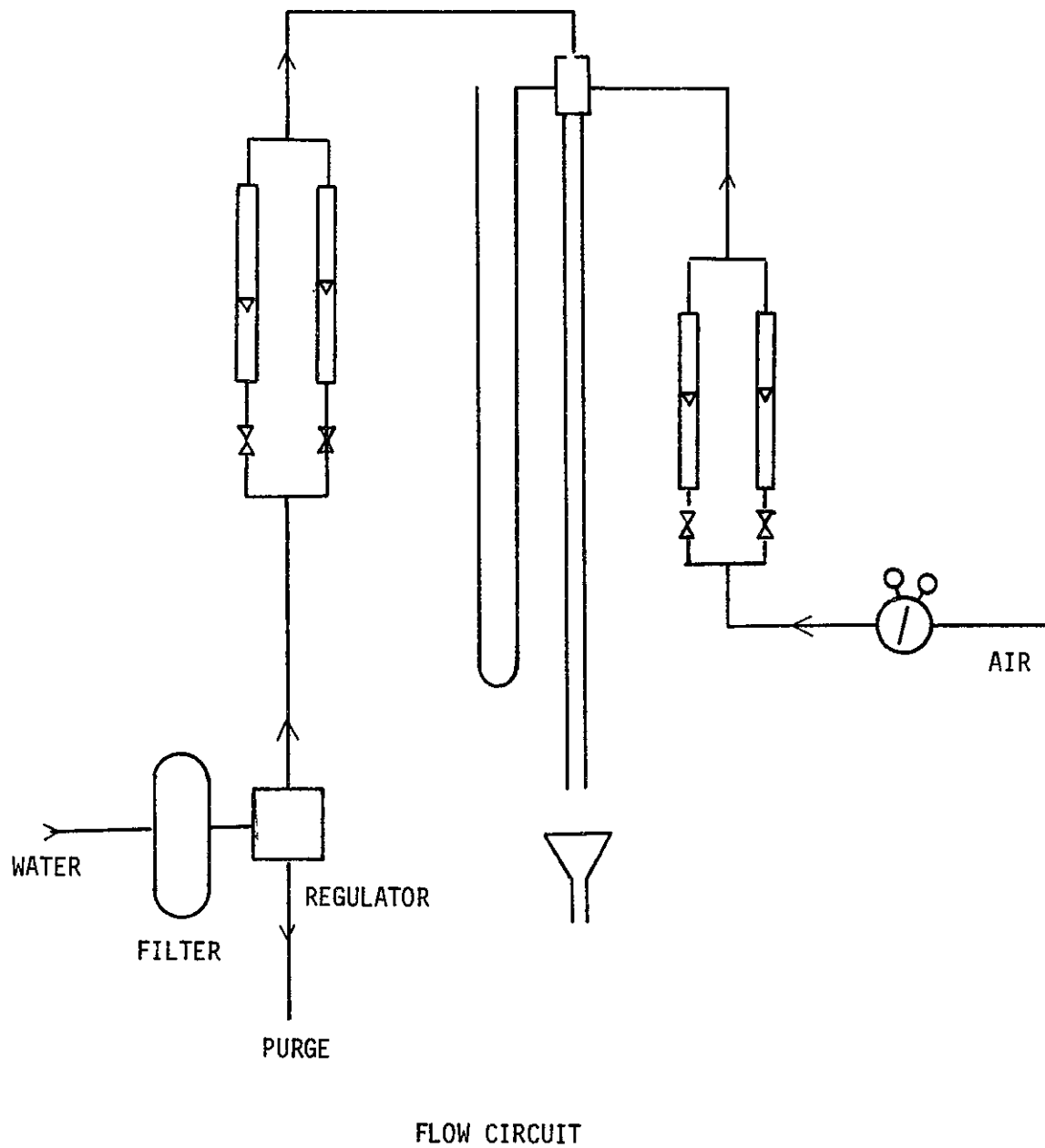


FIGURE 1.4 FLOW CIRCUIT FOR WATER STUDIES IN MONOLITHS

and liquid flow rates, caused by the hydrostatic head of liquid. With uneven liquid distribution, reversal of gas flow will presumably occur in this region, slug-type flow of liquid causing a pumping action to return some gas upwards through those channels in which liquid flow, if it occurs at all, is solely as an annular film on the wall.

With either a good or a poor liquid distributor, pressure drop increases with an increase in either gas or liquid rate, as expected. Comparison of the performance of a stack of 3" vs. 6" monolith pieces (Fig. 1.5 vs. Fig. 1.7 at $V_g = 3.95$ cm/s and Fig. 1.6 vs. Fig. 1.8 at $V_g = 1.31$ cm/s) reveals the effect of essentially doubling the number of junctions between adjacent pieces of monolith. (The increase is from 7 to 15). In each case this brings the values of $\Delta P/L$ with the two types of distributor much closer together, the pressure drop with the poor distributor (no. 1) being raised and that for the good distributor (no. 3) being lowered. At the lower of the two liquid flow rates for which this comparison was made, the values of $\Delta P/L$ become quite close together when 3" blocks are studied (Fig. 1.8).

We believe that two quite different phenomena exist which work in opposite directions when the monolith lengths are reduced from 6" to 3", the total column length being held constant. If one starts with the no. 1 distributor, uniform distribution is obtained but on a larger scale than that of the cross-section of the cells. Consequently we postulate that some cells had little or no liquid flow while adjacent cells had much more than the average. Presumably the slight offset between adjacent monoliths allowed mixing to occur

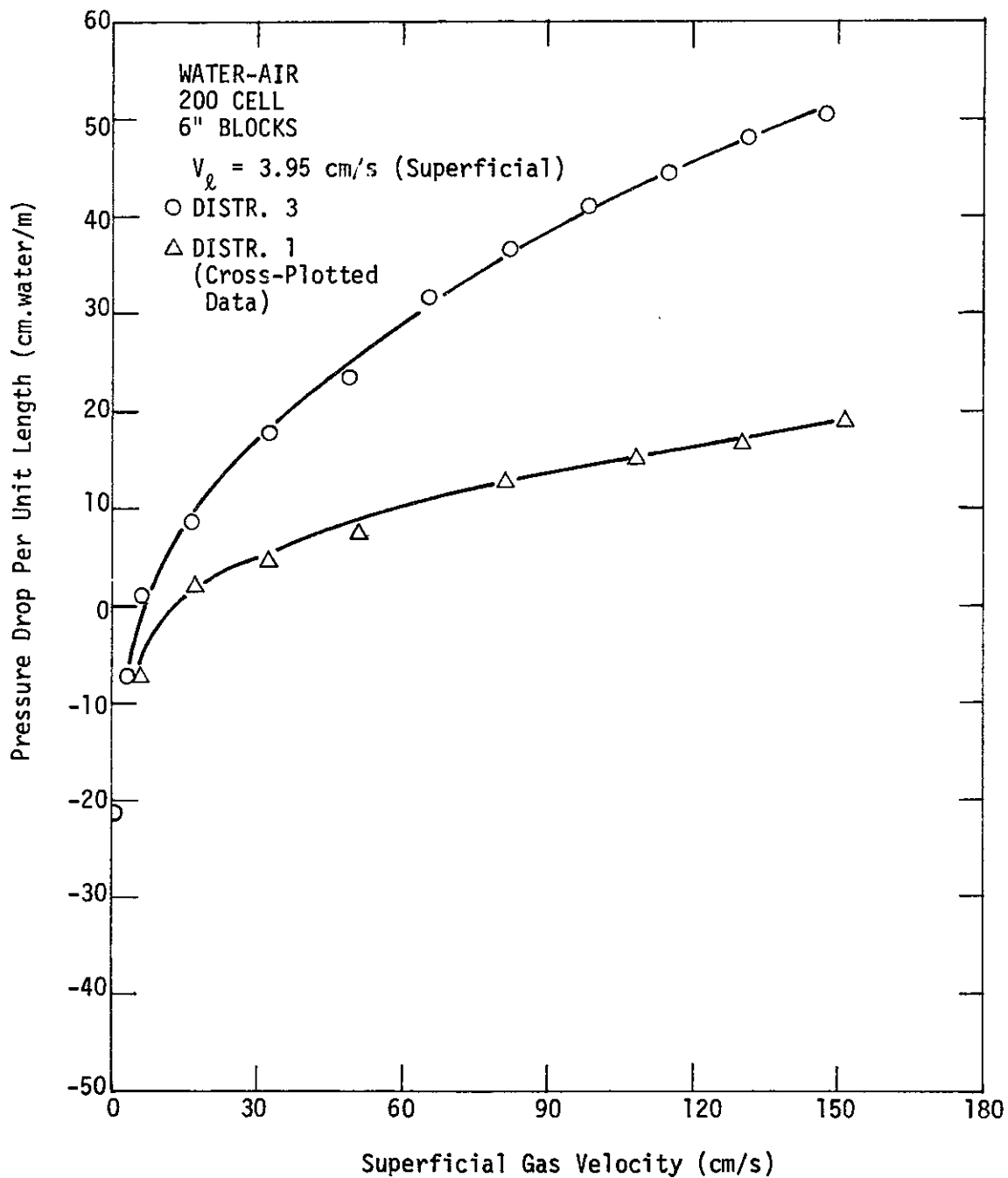


FIGURE 1.5 COMPARISON OF PRESSURE DROP
DATA FOR DISTRIBUTOR 1 AND 3.

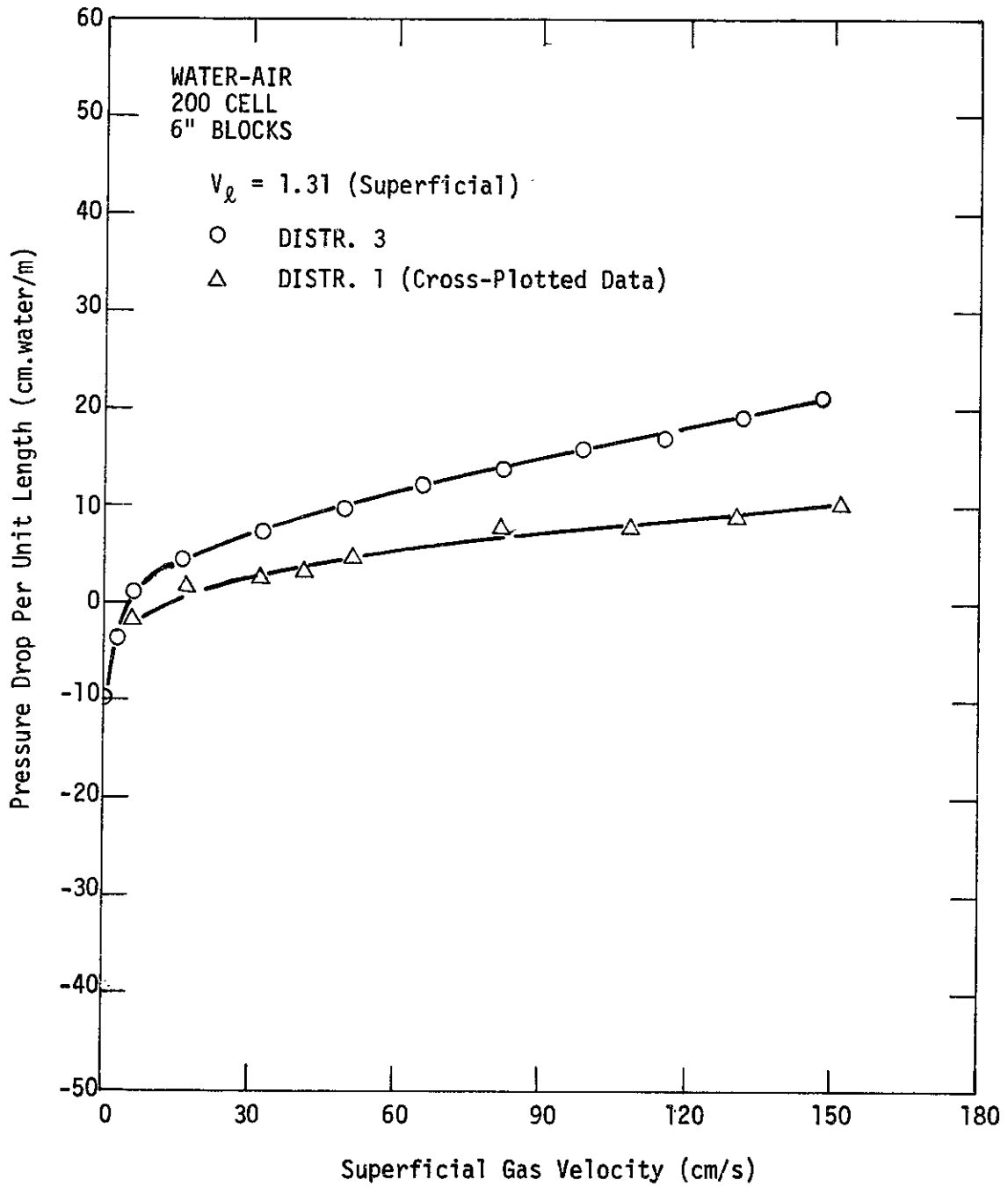


FIGURE 1.6 COMPARISON OF PRESSURE DROP DATA FOR DISTRIBUTOR 1 AND 3

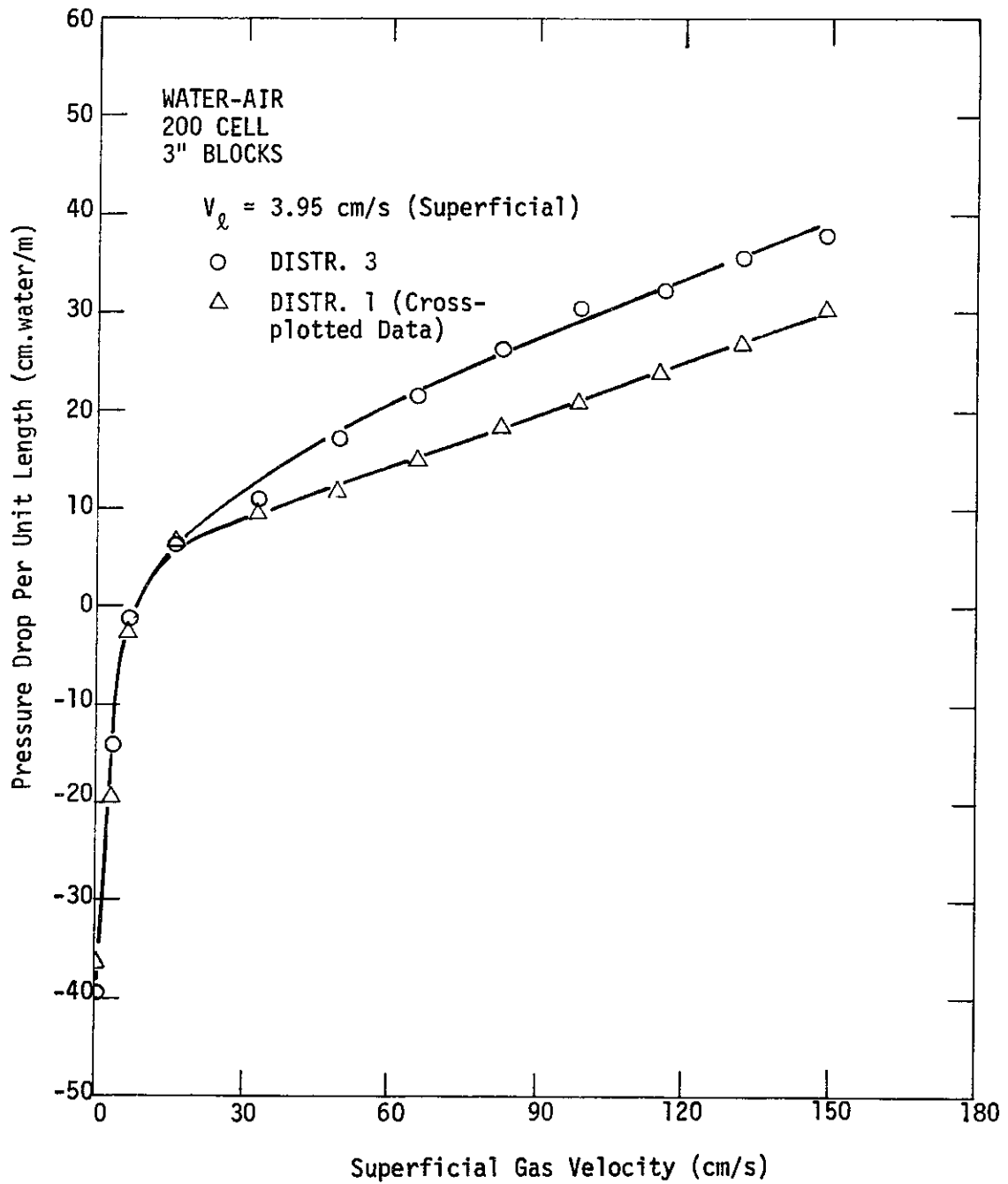


FIGURE 1.7 COMPARISON OF PRESSURE DROP DATA FOR DISTRIBUTOR 1 AND 3.

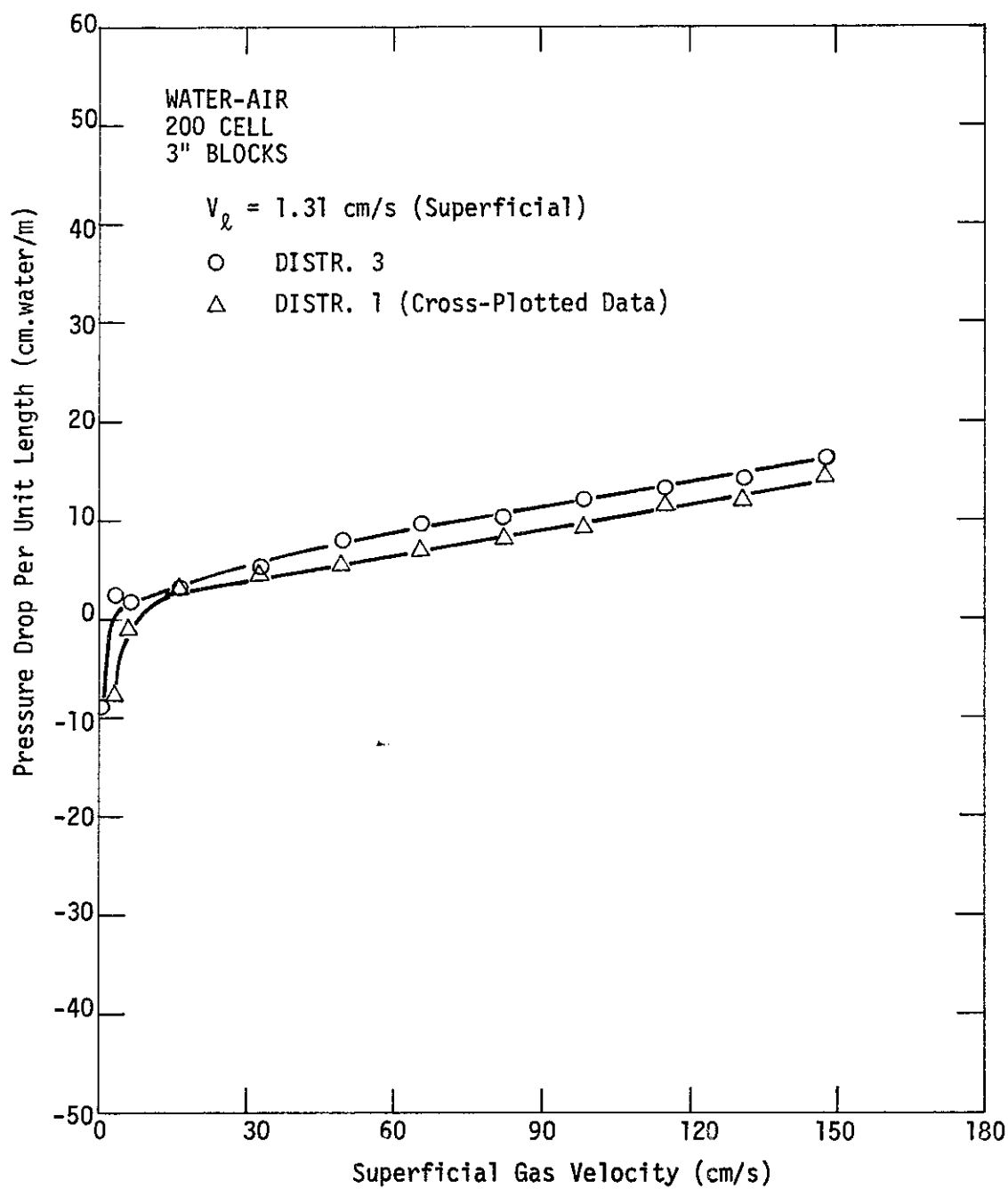


FIGURE 1.8 COMPARISON OF PRESSURE DROP DATA FOR DISTRIBUTOR 1 AND 3.

on a micro scale and thus more uniform distribution of liquid amongst the parallel passageways. This leads to a higher pressure drop. However, focusing on a single channel, the flow pattern changes with length. In essence, as bubbles and slugs of liquid follow one another down a tube it is observed that a liquid ring frequently appears within a bubble, which grows in thickness, finally forming a liquid web across the channel which splits the bubble in two. The appearance of additional menisci would presumably increase the resistance to flow caused by circulation in the slugs. It is thus postulated that considerably more bubble breakup occurs in the 6" lengths than in the 3" lengths, accompanied by a higher pressure drop per unit length.

Some of the pressure drop with 300 cell/in² monolith in a 4 ft column of 3" or 6" blocks are shown in Figures 1.9 and 1.10. Here again pressure drop per unit length as cm.water/m is plotted against superficial gas velocities at constant liquid flow rates. Pressure drop with 3" blocks is higher than 6" blocks. The opposite was true for 200 cell monoliths (Figs. 1.11 and 1.12). Both 200 cell/in² and 300 cell/in² monoliths had a measured web wall thickness of .027 cm, but the 300 cell material has a passageway dimension of .107 cm versus .1528 cm for the 200 cell material. Since passageways are smaller in the 300 cell bubbles should reach steady state more quickly than 200 cells and one does not expect very much difference due to bubble break up. The restrictions of the channel exits in 300 cell material by the web walls of the next block is greater than with 200 cell blocks and this causes a higher pressure drop across the block joints in 300 cell monolith columns. Indeed if this orifice effect is

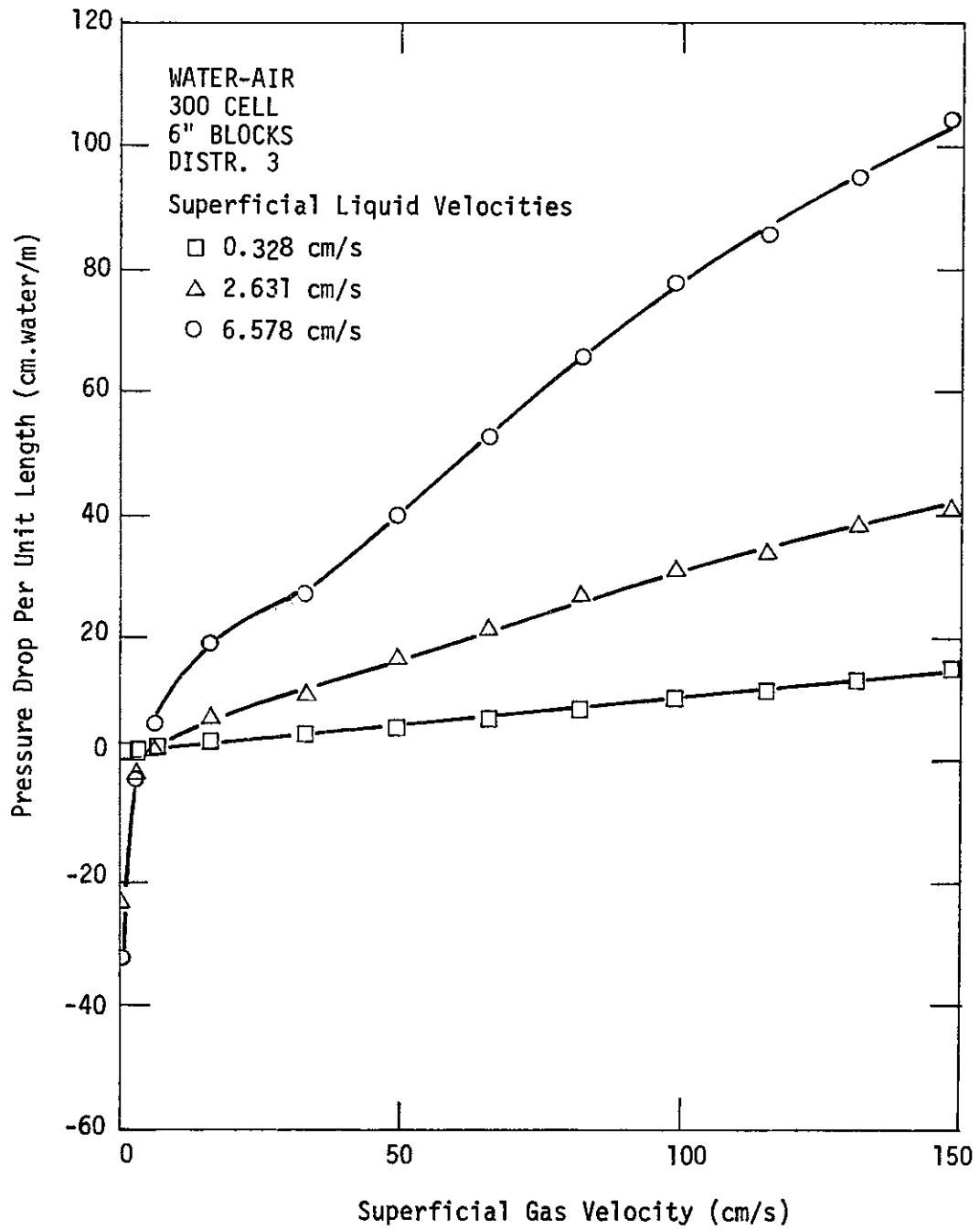


FIGURE 1.9 PRESSURE DROP

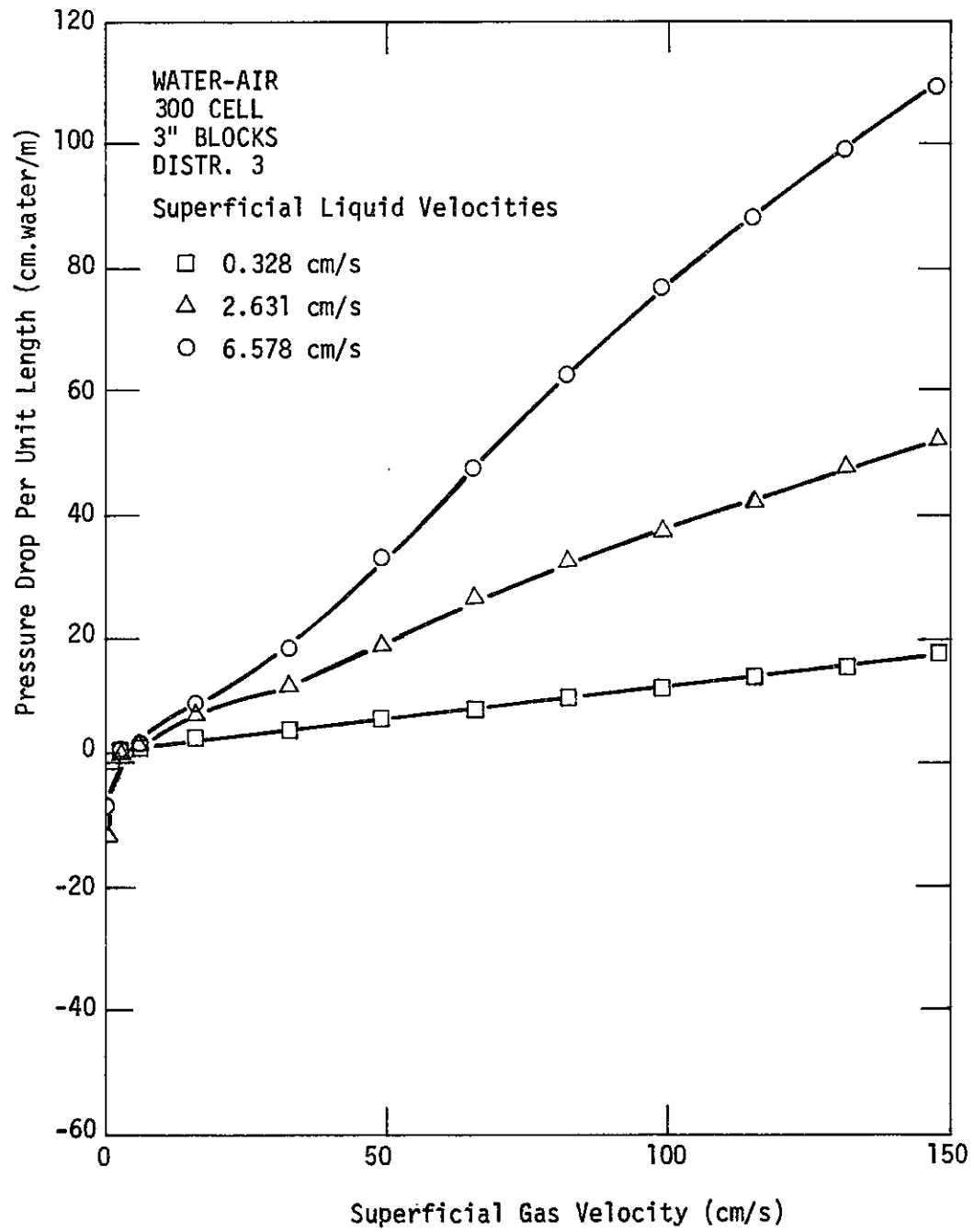


FIGURE 1.10 PRESSURE DROP

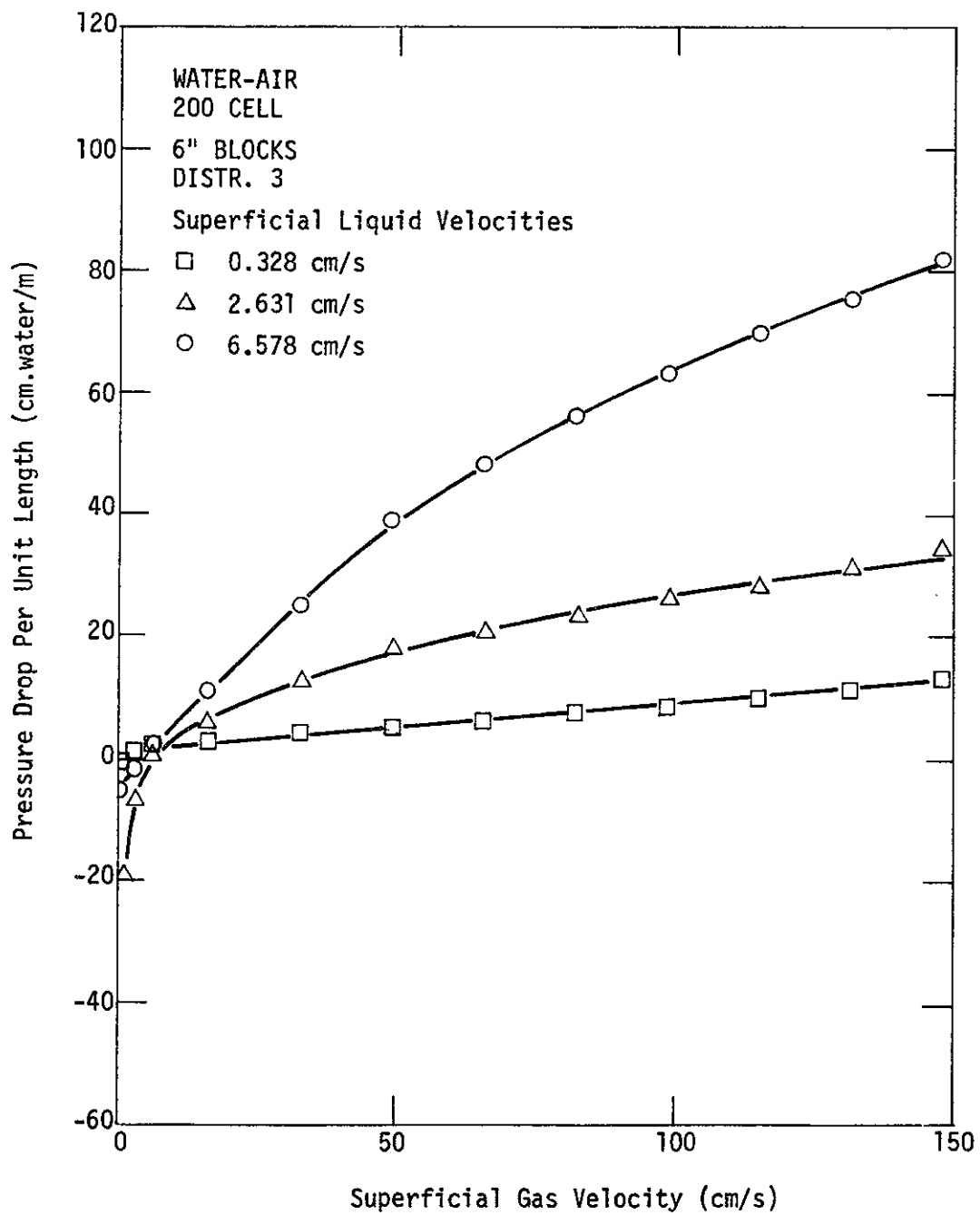


FIGURE 1.11 PRESSURE DROP

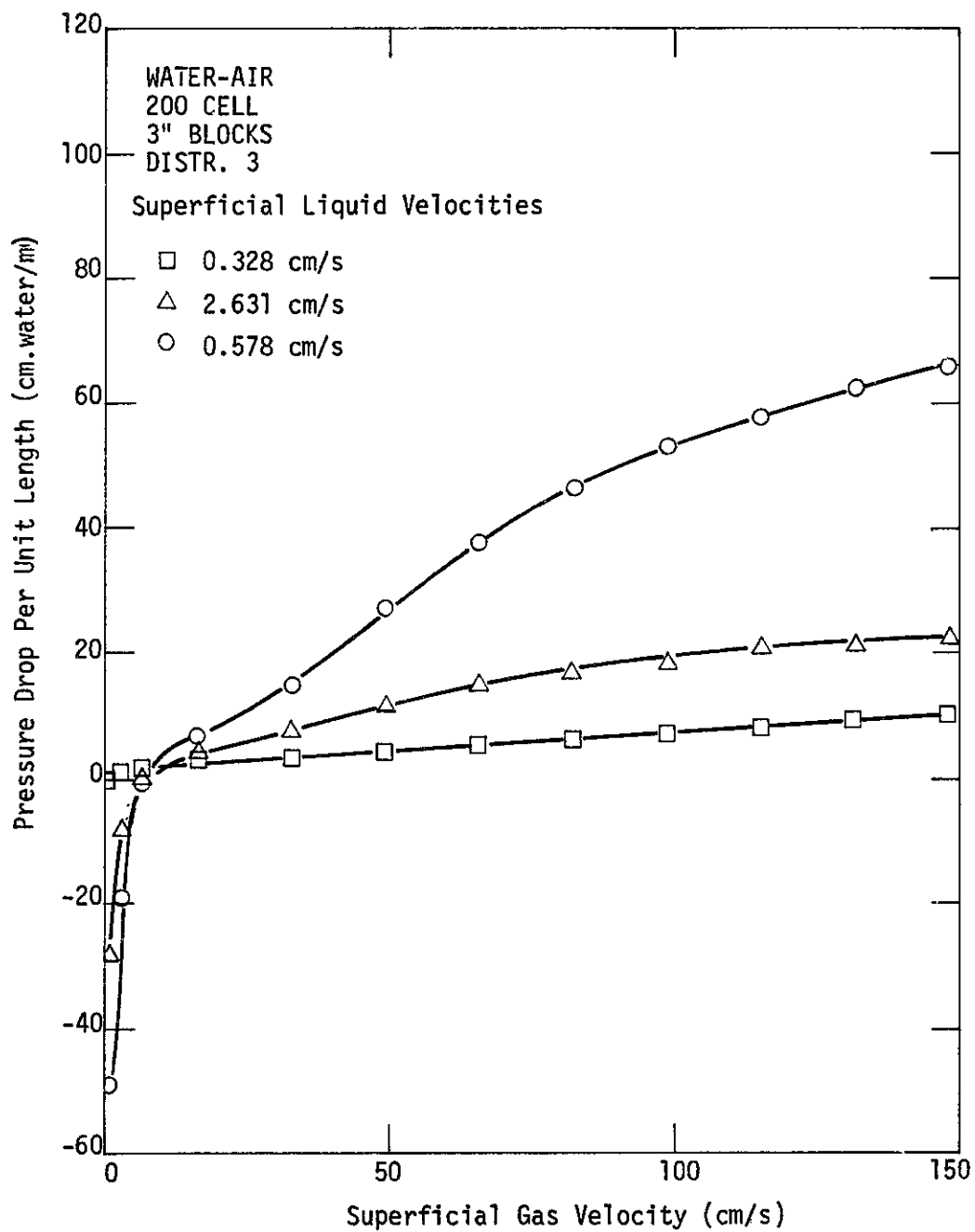


FIGURE 1.12 PRESSURE DROP

calculated and subtracted from measured pressure drop for 3" and 6" blocks of 300 cell columns with the equation given on page , it will be seen that the total of frictional and hydrostatic pressure drop in both systems (presumably hydrostatic pressure drop is the same for 6" and 3" blocks) will be close to each other.

Pressure drop data with distributor 3 for 200 cell/in² monoliths are compared to those in packed beds (Fig. 1.13). Packed bed data presented here are for 4 and 6 mm glass beads (McIlvried, 1956) and cylindrical alumina tablets of 1/8" diameter and length (M.W. Van Eek, 1976). Packed bed pressure drops are much higher than in monoliths for the same superficial gas and liquid velocities.

The above results may be compared to a brief study by Kiser (1975) performed on the same type of monolith structure but in a column 4" diameter and 4 ft long consisting of a stack of units each 3" high (Fig. 1.14). The highest liquid flow rate studied by Kiser was 1.24 cm/s but air flow rates of up to 90 cm/s were covered. Kiser's results agree closely with present results at the lowest air and liquid rates but his observed pressure drop was twice that obtained here at the highest combination of liquid and gas. The reasons for this difference are not clear. Kiser's distributor was a special Bick spray nozzle which is used to produce a uniform spray but no information is available on the degree of uniformity actually achieved. His study was not intended to be definitive and is cited only to illustrate further the sensitivity of pressure drop and flow pattern in monolith systems to geometrical details.

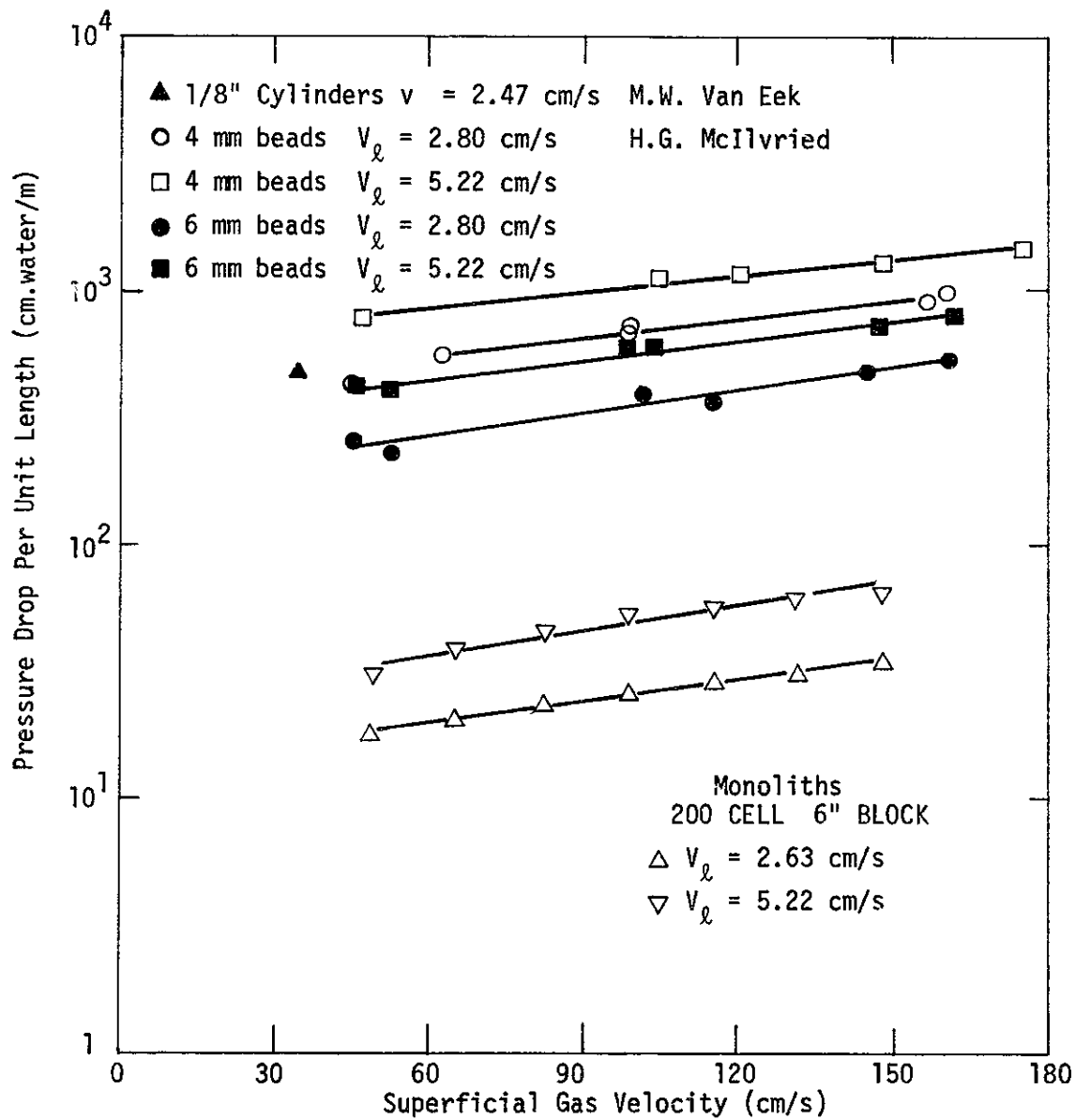


FIGURE 1.13 COMPARISON OF PRESSURE DROP IN MONOLITHS WITH THOSE IN PACKED BEDS

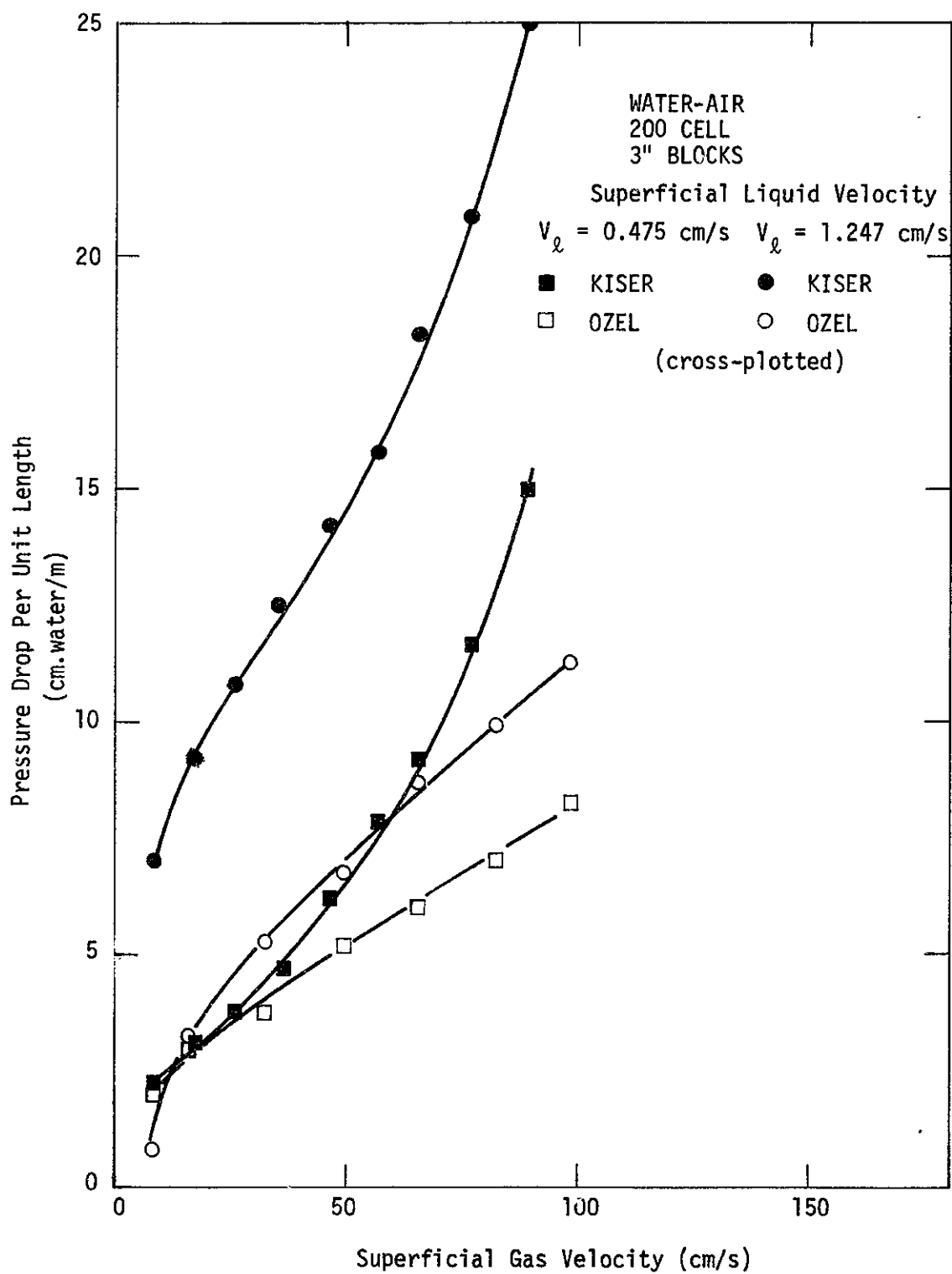


FIGURE 1.14 COMPARISON OF PRESENT RESULTS AND THOSE OF KISER

1-5

Cyclohexane-Air System

Figures 1.15 and 1.16 compare the pressure drop observed with cyclohexane and air with those for water and air (Figures 1.11 and 1.12) in 3" and 6" lengths of stacked monoliths. At any combination of superficial liquid and gas rate, the pressure drop observed with the hydrocarbon is moderately less, probably reflecting its lower surface tension. No foaming occurred in any of these studies.

1-6

Single Tube Studies

The pressure drop and, presumably, the degree of axial dispersion and mixing, is affected by the type of flow achieved in the monolith channels, specifically by whether the liquid passes downward as an annular film or as slugs. To obtain some idea of the hydrodynamic flow pattern as a function of gas and liquid flow rates in a single channel, some observations were made of water-air flow in a piece of precision bore capillary tubing 0.0791" (0.200 cm) in inside diameter and 102 cm long. This is slightly larger than the hydraulic diameter of the monolith channels (0.15 cm).

Over a considerable range the type of flow regime is determined by the mode of introduction of the liquid into the capillary, as shown in Figure 1.17. If water is introduced steadily down the side of a funnel atop the capillary, (distribution mode A) annular flow is established up to relatively high liquid flow rates, about 1.7 cm/s for this size capillary, and this limiting flow rate is independent of the gas rate from essentially zero to 150 cm/s. If however water is dropped steadily into the funnel (distribution mode B) (here drops of 0.037 cm^3 volume each were used) slug flow is obtained at relatively

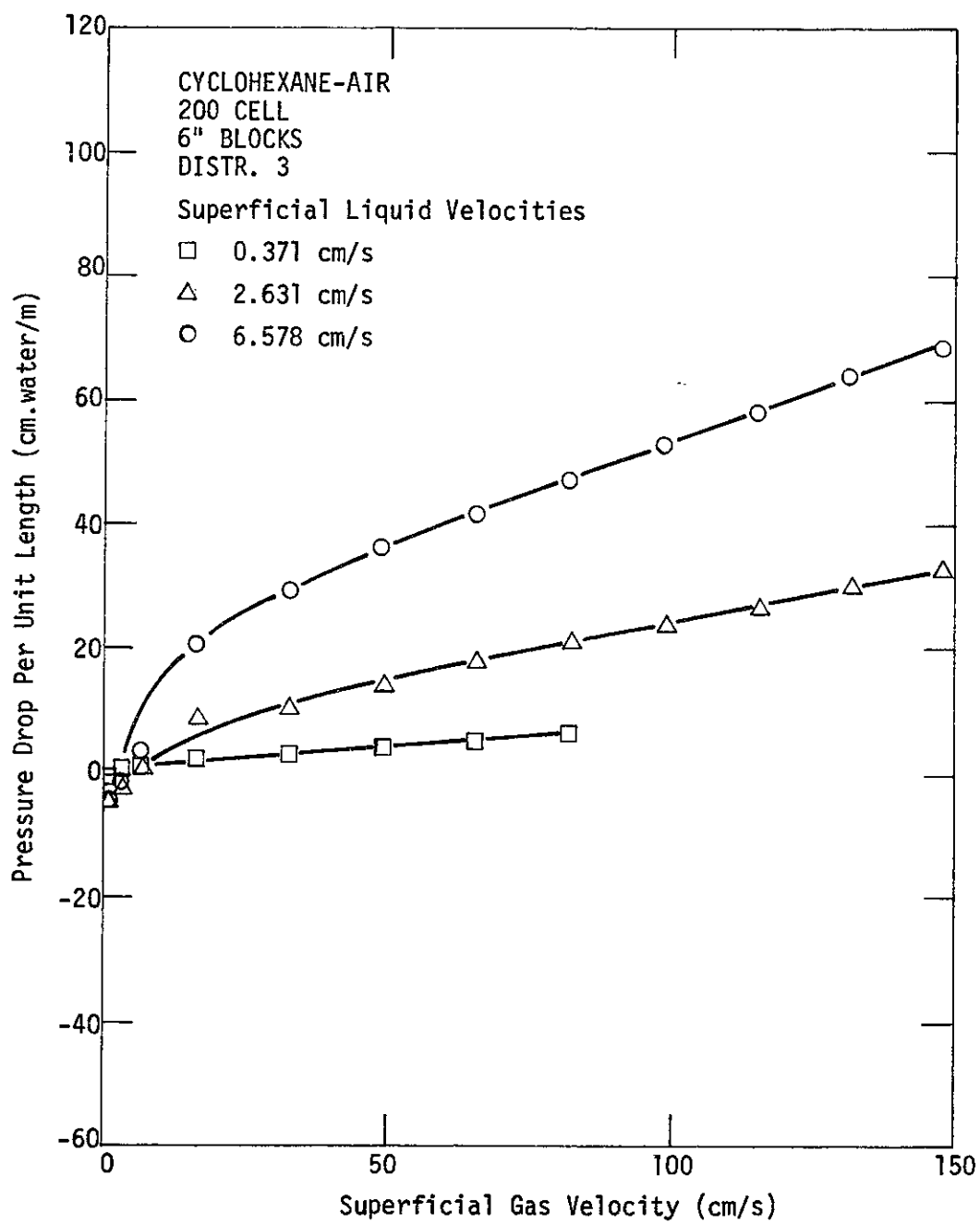


FIGURE 1.15 PRESSURE DROP

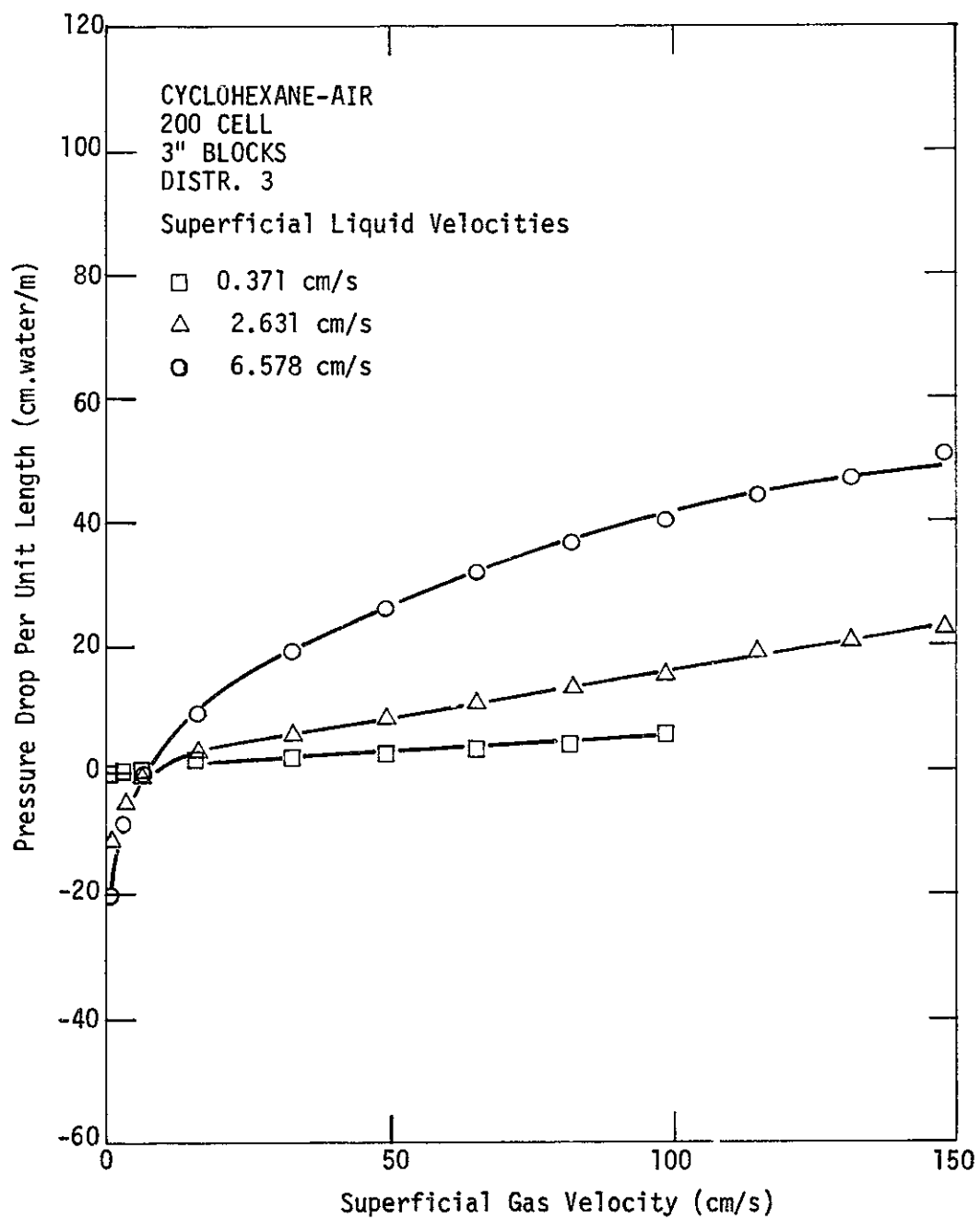


FIGURE 1.16 PRESSURE DROP

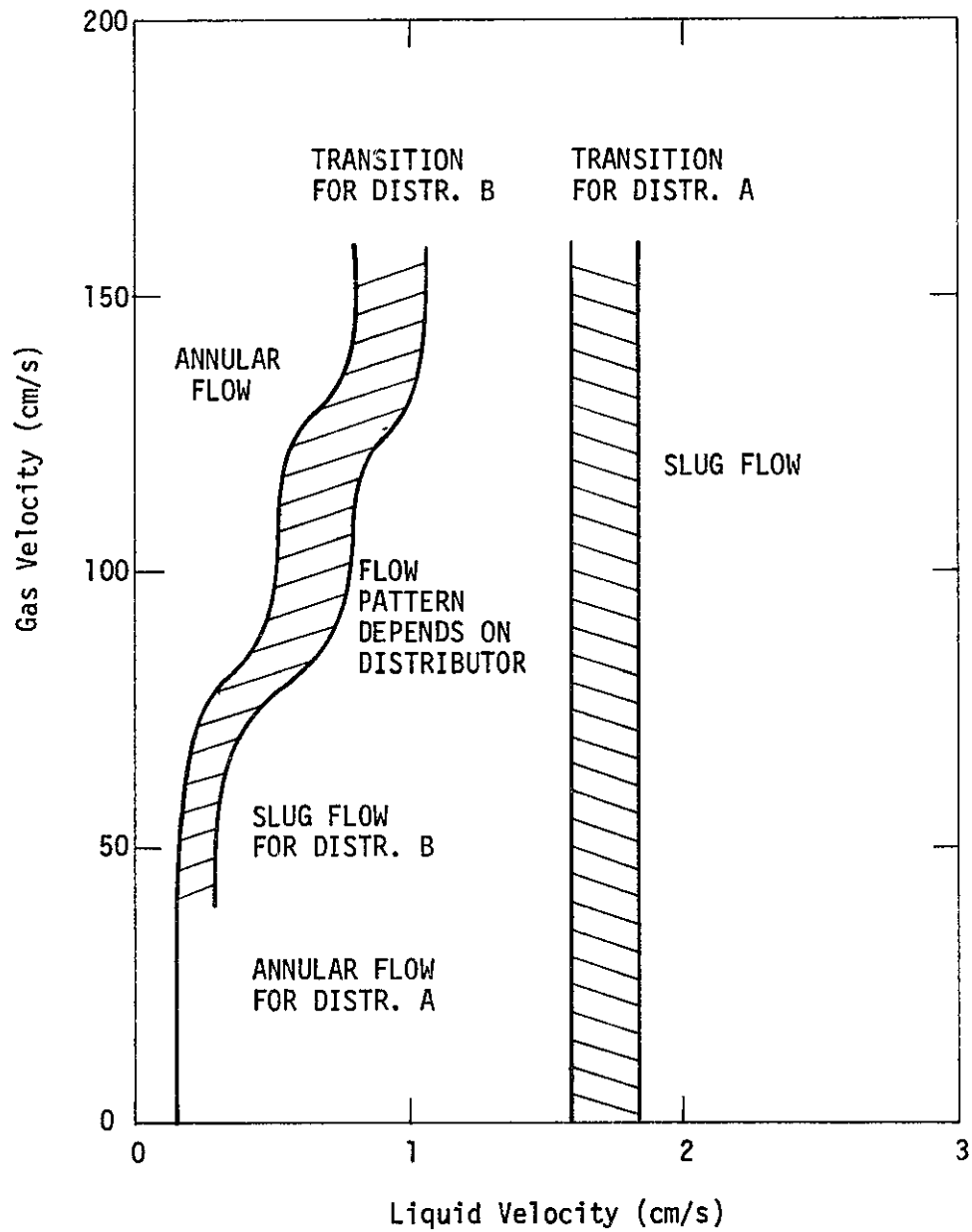


FIGURE 1.17 FLOW IN A SINGLE CAPILLARY —
REGIONS OF ANNULAR vs. SLUG FLOW

low liquid rates but the value of V_ℓ at which annular flow changes to slug flow varies substantially with gas flow rate.

Within the slug flow region, the behavior and appearance of successive slugs of liquid changes substantially as gas flow rate is increased at fixed constant liquid flow rate. At a V_ℓ of .79 cm/s, for example, increasing gas rate gradually decreases the length of liquid slugs and the distance between liquid slugs, of course, gradually increases. Liquid slugs become interspersed with annular rings of liquid which flow downward, the gas phase being continuous.

A ring typically grows in thickness with time, eventually to the point that it fills the tube cross-section, thus splitting the bubble in two. Consequently the flow pattern and average bubble size will be different at the bottom of the capillary than at the top, so the average behavior of a channel is a function of its length. The difference between pressure drops observed with monolith stacks of different segment sizes is ascribed to this, as discussed in previous sections. The characterization in Figure 1.17 is limited to a smooth-walled tube of this size and length.

Figure 1.18 shows pressure drop as a function of V_ℓ for various values of V_g as observed in annular flow and Figure 1.19 the same for slug-type flow. In annular flow, $\Delta P/L$ is independent of V_ℓ for a fixed low value of V_g , reflecting the region in which the liquid film insignificantly reduces the effective diameter of the tubing and in which the ΔP is caused essentially by the gas flow. At very low values of V_g the drag of liquid on gas causes a slight drop in ΔP with increased liquid flow rate. At the highest gas flow rates, ΔP is proportional to V_ℓ .

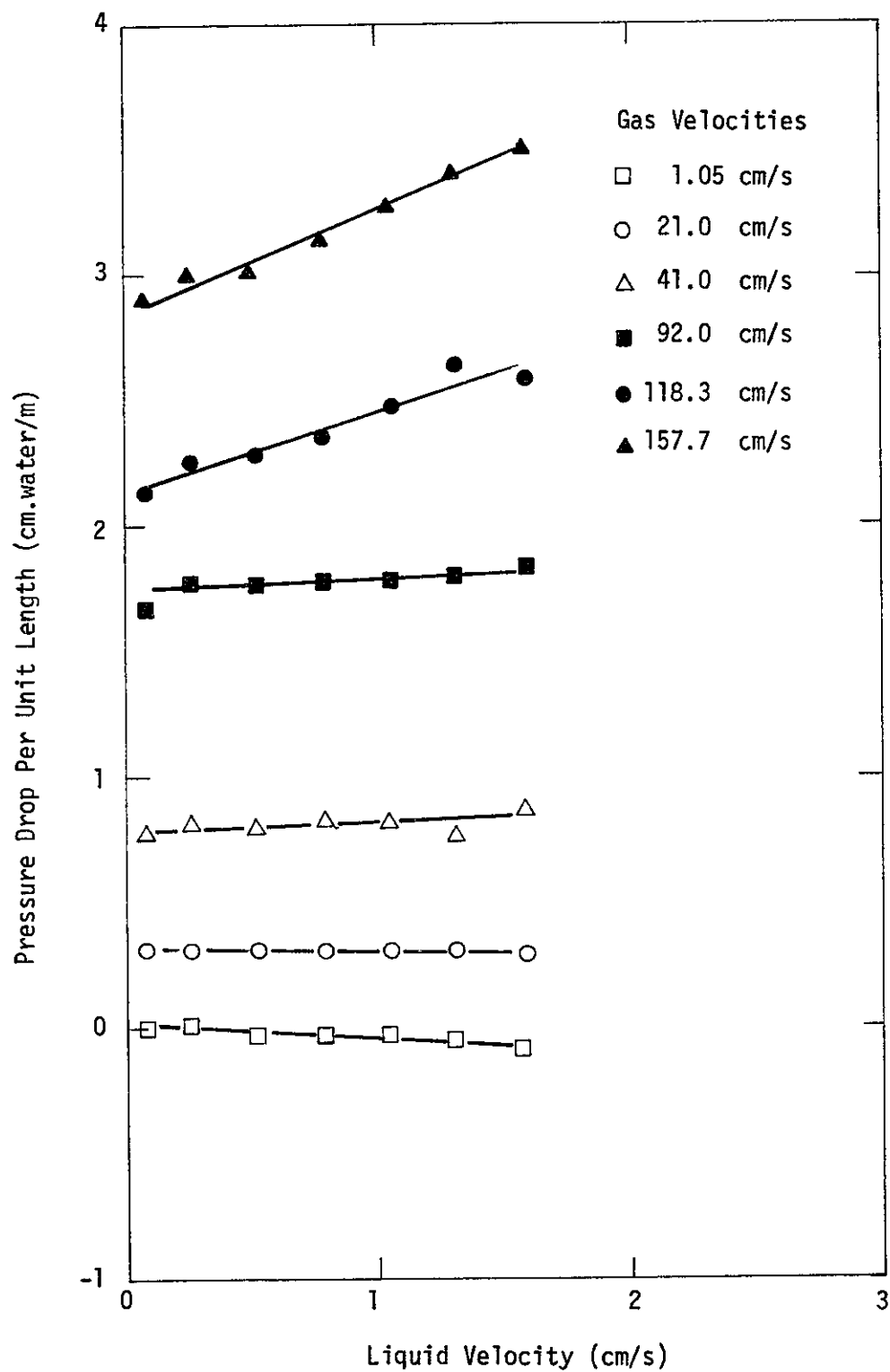


FIGURE 1.18 PRESSURE DROP IN A 0.200914 cm
CAPILLARY TUBE FOR ANNULAR FLOW

Figure 1.19 shows pressure drop as a function of V_ℓ for various values of V_g in the slug flow regime. ΔP is now a non-linear function of V_ℓ and the pressure drop is now negative over a considerable range in which it was positive with annular flow. Thus pressure drop information can be used to obtain some insight into the flow pattern established in a monolith.

Figure 1.20 compares the pressure drop observed with annular vs. slug flow for a fixed representative liquid flow rate as gas rate is increased. As expected, under any combination of liquid and gas flow rates, transition from annular to slug flow substantially increases the pressure drop, provided that this is positive. At low rates, however, under slug flow conditions the hydrostatic head of the liquid can cause a pumping action on the gas, producing a negative pressure drop.

Figure 1.21 shows values of $\Delta P/L$ vs. V_1 for monolith and capillary for comparable values of V_1 and V_g , where both are calculated per unit of open cross-sectional area. The capillary data are for drop-wise introduction. The considerably larger pressure drops in the monolith reflects their somewhat smaller passageways.

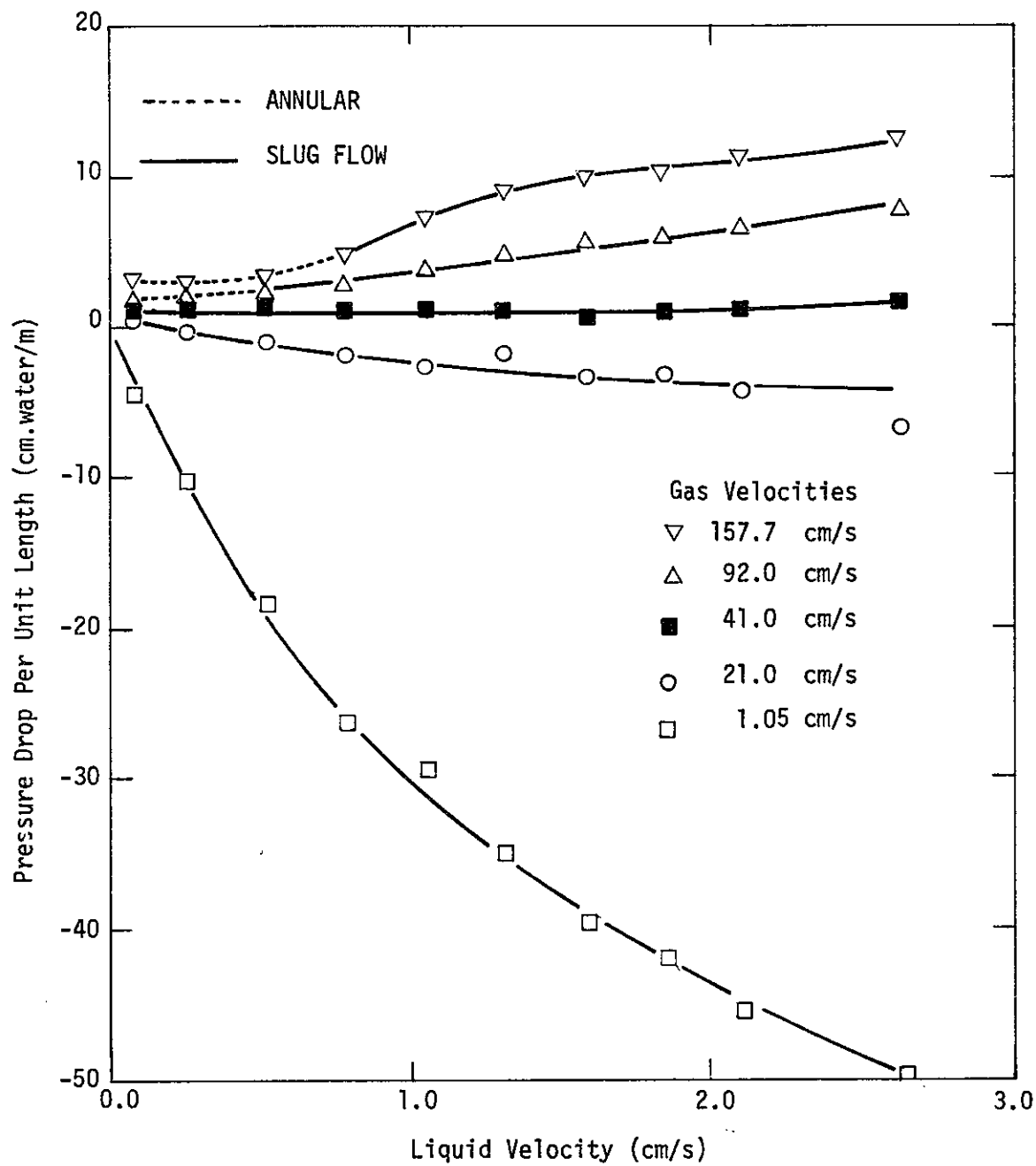


FIGURE 1.19 PRESSURE DROP IN A .200914 cm I.D. CAPILLARY TUBE WITH DISTRIBUTOR B.

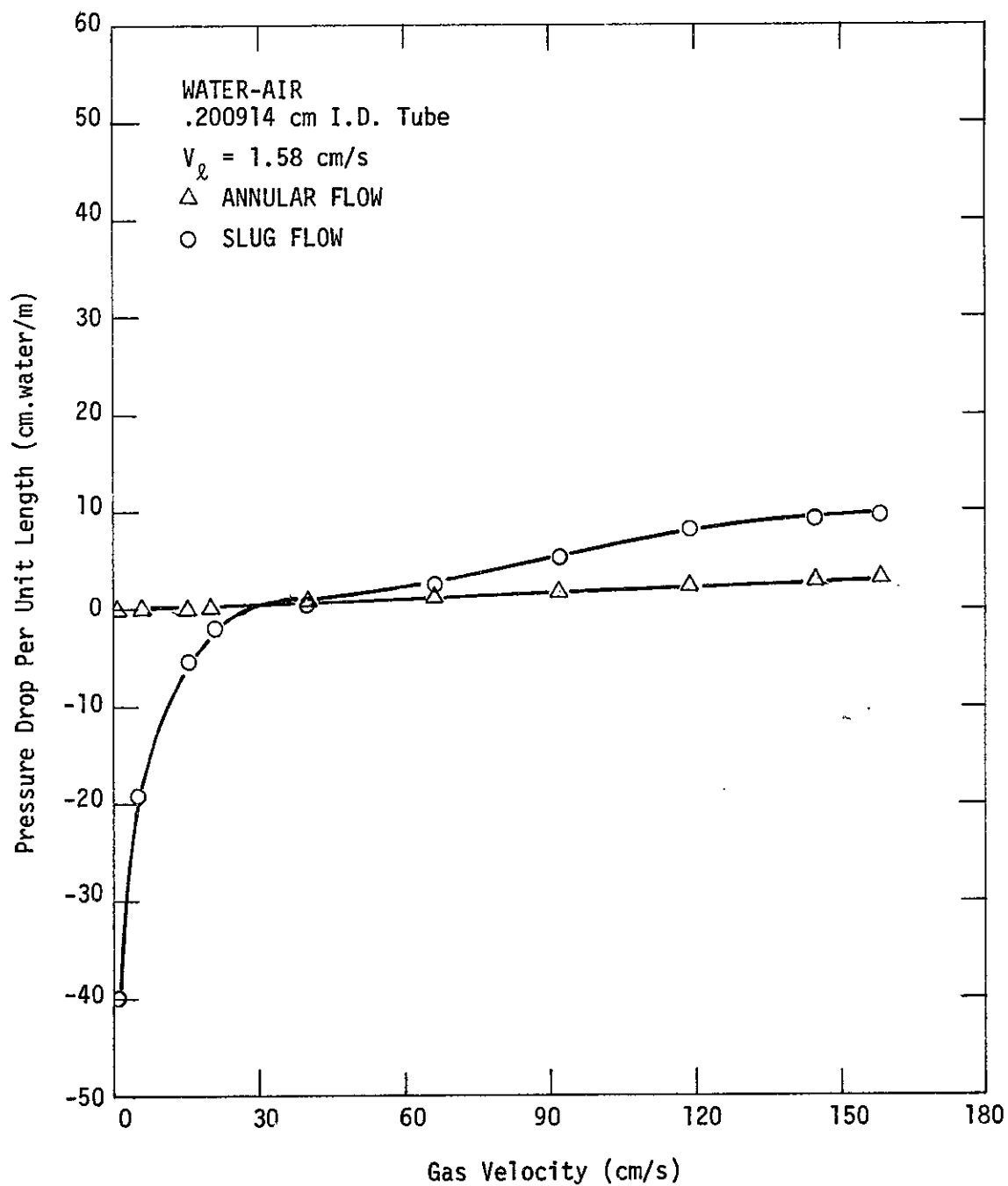


FIGURE 1.20 COMPARISON OF PRESSURE DROP FOR SLUG AND ANNULAR FLOW IN CAPILLARY TUBES

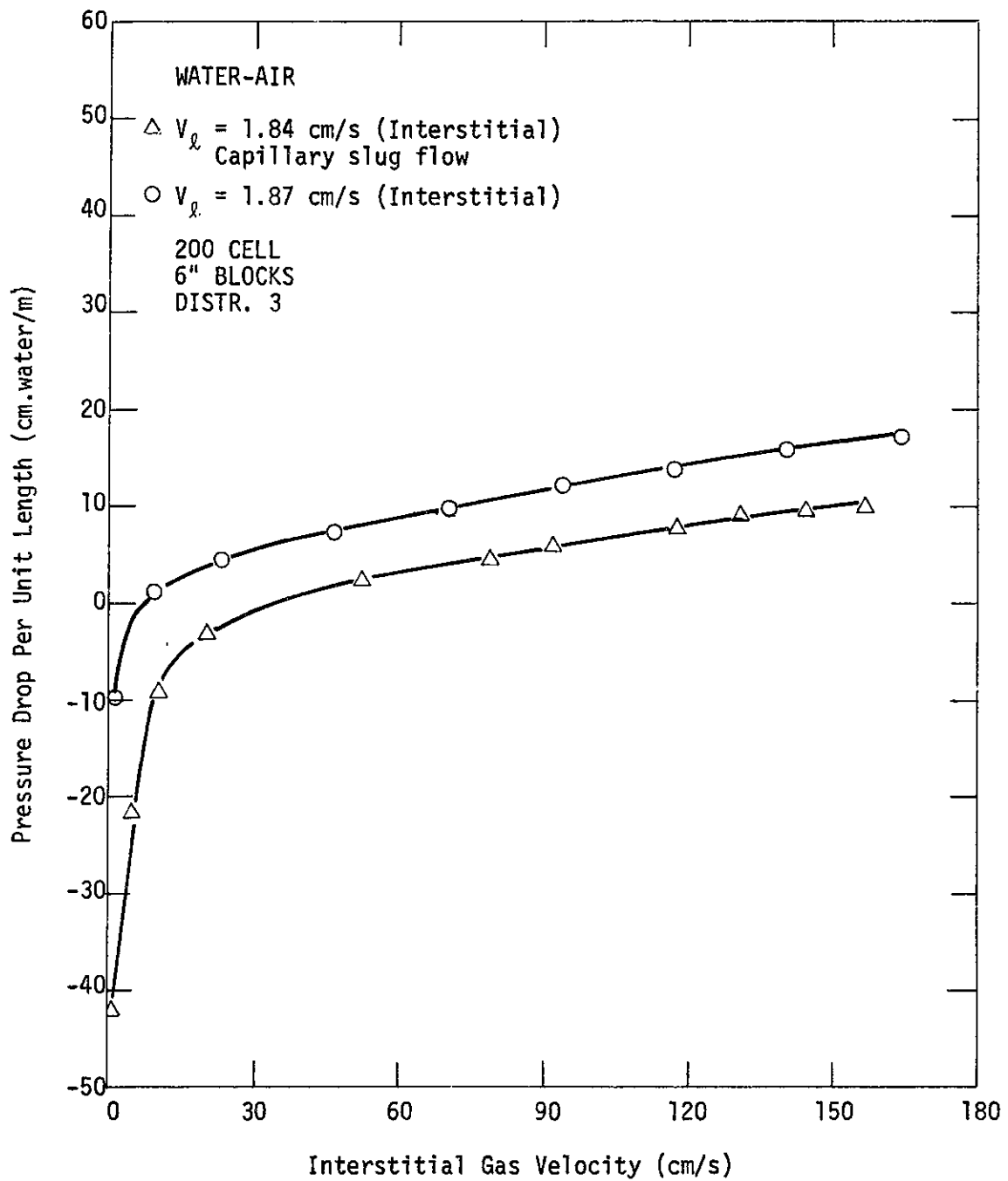


FIGURE 1.21 COMPARISON OF PRESSURE DROP FOR
CAPILLARY SLUG FLOW AND MONOLITHS

CORRELATION OF RESULTS

The measured pressure drop, ΔP_m , may be taken as the algebraic sum of the frictional pressure drop, the static head, $g\rho_L L$, and orifice effects:

$$\Delta P_m = \Delta P_f + \Delta P_{or} - g\rho_L L \quad (I-1)$$

The orifice effects are caused by the partial obstruction of the exit of one channel by the web of the next block. If one assumes that gas and liquid move as slugs through the orifice with the same velocity of $(V_G + V_L)$, the following equation results from the Bernoulli relationship:

$$\Delta P_{or} = N \left(\frac{V_L}{V_T} \rho_L \left(\frac{V_{or}^2 - V_T^2}{2} \right) + \frac{V_G}{V_T} \rho_G \left(\frac{V_{or}^2 - V_T^2}{2} \right) \right) \quad (I-2)$$

This assumes an inviscid fluid, a friction loss factor of unity and applies a volume average density of the fluid mixture. No information seems to be available on how to adjust this for the two-phase flow encountered here, although the true friction loss factor is presumably somewhat less than unity. The minimum ratio of average orifice area to cell cross-sectional area is 0.68 for the 200 cell/in² monoliths and 0.56 for the 360 cell/in² monoliths. The geometry here is such that this ratio would be expected to be encountered at most block intersections. Only when two adjacent blocks are nearly aligned would it be higher. As calculated from Eq. I-2 ΔP_{or} is generally fairly small relative to ΔP_m as calculated from Eq. I-1. It is concluded that

the frictional pressure drop, ΔP_f is the dominating term over most of the range of conditions studied. Attempts were made to correlate ΔP_f by dimensional analysis and multi-linear regression methods but none of the relationships obtained seem useful.

CONCLUSIONS

1. Stacked monolith blocks have considerable potential for use as gas-liquid contactors in devices such as trickle-bed reactors.
2. The pressure drop in these systems is very sensitive to the nature of the liquid distributor.
3. Comparison with conventional catalyst supports shows that for equivalent superficial areas per unit volume, the pressure drop for monoliths is an order of magnitude less than for conventional packing.
4. The observed pressure drop has been analyzed in terms of contributions from static head, orifice effects and frictional pressure drop. The flow pattern seems to be too complicated to permit correlation of the data in useful numerical form.

2 - INTRODUCTION

Trickle bed reactors first appeared in the early thirties in Germany. In these reactors a liquid phase and a gas phase flow concurrently through a fixed bed of catalyst particles while reaction occurs. The reaction is usually between a reactant gas phase and a reactant liquid phase on the catalyst surface, but sometimes it is between gases dissolved in an inert liquid. The inert liquid may serve to remove heat of reaction, or to remove unwanted side products or polymer deposits from the catalyst surface.

Petroleum stocks and organic liquids with high boiling points are preferably processed in the liquid phase. Their processing as vapors in packed bed reactors would require evaporation of the liquid phase, possibly causing some decomposition of reactant liquid and inevitably larger amounts of energy. For many systems, trickle beds are also cheaper to operate and construct than vapor phase reactors since they do not need peripheral equipment such as evaporators and condensers.

Trickle beds share the same advantages that packed beds have, namely no problem of catalyst separation; possibility of reactivation in situ; continuous operation; a good approximation to plug flow. It is also fair to mention that they have their unique problems.

A substantial problem is liquid channelling. The liquid phase moving through the fixed bed, after some distance, may begin to channel or flow along the reactor wall. Moreover, within the bed itself, liquid tends to flow as rivulets, leading to a partially

wetted bed and, in case of volatile liquids, may cause some undesired gas phase reactions to occur on the dry catalyst pellets. In the literature it is reported that only a small outer portion of the catalyst pellets can be utilized under trickle bed conditions with a relatively fast reaction, causing a low catalyst effectiveness factor (Satterfield, 1969). Higher effectiveness factors can be achieved by use of small pellets, down to 1 mm, but such small pellets may cause an excessive pressure drop in the reactor, which may be expensive to handle.

Liquid lenses exist between the catalyst pellets in trickle beds and may constitute an undesired feature. The liquid in some of these lenses may be replaced by the trickling-down liquid phase continuously, but some of them may have only poor liquid exchange causing a broad RTD distribution of the liquid, especially tailing. Mass transfer is also affected by these lenses depending on flow rate (Satterfield, 1975).

A possible alternative to a trickle bed reactor is the slurry reactor. In a slurry reactor, a slurry of fine catalyst particles and reactant liquid is agitated by a stirrer or by bubbling through reactant gas from a gas distributor at the bottom of the reactor. They can be operated either as batch reactors or as CSTR's. Many times it is found that removal of catalyst from the slurry reactor or product stream may require a substantial amount of equipment and investment. Other advantages or disadvantages can be stated briefly as (Satterfield, 1975);

Advantages

1. A high heat capacity to provide good temperature control

2. A potentially high rate of reaction per unit volume of reactor if catalyst is highly active.
3. Easy heat recovery
4. Adaptability to either batch or flow processing
5. The catalyst may be readily removed and replaced, especially important if its working life is relatively short.
6. They may permit operation at catalyst effectiveness factors approaching unity, of especial importance if diffusion limitations cause rapid catalyst degradation or poorer selectivity.

Disadvantages

1. The broad residence time distribution, equivalent to a CSTR. Therefore it is very difficult to get high conversion except by staging.
2. High ratio of liquid to solid in a slurry reactor allows homogeneous side-reactions to become more important, if any possible.
3. Large amounts of a flammable reacting liquid in the reactor may comprise a hazard.

In the usual trickle bed reactor the catalyst packing is pellets or extrudates typically 1/4 - 1/16" in diameter but it appears that monolith catalyst supports may have some advantages. Monolith catalyst supports now are produced on a large scale for automobile catalytic converters and are available in large quantities. As used in automobiles, a monolith catalyst support comprises in effect a block of solid containing within it an array of parallel, uniform, straight non-connecting channels. The gross void fraction is high and the solid structure might be

better visualized as a three-dimensional web whose cross-section is uniform with length. The solid itself is also porous, with pores in the size range of 1 - 10 microns. As a first step in evaluating their potential for trickle bed reactors, this study focussed on the hydrodynamics and two phase flow characteristics of these supports. Particular emphasis was on the effect of gas and liquid flow rate on pressure drop and type of flow and their flow distribution. Some of the possible advantages of monoliths for use in trickle bed reactors are;

1. Low pressure drop relative to conventional packed beds.
2. The high compressive strength may permit deep beds to be constructed without the necessity of using intermediate supports and gas-liquid redistributors, which greatly increase capital costs.
3. The "controlled channelling" that they provide may permit better contacting and better liquid distribution than that obtained in conventional trickle bed reactors, especially at low liquid flow rates.
4. The uniformity of passageways may minimize axial dispersion.
5. With liquids containing fine solids, such as those derived from liquifaction of coal, bed plugging may be minimized, or avoided.
6. The high superficial area can allow a higher effectiveness factor to be achieved under potentially diffusion-limiting conditions.

Monoliths are currently manufactured by several companies and by more than one process, so that a variety of cross-sectional

shapes, sizes and wall (web) thicknesses are or can be readily obtained. This study utilized monoliths supplied by the Corning Glass Works, which are manufactured by extrusion of a thick inorganic dough through a complicated die, followed by drying and firing of the extrudate. All the work here was done with monoliths having a square cross-section channel, nominal wall thickness of 10 mills (.254 mm) and a nominal 200 channels per square inch of cross section. As measured, our samples had a wall thickness of .27 mm. This is slightly thicker than nominal values, probably reflecting some die wear. This particular configuration is currently used in the automobile manufacturing industry. A few studies were also made with monoliths having a nominal 300 channels/in². The actual count was 360 channels/in² and measured wall thickness was .27 mm. Table 1 presents equations for superficial (outside) area per unit gross volume and void fraction for monoliths with square channels as a function of wall thickness and channel density. The derivation of these equations are given in Appendix A. In Table 1, values for representative dimensions are also given. For comparison the area/volume ratio and representative values are given for packing of spheres (McGeary, 1961). In general monoliths have substantially higher void fraction and higher surface/volume ratio than conventional reactor catalyst packing. Although 1/16" or 1/32" pellets are comparable to monoliths on an area/volume basis and can be used commercially, they will cause a high pressure drop. In Figure 1 effectiveness factors for spheres and monoliths are given as a function of the Thiele modulus (Satterfield, 1971). Here monolith webs are treated as flat plates

of the same thickness as the web, exposed from both sides. The effectiveness factor as used here is defined as the ratio of actual reaction rate to that which would occur if all of the surface throughout the inside of the catalyst were exposed to reactant of the same concentration and temperature as that existing at the outside surface of the particle. The definitions of the Thiele modulus are given in the Table 2. For comparison of spheres and flat plates, one compares ϕ_s to $3\phi_L$ as in Figure 1. The ratios of Thiele modulus for spheres to 3 times the Thiele modulus for monoliths are given in the same table. Since typical monoliths have much lower $3\phi_L$ values than ϕ_s values for typical spherical packing, they have higher effectiveness factors.

TABLE 1
COMPARISON OF SUPERFICIAL AREAS AND
VOID FRACTION FOR MONOLITHS AND SPHERES

PACKING TYPE	SPECIFICATIONS	SUPERFICIAL AREA (CM ² /CM ³)	VOID FRACTION
SPHERICAL	d = DIAMETER (CM)	$\frac{3.75}{d}$	0.375*
MONOLITH WITH SQUARE HOLES	a = WALL THICKNESS (CM) M = $\frac{\text{HOLES}}{\text{UNIT AREA}}$ $\frac{1}{(\text{CM}^2)}$	$4\sqrt{M(1-2a\sqrt{M})}$	$(1-2a\sqrt{M})$

CALCULATED VALUES FOR MONOLITHS AND SPHERES

	200 CELLS/IN ²		360 CELLS/IN ²	1/4"	1/8"	1/16"	1/32"	
	a=.0270 cm	a=.054 cm	a=.027 cm	Dia.	Dia.	Dia.	Dia.	
AREA SUPERFI.	18.625	14.68	23.08	5.91	11.81	23.61	47.24	cm ² /cm ³
VOID FRACTION	.70	.43	.60	.375	.375	.375	.375	

* McGreary (1961)

TABLE 2

THIELE MODULUS FOR FIRST ORDER REACTIONS

$$\text{MONOLITHS} \quad \phi_L = \frac{a}{2} \sqrt{\frac{k_v}{D_{\text{eff}}}}$$

$$\text{SPHERES} \quad \phi_S = R \sqrt{\frac{k_v}{D_{\text{eff}}}}$$

RATIO OF THIELE MODULUS FOR SPHERES
AND MONOLITHS ($\phi_S/3\phi_L$)

Monolith with a =	Spheres with Diameter of			
	2R = 1/4"	2R = 1/8"	2R = 1/16"	2R = 1/32"
a = 0.027cm	7.84	3.92	1.96	.98
a = 0.054cm	3.92	1.96	.98	.49

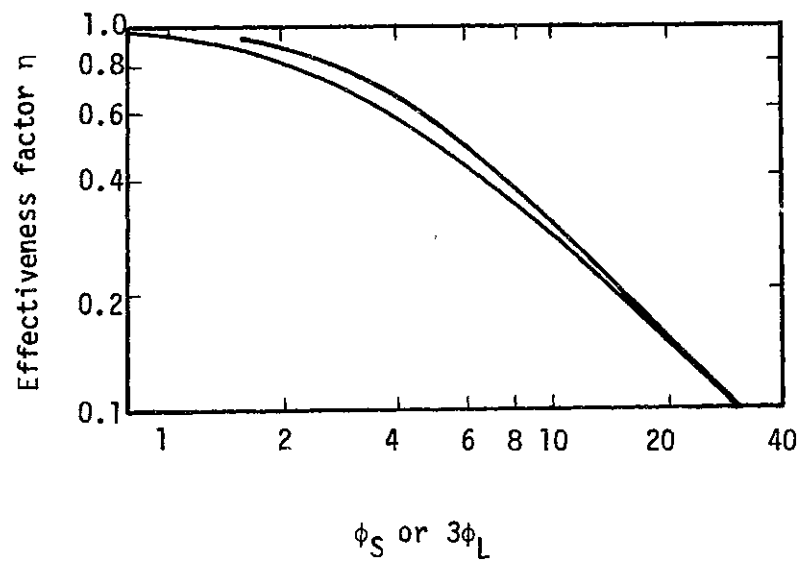


FIGURE 1. EFFECTIVENESS FACTOR WITH FIRST ORDER KINETICS

3 - OBJECTIVES

For use in a trickle bed we visualize the sections of monolith being stacked side by side, one layer on top of another. It would probably be very difficult for the array of parallel passageways to be exactly aligned from one layer to the next, so some degree of restriction will exist between layers. The first step in evaluating the potential of these supports for trickle bed reactors is to study the hydrodynamic and two-phase flow characteristics in these supports with particular emphasis on determining the effect of gas and liquid flow rate on the type of flow encountered and the corresponding pressure drop. Studies were made here with single capillaries representative of the individual passageways to be found in monolith catalyst supports and with industrially manufactured monoliths as such. Some questions of concern are as follows.

- A. Under what combinations of gas and liquid flow rates do the liquid and gas move down the walls of the tube in parallel as opposed to the liquid moving in slug flow? The flow pattern will significantly affect the pressure drop encountered.
- B. How is the pressure drop affected by such physical properties of the liquids as viscosity and surface tension? To answer this some experiments were conducted with hydrocarbons and air as well as water and air.
- C. How does the pressure drop through a monolith structure vary with the evenness of distribution of liquid over the structure?

- D. What is the effect of the passageway dimensions?
- E. What other variables affect the pressure drop?

4 - BACKGROUND AND REVIEW OF RELATED STUDIES

Two phase flow through the narrow passageways of monolith catalyst supports is essentially vertical two phase capillary flow. Two phase capillary flow has been used for measuring the flow rates of a liquid flowing through capillary tubes by injecting an air bubble into the stream and then measuring the travel velocity of the air-bubble. Hence Fairbrother et al. 1935, suggested that the air bubble velocity may not be an index of liquid flow rate, since a liquid film exists between a cylindrical air bubble and the tube wall and therefore the liquid is dragged behind the gas. Taylor (1961) and others have showed experimentally this is so. All these studies were made in horizontal round tubes with very low ratios of air flow to liquid flow but no pressure drop measurements were made. Suo and Griffith (1964) experimentally measured the liquid film thickness between tube wall and cylindrical air bubble and pressure drop for slug flow in horizontal round tubes.

Blood flow in capillary veins has some similarities with the two phase flow of interest here. Red blood cells move like plugs with a plasma film between cell membrane and vein walls as illustrated in Figure 2. Different mathematical models have been set up by many researchers (Fitz-Gerald, 1969, Lew and Fung, 1970, Aroestry and Gross, 1970, etc.) to represent this phenomenon. All these models assume that the cell membrane is not elastic enough to permit continuity of shear stress and velocity profile. In other words the cell membrane behaves like a solid surface in terms of shear stress and velocity profile. Under these assumptions

4 - BACKGROUND AND REVIEW OF RELATED STUDIES

Two phase flow through the narrow passageways of monolith catalyst supports is essentially vertical two phase capillary flow. Two phase capillary flow has been used for measuring the flow rates of a liquid flowing through capillary tubes by injecting an air bubble into the stream and then measuring the travel velocity of the air-bubble. Hence Fairbrother et al. 1935, suggested that the air bubble velocity may not be an index of liquid flow rate, since a liquid film exists between a cylindrical air bubble and the tube wall and therefore the liquid is dragged behind the gas. Taylor (1961) and others have showed experimentally this is so. All these studies were made in horizontal round tubes with very low ratios of air flow to liquid flow but no pressure drop measurements were made. Suo and Griffith (1964) experimentally measured the liquid film thickness between tube wall and cylindrical air bubble and pressure drop for slug flow in horizontal round tubes.

Blood flow in capillary veins has some similarities with the two phase flow of interest here. Red blood cells move like plugs with a plasma film between cell membrane and vein walls as illustrated in Figure 2. Different mathematical models have been set up by many researchers (Fitz-Gerald, 1969, Lew and Fung, 1970, Aroestry and Gross, 1970, etc.) to represent this phenomenon. ~~All these models assume that the cell membrane is not elastic~~ enough to permit continuity of shear stress and velocity profile. In other words the cell membrane behaves like a solid surface in terms of shear stress and velocity profile. Under these assumptions

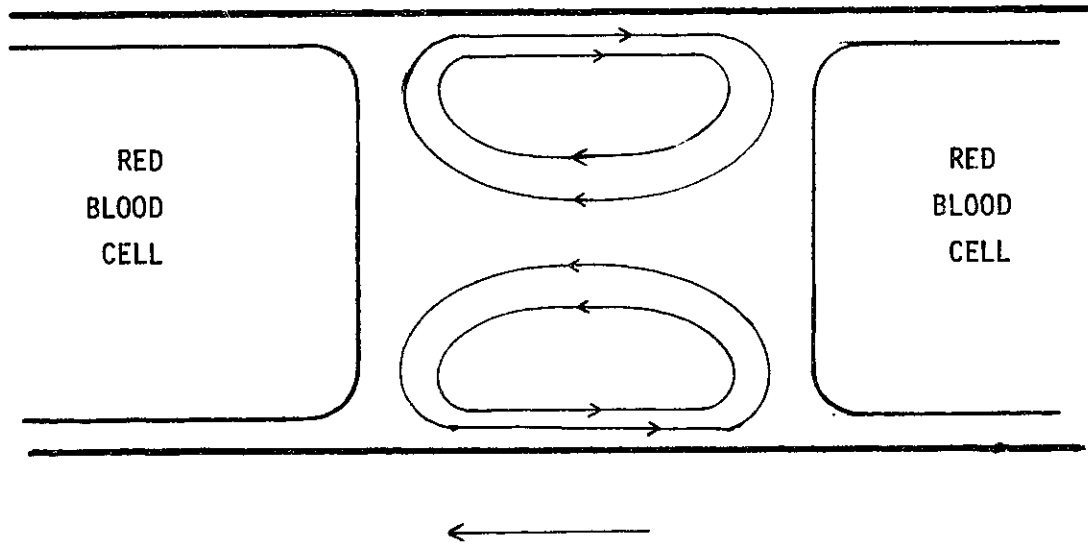


FIGURE 2. BOLUS FLOW

they were able to calculate velocity profiles in the plasma slugs and the pressure drop required to force red blood cells through the capillary veins. In plasma slug a flow pattern called bolus flow exists, Figure 2. This pattern or circulation increases the transport of macromolecules, but does not facilitate the transport of O_2 since Reynolds numbers are around 10^{-2} and the Peclet Number is less than 10 in blood veins (Fitz-Gerald, 1972, Aroesty and Gross, 1970).

Levich, 1962, gives boundary conditions at the gas bubble and liquid surfaces for shear stress and velocities. On the bubble surface the tangential velocity and shear stress is continuous across the surface. Obviously normal velocities should be zero at both sides of the bubble surface.

All these studies are indirectly related to our specific purpose, though most of them have a different physical system such as blood flow, or their physics and experimental conditions are quite different than ours, like the Suo and Griffith study for horizontal slug flow in round capillaries. Since a static head term did not exist in their studies, one of the very important factors in our problem does not exist in their study.

In the field of two phase vertical slug flow a tremendous amount of research has been done, although, almost all of it is for cocurrent upflow, and it is concerned with tubes larger than about 1/4" i-d. The liquid film between bubble and the tube wall is much thicker than in capillary flow and therefore the effect of gravity is very important on this film. Most of the researchers report that there is a down flow of liquid in the film due to

gravity even for the cocurrent up flow system. Gas bubbles are usually shorter and bullet shaped rather than cylindrical. These studies were done with round tubes and with particular application to nuclear reactor cooling. In spite of the large amount of research in this field it is interesting that the experimental data are still not completely consistent and a conclusive correlation for pressure drop has not yet been established. Available correlations are based on the semi-empirical Martinelli-Lockhard correlation (1949) which is derived for horizontal non-slug flow. It assumes that two phase pressure drop is only a function of single phase pressure drop for gas and liquid phases. The single phase pressure drops are calculated as if gas or liquid were flowing alone in the tube with its superficial velocity based on tube cross-section.

This approach has been taken by many researchers as a basis to correlate types of two phase flow that the original correlation was not intended for, such as slug flow, vertical flow, etc. Though its accuracy is very low (at best $\pm 60\%$) it is easy to use and has an apparent generality.

5 - EXPERIMENTAL STUDIES

5-1

Single Capillary Studies

This apparatus was designed primarily to study the flow regimes and pressure drop occurring under controlled introduction of a liquid phase into an individual capillary tube. This was managed by use of a specially designed column head, details of which are shown in Figure 3. The column head was machined from a 2" long 1 1/2" diameter Plexiglas rod. In preliminary work it was found that due to stresses created in the Plexiglas rod during its extrusion and machining, an hour or so following the machining the rod literally shattered into pieces. These stresses were relieved by first heating the Plexiglas rod at 250°F for more than 10 hours and then machining it. This procedure effectively prevented the self-shattering of the rod.

The column head was machined to contain a series of differently shaped interconnecting passageways. The first one was a cylinder of 1.5 cm i.d. and 4 cm in height, and was connected to the lower conical piece. The conical passageway was 1.5 cm i.d. on top, .200914 cm i.d. on the bottom and 2.3 cm long. The cylindrical piece at the bottom of the column head had the same i.d. as the o.d. of the capillary tube. In other words the capillary tube fitted snugly into this cylindrical cavity and was sealed into it. The cylindrical cavity at the top of the column head was tapped from both sides for the gas inlet and for a pressure tap. The opening at the top of the column head was fitted with a screwed-in plug which itself had a hole in its center into which a hypodermic needle

or a small nozzle could be fitted.

To introduce liquid into the capillary as an annular film a hypodermic needle was used to inject the liquid phase onto the conical surface of the column head. The liquid phase spread over the surface and covered it with a liquid film which entered the capillary as an annular film. This is termed distributor A, Figure 3.

For dropwise liquid introduction, a small nozzle was used. The liquid drops formed at the tip of the nozzle and fell onto the entrance of the capillary tube, forming liquid slugs immediately. The volume of each liquid drop was found to be independent of liquid flow rate and amounted to $.037 \text{ cm}^3$. This system is termed distributor B, Figure 4.

Prefiltered high pressure air (80 psig) from a compressor was depressurized to 10 psig by pressure regulators, then it was filtered again through a 7μ stainless steel in-line filter. Any oil retained in the air was washed out by sulfuric acid in a glass bead packed column. The sulfuric acid entrained by air was trapped in a bed of KOH beads. Oil-free air then was refiltered and sent to the flow rate control section. Air flow rates were controlled by needle valves and were measured by flow meters.

The liquid phase was distilled water and was recirculated through a glass tank, Figure 5. A trace amount of CuSO_4 was added to the water to prevent algae growth. Needle valves used to control the water flow rate were capable of flow rates down to 2 cc/day, so accurate and stable water flow rates could be obtained. For water circulation a stainless steel magnetically driven gear

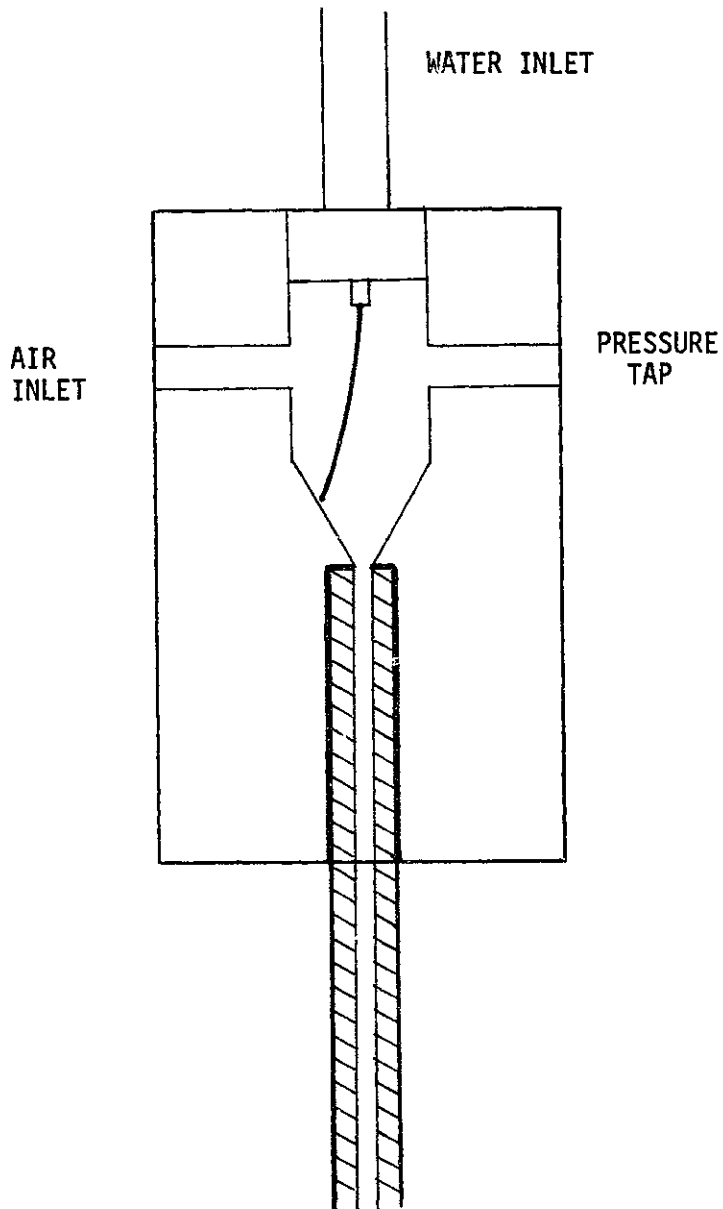


FIGURE 3. DISTRIBUTOR A

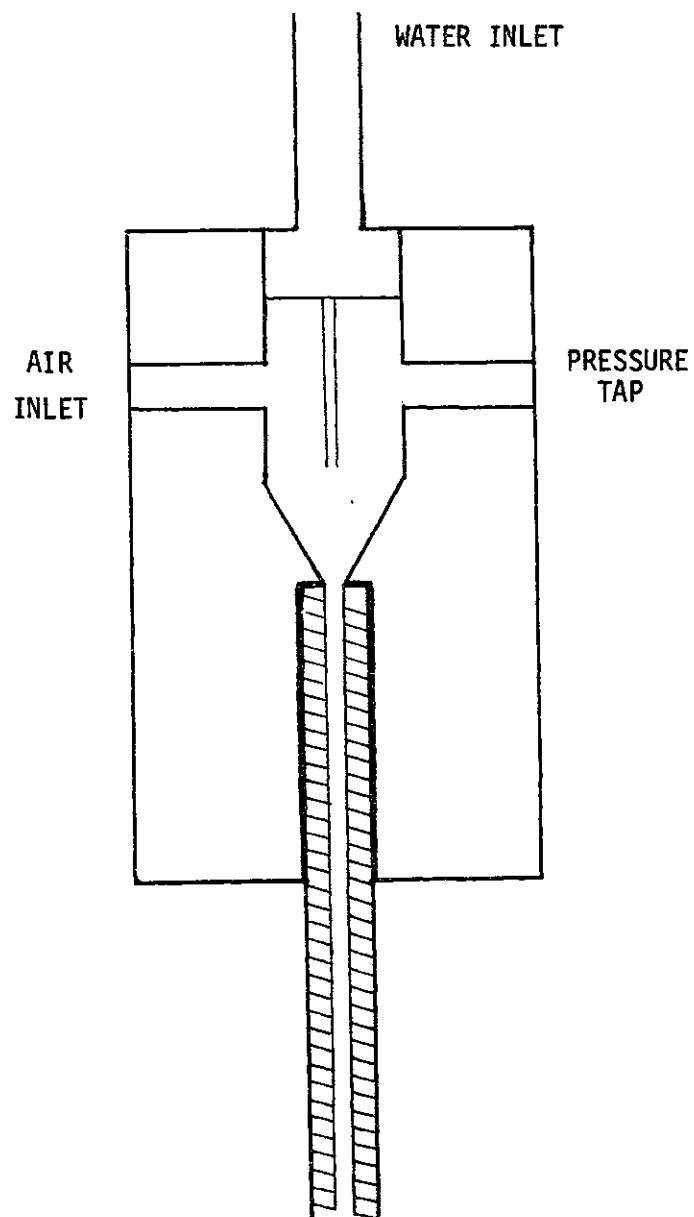


FIGURE 4. DISTRIBUTOR B

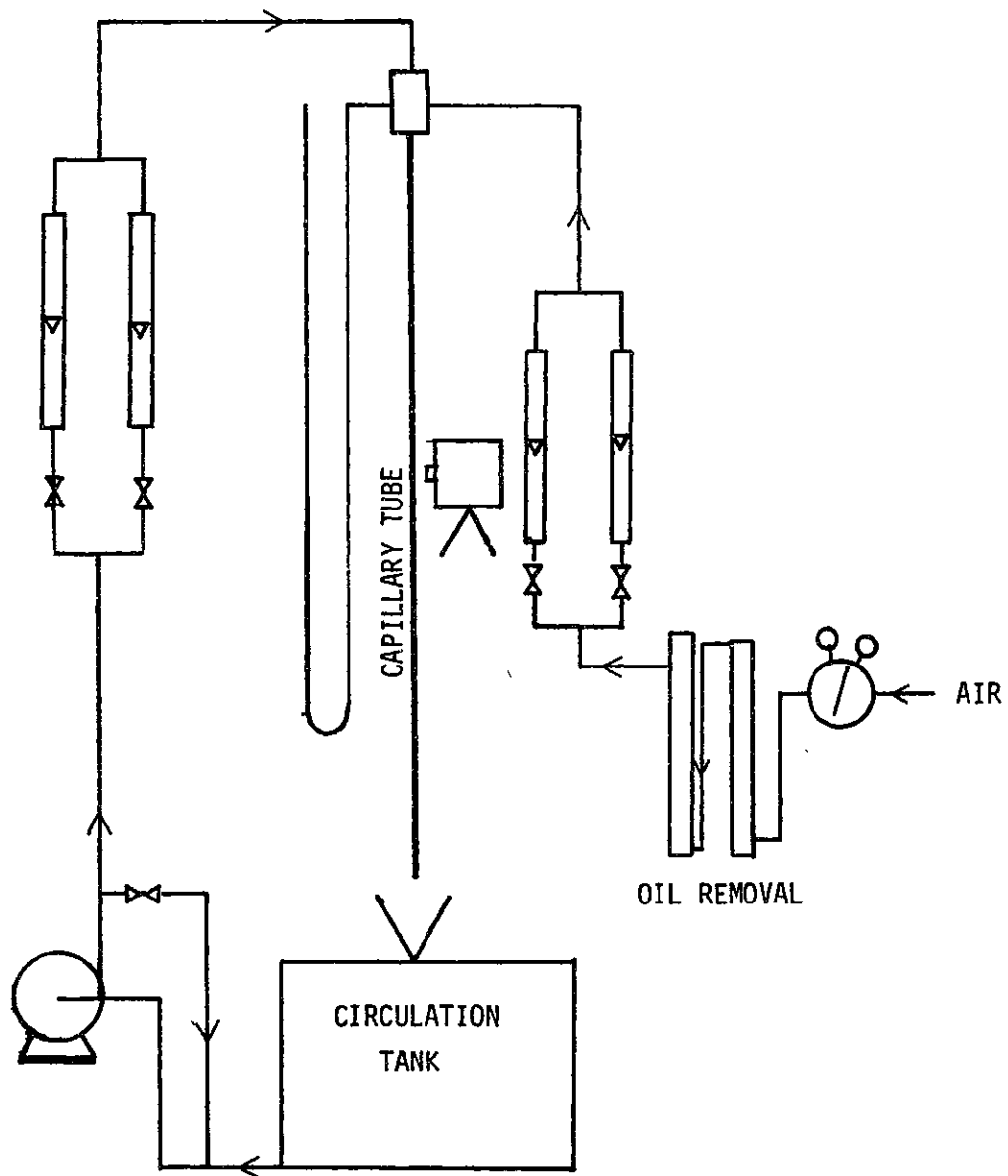


FIGURE 5. FLOW CIRCUIT FOR CAPILLARY STUDIES

pump was used. These precautions were required since the flow meters used to measure water flow rates were so precision made that any piece of rust or solid material deposited on the flow meter float would prevent its free moving. Some of the water pumped by the gear pump was directly sent back to the recirculation tank to be able to obtain different liquid flow rates. Water coming from the flow meters was sent to the top of the column head. The capillary tube attached to the bottom of the column head was supplied by Wilmad Glass Co., Buena, N.J. and was 102 cm long precision bore with a i.d. of $.0200914 \pm .000254$ cm. This size capillary was chosen as a near approximation to the hydraulic diameter of the individual channels in 200 cells/in² monoliths with which studies could be made at flow rates measurable with available rotameters. Pressure drop measurements were taken between the pressure tap at the column head and atmospheric pressure by an inclined monometer.

For studying flow regimes a high speed camera was placed adjacent to the mid section of the capillary tube and Kodak high speed Tri-X film was used.

5-2

Monolith Columns

Monolith columns used in these experiments were built by two different methods. The first method was adequate for use with water but not for organic solvents due to the sealant used. The second method used was more practical and columns built by it were solvent proof. Data were taken with columns built by both methods.

In the first method, monolith blocks either 6" or 3" in length and 1" in diameter were placed on top of each other. The arrangement was random, i.e., no attempt at alignment of passageways from one block to the next was made. 1 in. wide glass cloths were cut into 4" lengths and dipped into rubber cement. These glue-covered pieces of glass cloth were wrapped around the monolith blocks at the joints, holding the blocks together. The peripheral surface of the monolith column was then covered with this rubber cement by painting it on. After letting it dry, the outside surface of the column was covered by G.E. 108 silicone rubber. The column head and liquid distributor were placed on the column as explained later. Since both rubber cement and silicone rubber were affected by organic solvent, columns built by this method could not be used with organic solvents.

In the second method, monolith blocks 1 in. in diameter were randomly force-fitted on top of each other in a 1" i.d. Teflon tube. Teflon has a much higher temperature expansion coefficient than do the monoliths, so the Teflon was expanded at elevated temperature, the blocks were inserted and held tightly in place on cooling.

An 8 ft long and 2 1/2" i.d. oven was built to house and heat 6" long, 1" i.d., 1 1/4" o.d. Teflon tubes. The temperature inside the oven was controlled by electronic temperature controllers to about 250 °C. After the monolith and Teflon tube reached a steady temperature the monolith blocks were slid into the Teflon tube from one end. After all the monolith blocks were placed in the Teflon tube, they were pushed inwards from both ends to insure that no empty space was left between them. Then the oven was

immediately cooled to room temperature by blowing air into the oven to prevent Teflon recrystallization.

The monolith blocks used in this study were core drilled. Because of this, monolith passageways on the 1" diameter circle were cut through by the saw, leaving pieces of the passageways at the circumference. In other words, walls of the web extended beyond the main structure (Figure 6). These partial passageways were filled in the first method of column building by application of rubber cement to the periphery but remained open in the second. Therefore the effective cross sectional area of the column was smaller than a 1" diameter circular area in the first method due to blockage of these outer passageways. Consequently the actual superficial and interstitial velocities of the liquid and the gas are slightly higher than in the case of an exact 1" diameter circle. This effect has been considered in our calculations of flow rates in this type of column. In the columns built by the second method, either these partial passageways become smaller-area passageways due to Teflon tube coverage of their open side or they may become an empty space created between the chordial web and Teflon tube due to broken extended webs. These two artifacts may cause some flow complications but their effects act in opposite directions so as to tend to cancel each other out.

Three different types of liquid and gas distributors were used. The first type was simply a shower head fitted into a Plexiglas tubing (Figure 7). A 4" long Plexiglas with 1 1/4" i.d. was fitted with a Teflon shower head at the top and an O-ring was placed between shower head and Plexiglas tubing to prevent gas

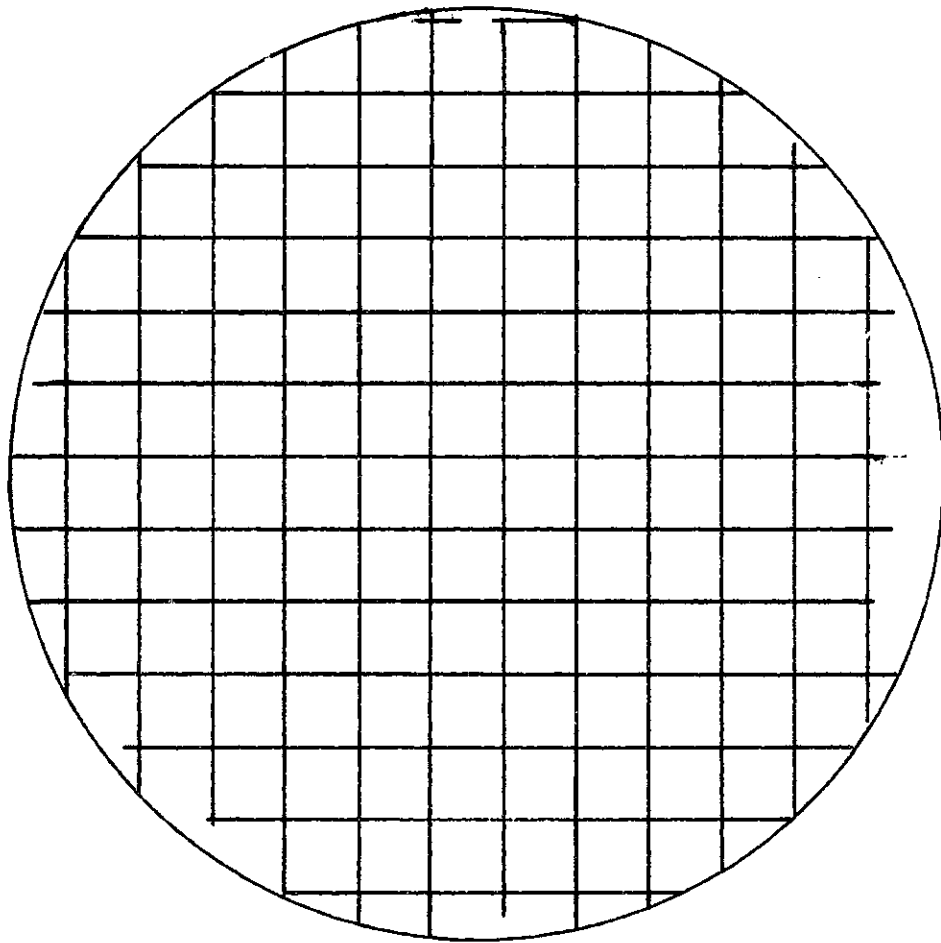


FIGURE 6. CROSS-SECTION OF THE MONOLITH COLUMN

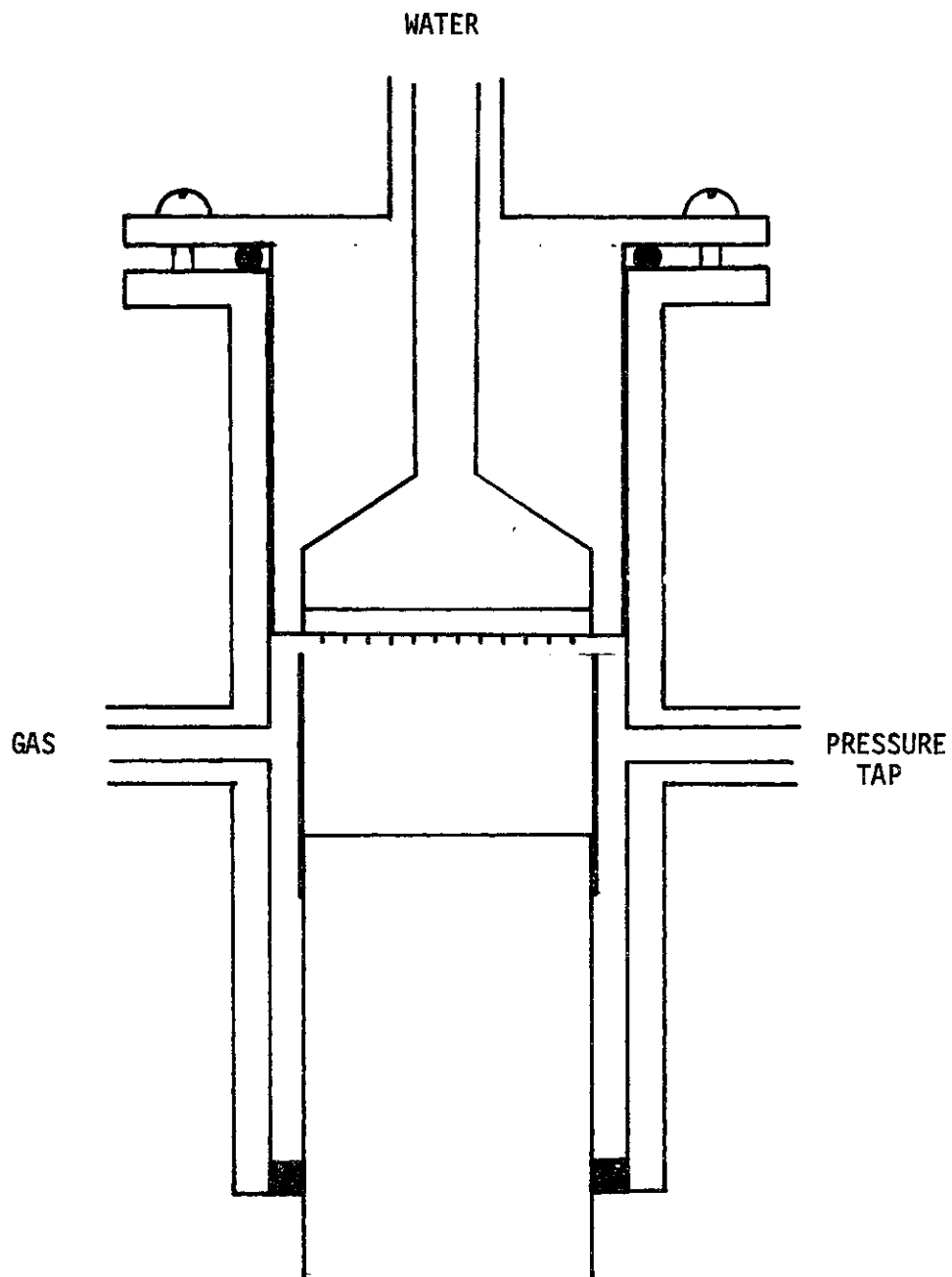


FIGURE 7. DISTRIBUTOR 1

leaks. These two were held together by a set of 4 screws and bolts. The shower head had 37 small Teflon tubes for dripping the liquid down in a 1" diameter circle. Here 37 small tubes were used instead of 37 holes on the shower plate to prevent liquid spreading on shower plate by creating liquid drops on the tip of small tubes.

A 1 in. plastic shield was placed around the upper half of the monolith column to protect liquid predistribution from interference from the incoming gas. The incoming gas moved upward in the annular space between the Plexiglas tubing and this plastic shield, then entered into the empty space over the monolith column through the circular opening between plastic shield and Teflon shower head. The space between the lower end of the Plexiglas tubing and the monolith column was sealed with G.E. 108 silicone sealant. The pressure tap was placed opposite to the gas inlet on the Plexiglas tubing.

In the second type of liquid distributor, the plastic shield height was increased to 1 1/2" and the first one inch of it was filled with 4 mm glass beads as prepacking, Figure 8. These two types of liquid distributor were used only with columns built with the first method. The third type of liquid distributor differed from the first two by its prepacking. After the monolith blocks were placed in the Teflon tubing, the part of the Teflon tubing corresponding to the top of the monolith blocks was heated and 27 pieces of 1/16" - 1/8" thick monolith slices were placed on top (Figure 9). A 1/16" o.d. stainless steel tubing was placed between the first monolith slice and blocks as a pressure tap.

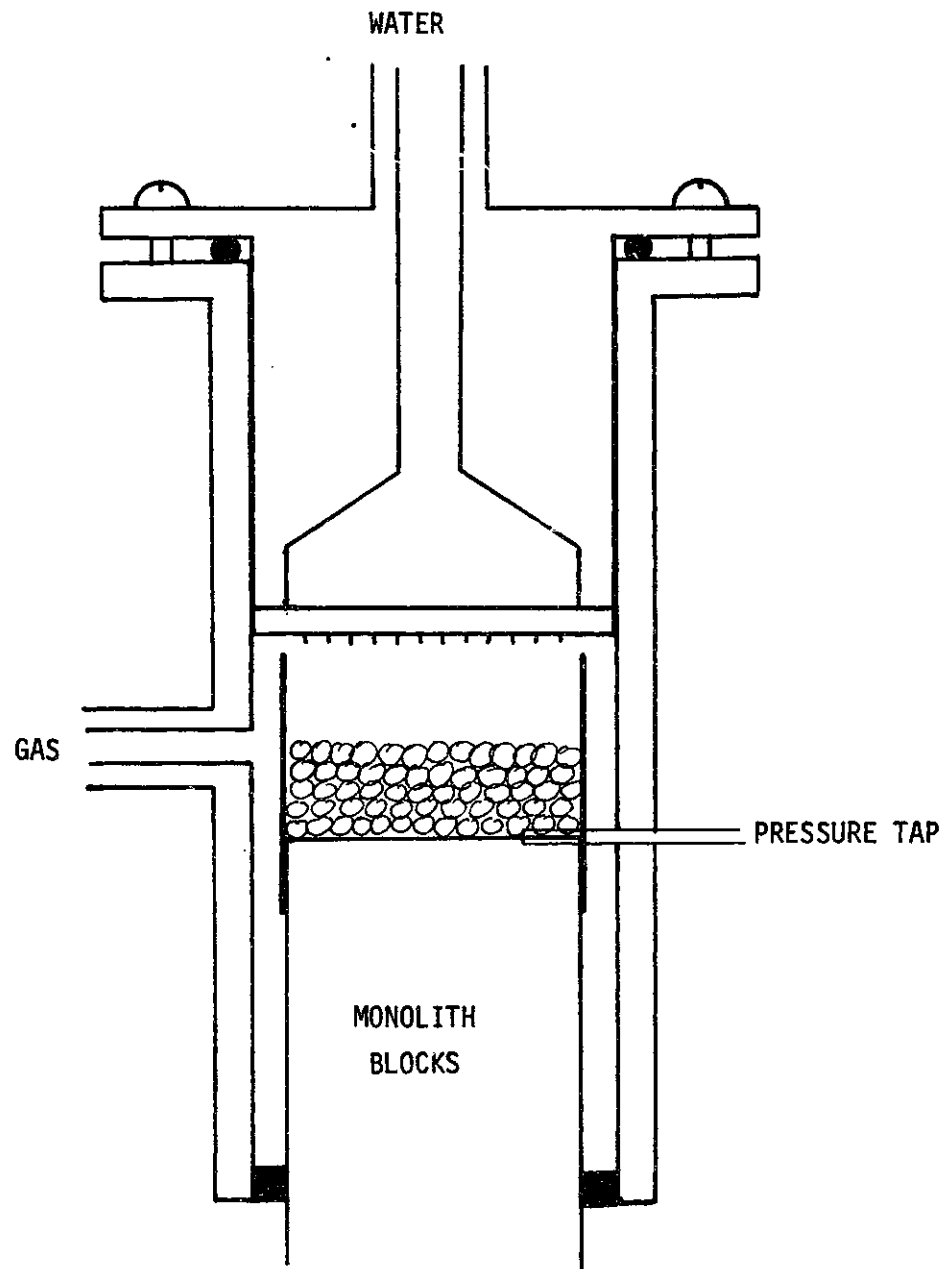


FIGURE 8. DISTRIBUTOR 2

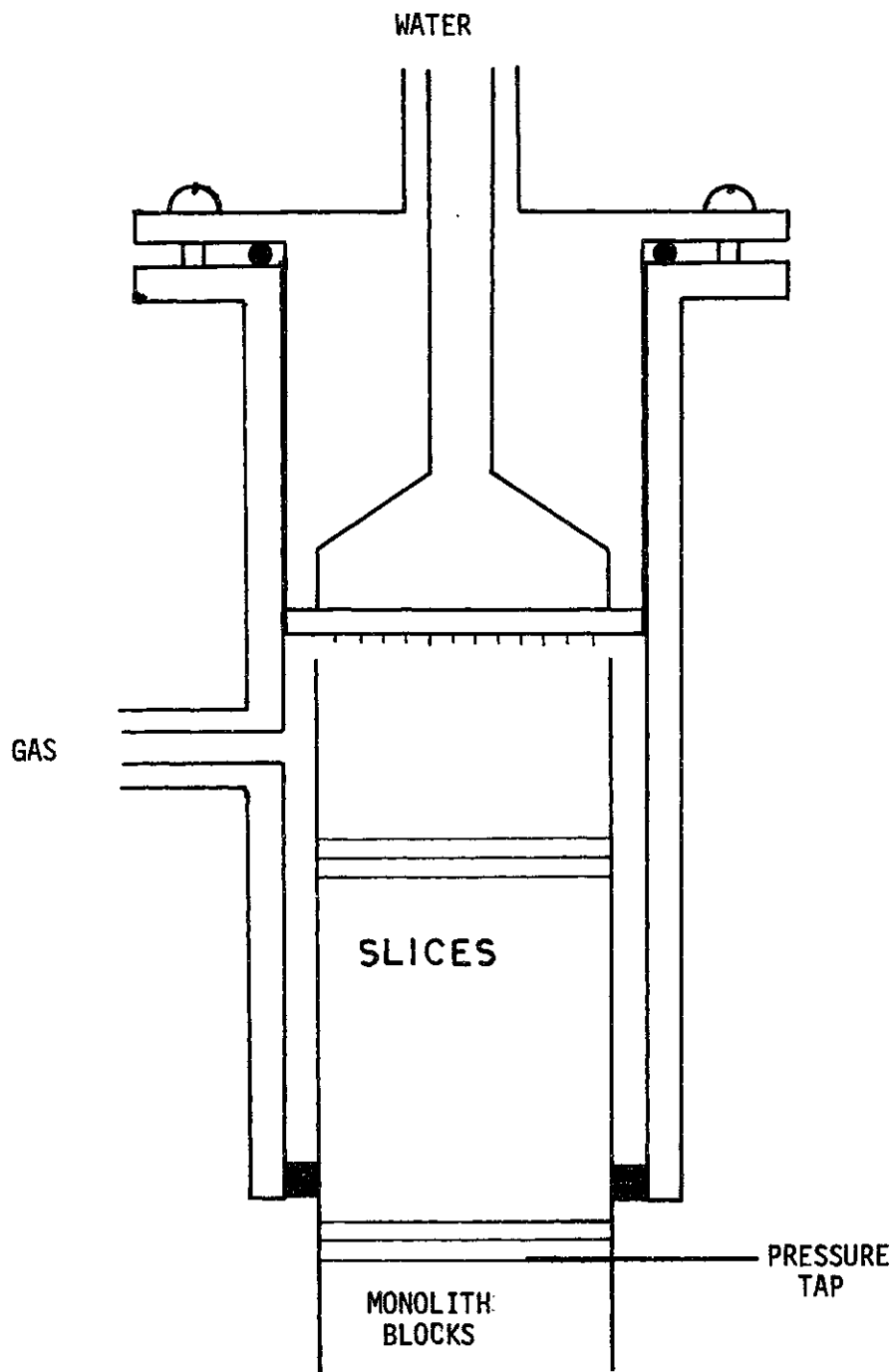


FIGURE 9. DISTRIBUTOR 3

Here the annular space between Teflon column and Plexiglas (1 3/8" i.d.) column head was sealed with a specially cut rubber stopper.

5-3

Flow Circuits

Different flow circuits were used for water and for cyclohexane. That for water is shown in Figure 10. Water from the Cambridge City Water system was passed through a synthetic spool filter, then through a 15 μ stainless steel in-line filter. Filtered water was pressure regulated by a liquid pressure regulator. Liquid flow rates were controlled by needle valves and measured by a rotameter.

Pressurized filtered air from the compressor was depressurized to 10 psig by gas pressure regulators; its flow rate was regulated by needle valves and measured by a rotameter. Water coming from the bottom of the column was dumped into the drain and air was released to the atmosphere. The pressure drop was measured between the pressure tap on the column head and the atmosphere since the lower end of the column was open to the atmosphere. Another pressure probe at the bottom end of the column was installed and pressure measurements between two probes were taken. There were no measurable end effects. Therefore, pressure drop measurements were taken between atmosphere and tap probe.

For cyclohexane measurements a recirculation tank and a gear pump was installed in the system. The circuit diagram is given in Figure 11. Different liquid flow rates were obtained by recirculating cyclohexane between the inlet and outlet of the pump. Cyclohexane coming from the bottom of the column was returned to

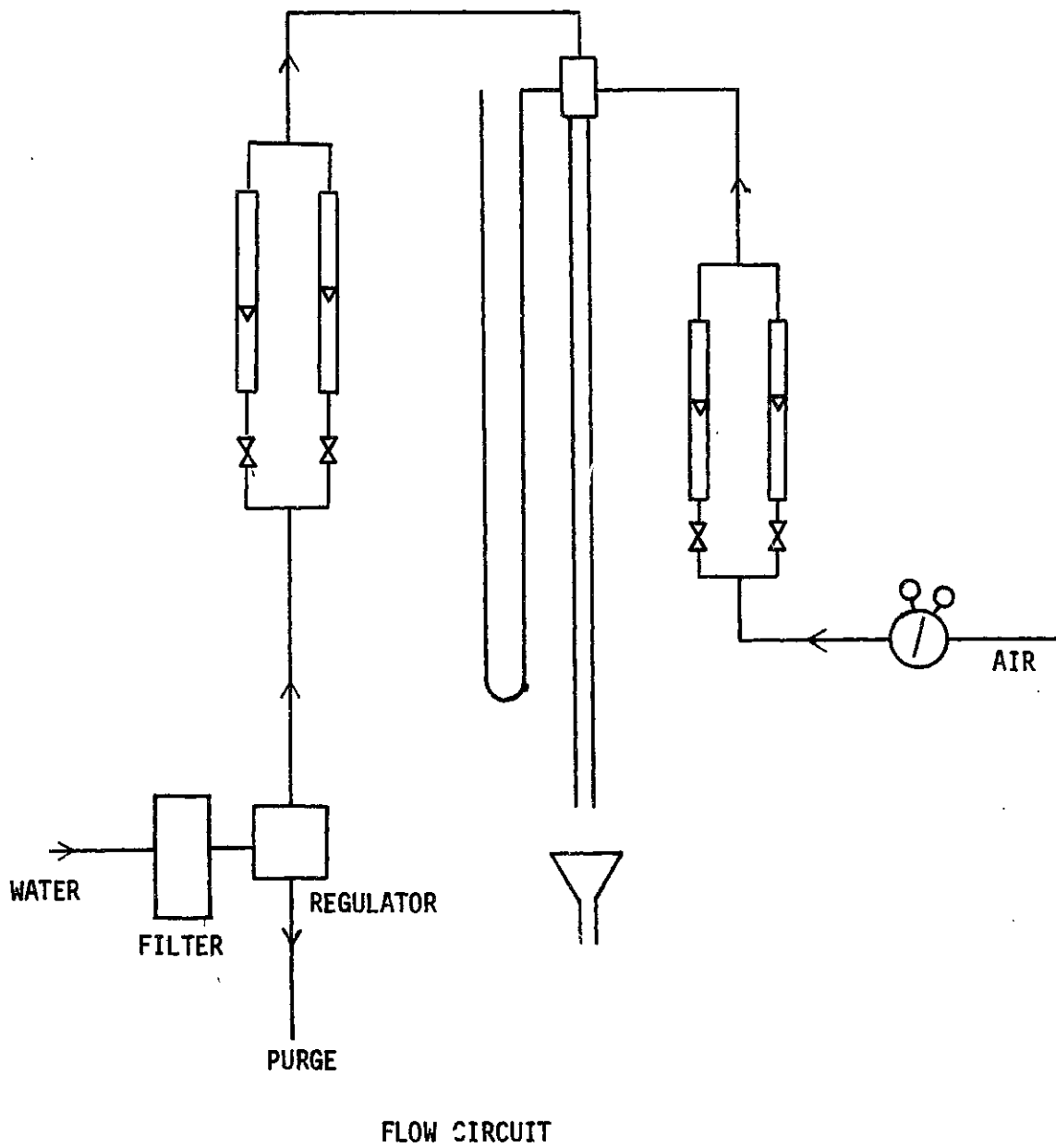


FIGURE 10. FLOW CIRCUIT FOR WATER STUDIES IN MONOLITHS

the recirculation tank. Air was released to a hood system. Measurements showed that there was no significant change in the liquid flow rate due to evaporation in the column.

6 - RESULTS AND DISCUSSION

6-I

Studies with Single Capillary Tubes

Early studies with the monoliths showed that the pressure drop could be very sensitive to the mode of distribution of liquid onto the top face of the first monolith and these effects were especially pronounced at low flow rates. Basically the pressure drop reflects in part whether the flow in individual capillaries is annular or slug-type and, in the case of monoliths, whether the type of flow is identical in parallel passageways.

In order to isolate some of these variables, studies were made with a single capillary and the nature of the flow pattern was determined as a function of liquid and gas flow rate, as shown in Figure 12. At liquid velocities above about 1.6 to 1.8 cm/s slug flow was observed, independent of gas flow rate or of the mode of distribution of liquid. At sufficiently low liquid velocities the type of flow was annular, independent of distributor nature but dependent on the gas velocity. In between is a substantial region in which the nature of the distributor dominates the flow pattern. Goldsmith et al. 1962, and Taylor, 1961 have reported that recirculation patterns that occur in liquid slugs and gas bubbles in slug-type flow are shown in Figure 13. It was not attempted to measure liquid-phase mass transfer in this study but it would be expected that circulation in the liquid slugs would increase the mass transfer in the liquid phase over that occurring at the same Reynolds number in single phase liquid flow. The same is true for the gas bubbles. These stream lines together

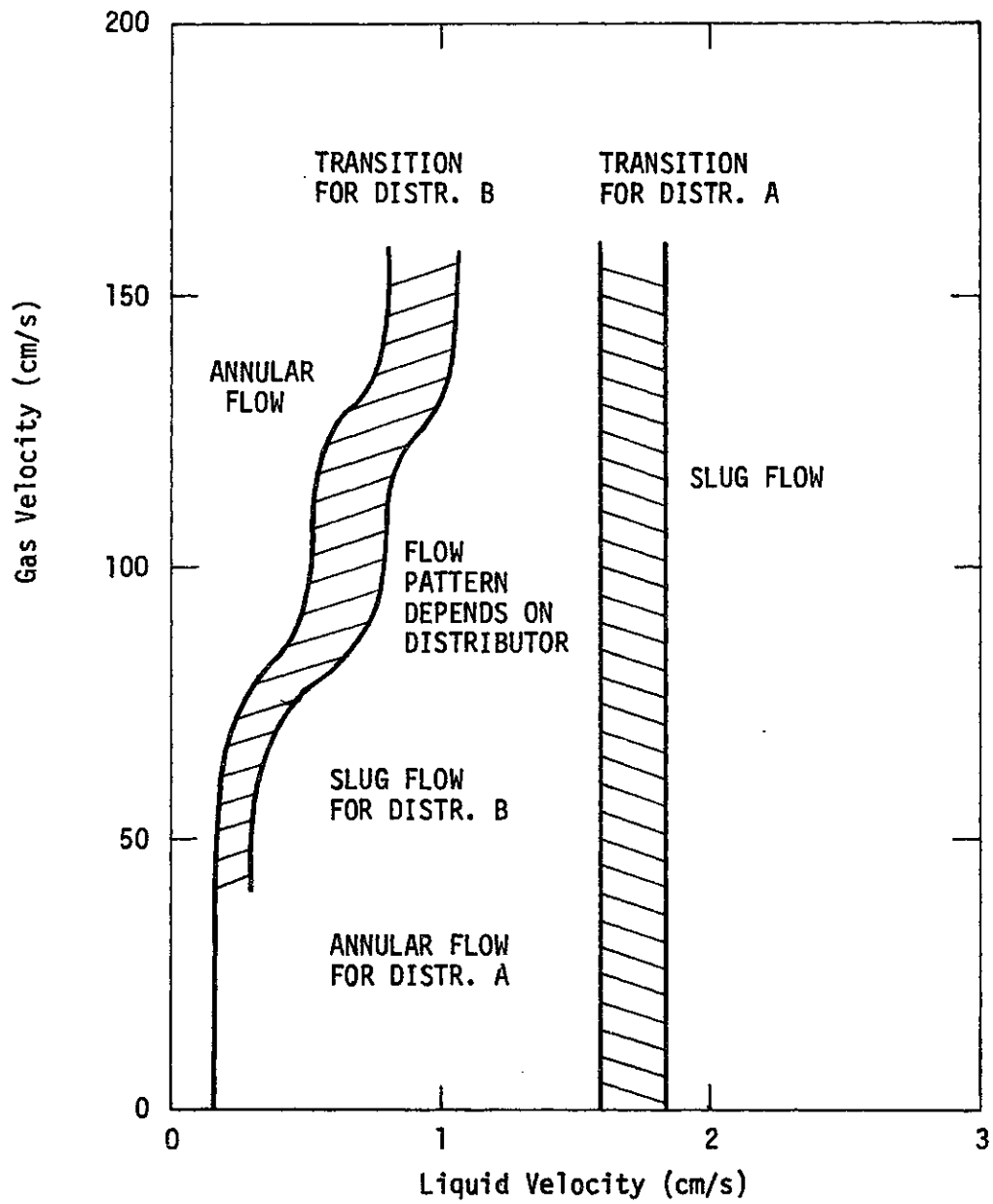


FIGURE 12. FLOW IN A SINGLE CAPILLARY —
REGIONS OF ANNULAR vs. SLUG FLOW

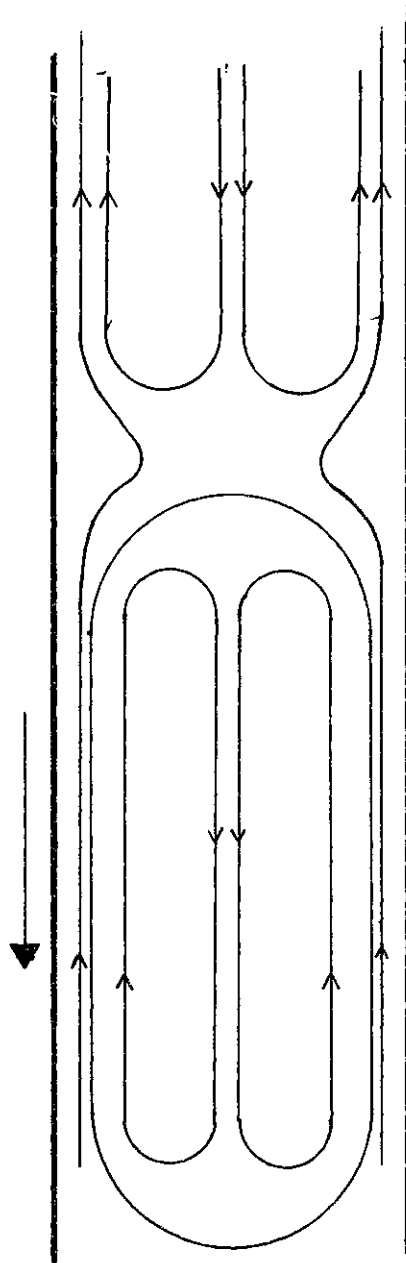


FIGURE 13. RECIRCULATION PATTERNS IN
CAPILLARY SLUG FLOW

with the blood bolus flow stream lines could be used to estimate stream lines in monolith channels.

In Figure 14 two phase pressure drop results are shown for water introduced annularly to the capillary by the liquid distributor described on page and Figure 3. Here liquid coming from the column head enters the capillary tube as an annular film. The gas phase flows down in the center. Measured pressure drop per unit length of column is plotted against liquid linear velocities at constant gas linear velocities. The pressure drop changes linearly with increasing liquid flow rates, with a decreasing slope at low gas flow rates and an increasing slope at high gas flow rates. The slight negative pressure drop at low gas and high liquid flow rates presumably means that the liquid flowing under gravity drags the gas phase along with it. At high gas flow rates the gas drags down the liquid in the liquid film.

The slug flow pattern was studied in more detail from a large series of photographs obtained under a variety of conditions. Slug flow begins to appear when the liquid phase reaches a definite flow rate, independent of the gas flow rate. As liquid flow rate is increased in the transition region, a wavy turbulence in the annular film appears. This develops into a torus in which the gas-phase hole in the center gradually shrinks, ultimately forming a liquid slug.

With drop-like introduction of the liquid phase (liquid distributor B), liquid drops formed at the tip of the nozzle and fell into the entrance of the capillary tube, forming liquid slugs immediately. The gas phase travelled as cylindrical bubbles

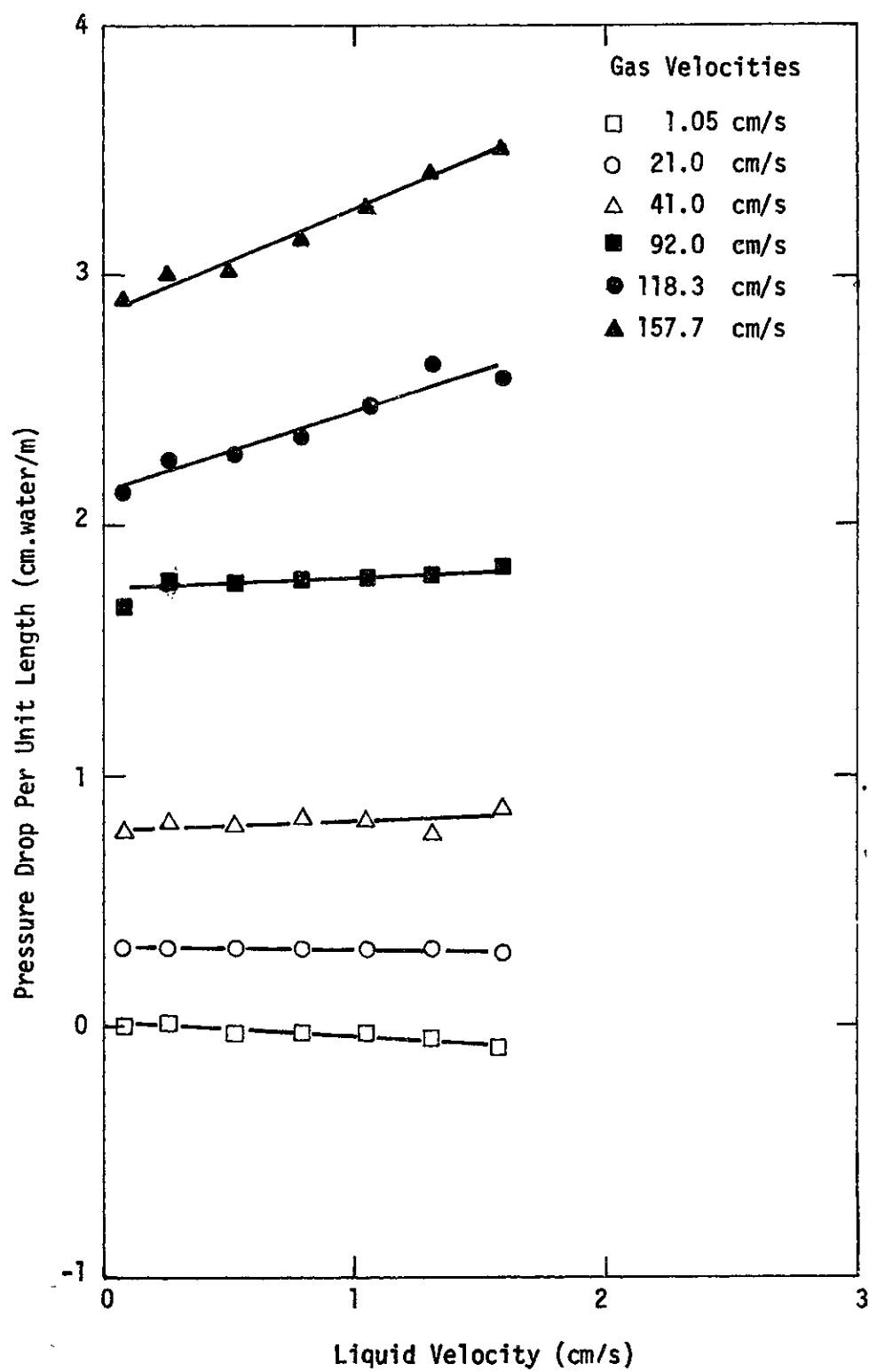


FIGURE 14. PRESSURE DROP IN A 0.200914 cm
CAPILLARY TUBE FOR ANNULAR FLOW

between the liquid slugs. However, a thin liquid film existed between the gas bubble and capillary wall and could be easily seen at low flow rates.

The pressure drop per unit length of column is plotted against the liquid flow rate at constant gas flow rate in Figure 15. The pressure drop increases non-linearly with increasing liquid flow rate. Even with moderately high gas flow rates, large negative pressure drops are observed. These two phenomena are characteristic of the slug flow. Here the static liquid head plays a relatively large role on pressure drop. Also velocity profiles and stream lines are presumably greatly different in annular flow. Pressure drops are compared for slug and annular flow at the same gas and superficial liquid flow rates in Figure 16. At low gas flow rates, slug flow gives a negative pressure drop due to the static head of liquid. But at high gas flow rates it gives higher pressure drops than annular flow. It is interesting to see that the pressure drop changes linearly with increasing gas flow rate in the annular flow regime.

At a constant low liquid flow rate in the slug regime, as gas flow rate is increased the length of the gas bubbles increases to the point that it became longer than the length of capillary tube, thus the flow pattern essentially reaches annular flow interspersed with slugs of liquid.

The ratio of the sum of the liquid slug lengths to the total length of liquid slugs and gas bubbles was experimentally determined by photographic measurements at different flow rates. In Figure 17 this ratio is plotted against the gas flow rate at constant liquid

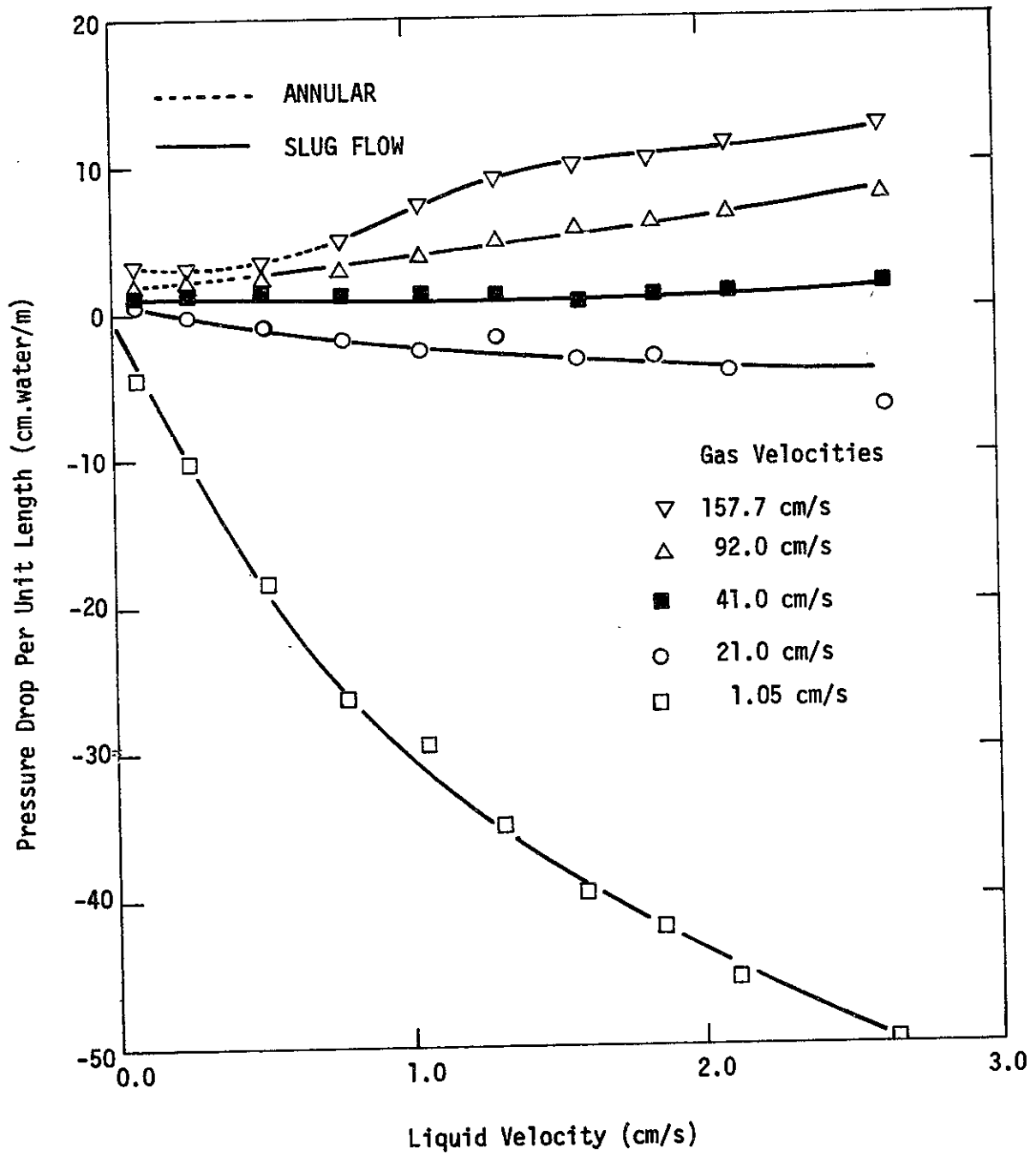


FIGURE 15. PRESSURE DROP IN A .200914 cm I.D. CAPILLARY TUBE WITH DISTRIBUTOR B.

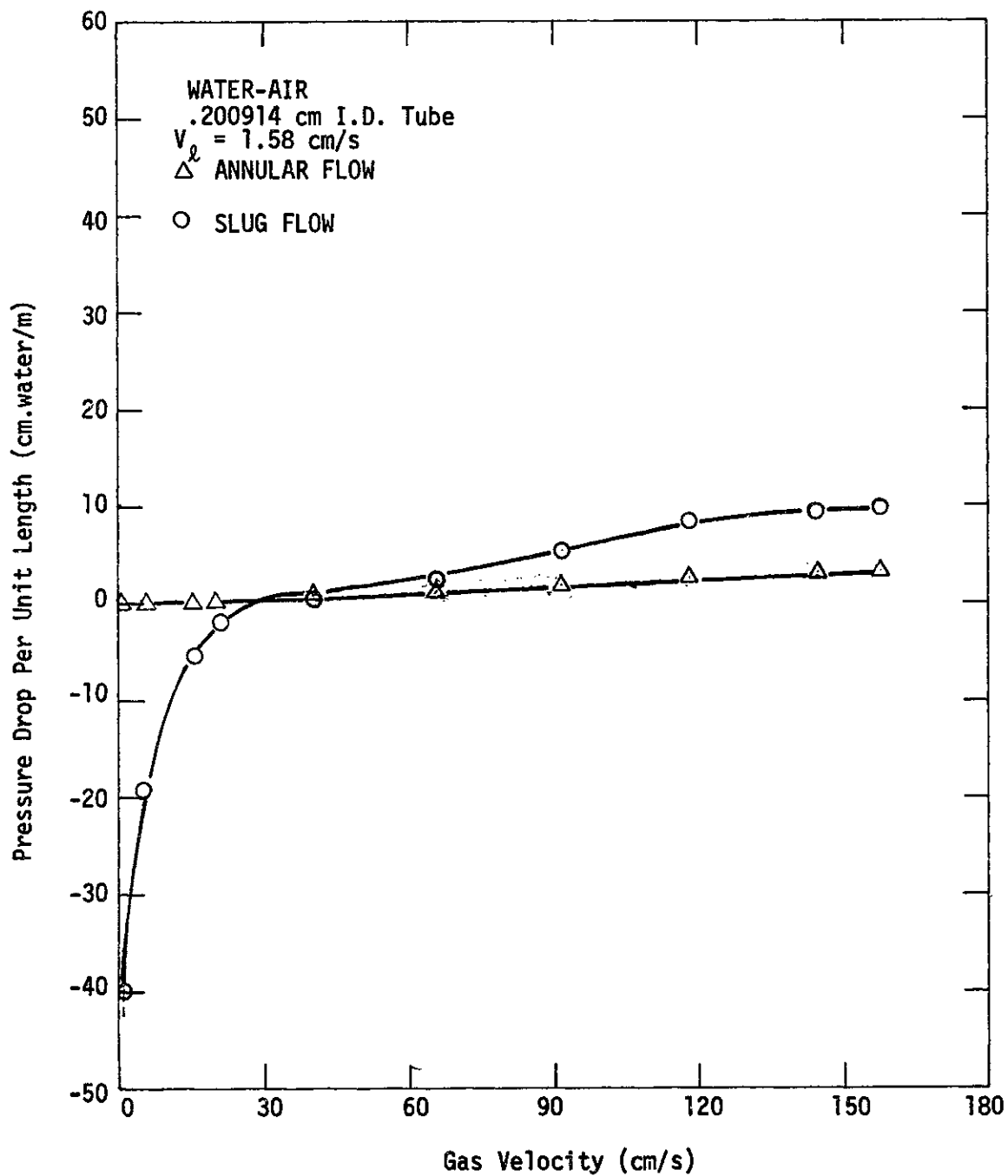


FIGURE 16. COMPARISON OF PRESSURE DROP FOR SLUG AND ANNULAR FLOW IN CAPILLARY TUBES

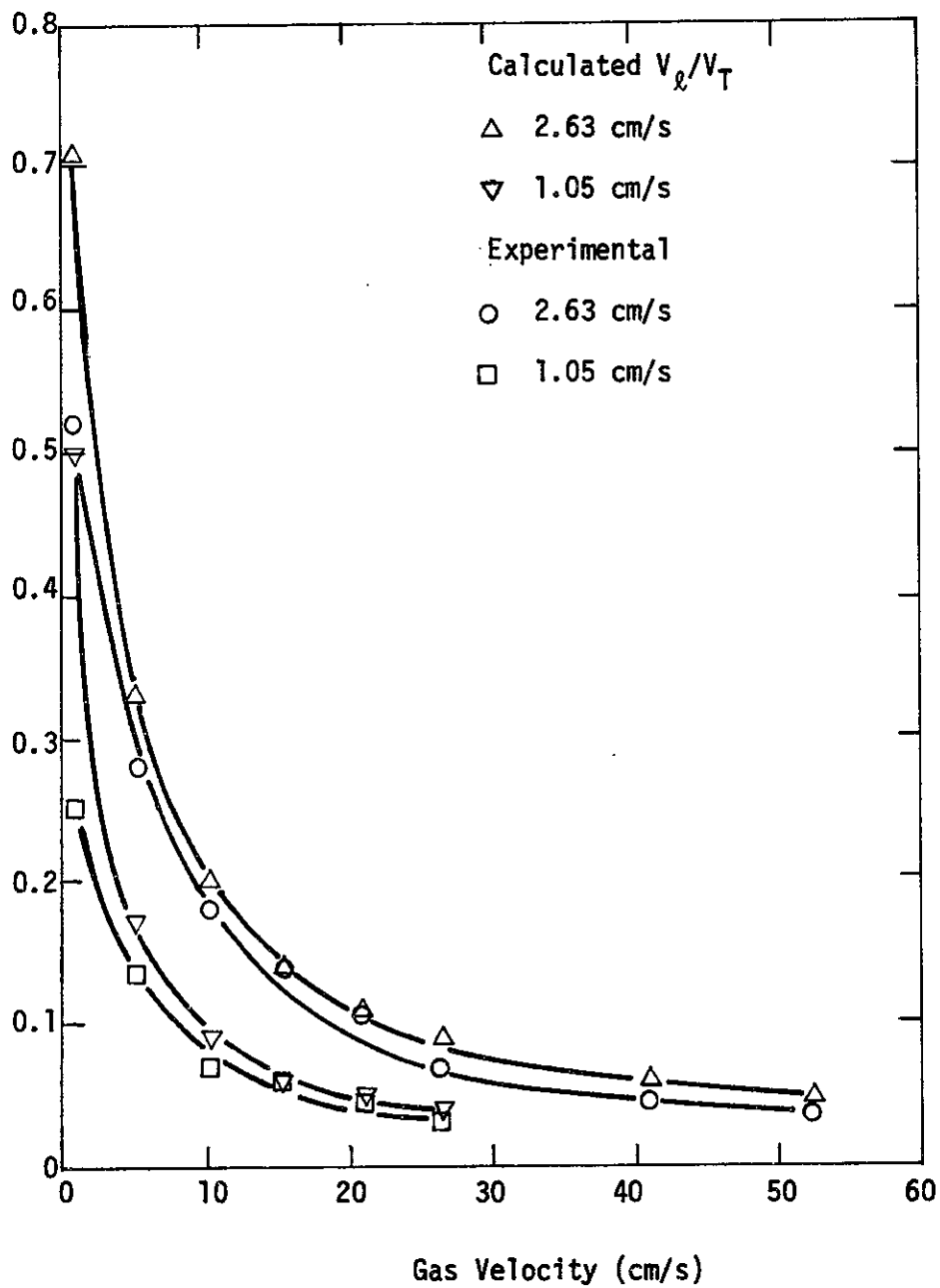


FIGURE 17. FRACTION OF CAPILLARY TUBE LENGTH OCCUPIED BY LIQUID SLUGS IN A 0.200914 cm I.D. CAPILLARY TUBE.

flow rate. On the same figure also the ratio of superficial liquid velocity V_L to total superficial velocity V_T is plotted against the same variables. Here V_L/V_T is the ratio of length of liquid slugs to total length of liquid and gas slugs if there were no liquid film between tube walls and gas bubble.

The difference seen in the two ratios is due to this liquid film. Deviation from V_L/V_T is very large at low gas flow rates, attributed to the existence of thicker liquid film than at high gas flow rates. At high gas flow rates this difference approaches a constant factor of about .75.

6-II - STUDIES WITH MONOLITHS

6-II-1

Effect of Liquid Distributor

The initial liquid distribution will presumably maintain itself with little change as it flows through successive sections, so it is vitally important to obtain uniform distribution initially. Several types of distributors investigated were found wanting. Figures 7, 8, & 9 illustrate three, the third of which was chosen for all subsequent studies. The first comprised a flat shower head with 37 small pipes which dripped liquid uniformly over the cross section. However, there are about 157 cells in a 1" diameter section of 200 cell/in² monolith and liquid did not distribute itself uniformly through all these cells, as shown by the fact that the pressure drop was irreproducible and changed significantly with a slight rotation of the shower head, i.e. the scale of uniformity provided by the pipe distributor was considerably larger than the cross-section of the cells. Nevertheless, some data were taken with this distributor for comparison with other distributors. In the second distributor configuration a layer of 4 mm spheres was placed on the top of the monoliths and the pipe distributor was retained as a predistributor. As one might expect some of the spheres sat at the openings of monolith channels causing their plugging. At low liquid flow rates, reproducibility improved somewhat but at moderately high liquid flow rates some flooding above the layer of spheres occurred. None of the data obtained with distributor no. 2 (Figure 8) were retained since they were of dubious value.

The best reproducibility and minimum pressure fluctuations were obtained by placing a sandwich of thin monolith slices (27 slices each about 1/8" thick) above the monolith array, randomly arranged. The detailed design is shown in Figure 9. The pipe distributor was retained as a predistributor. In a random stack of monolith blocks, a single passageway of a block usually will connect with 3 or 4 passageways of the next block. Therefore, liquid travelling in the passageway of the first block will become distributed to 3 or 4 channels of the next block each time it flows through a monolith slice.

The marked effect of the nature of the distributor is demonstrated on Figures 18 through 21 which show the observed pressure drop (cm of water per meter length of monolith stack) as a function of superficial air flow rate (cm/s at room temperature and atmospheric pressure) for each of two representative values of the superficial liquid flow rate of water and for a stack of 3" monoliths as compared to 6" monoliths. As noted above, with distributor no. 1 the pressure drop varied substantially with a slight degree of rotation which presumably altered the degree of uniformity of distribution. The values shown are the highest observed, which occur with the most uniform distribution (see below). Regardless of the type of distributor, a negative measured pressure drop is encountered at low gas and liquid flow rates, caused by the hydrostatic head of liquid. The regions of gas and liquid flows in which this occurs is somewhat larger with a poor distributor than with a good distributor. With uneven liquid distribution, reversal of gas flow will presumably occur in this region, slug-type flow of liquid causing a pumping action to return some gas upwards through those

channels in which liquid flow, if it occurs at all, is solely as an annular film on the wall.

With either a good or a poor liquid distributor, pressure drop increases with an increase in either gas or liquid rate, as expected. Comparison of the performance of a stack of 3" vs. 6" monolith pieces (Fig. 18 vs. Fig. 20; at $V_L = 3.95$ cm/s and Fig. 19 vs. Fig. 21, at $V_L = 1.31$ cm/s) reveals the effect of essentially doubling the number of junctions between adjacent pieces of monolith. (The increase is from 7 to 15.) In each case this brings the value of $\Delta P/L$ with the two types of distributor much closer together, the pressure drop with the poor distributor (no. 1) being raised and that for the good distributor (no. 3) being lowered. At the lower of the two liquid flow rates for which this comparison was made, the values of $\Delta P/L$ become quite close together when 3" blocks are studied (Fig. 21).

We believe that two quite different phenomena exist which work in opposite directions when the monolith lengths are reduced from 6" to 3", the total column length being held constant. If one starts with the no. 1 distributor, uniform distribution is obtained but on a larger scale than that of the cross-section of the cells. Consequently we postulate that some cells had little or no liquid flow while adjacent cells had much more than the average. With 3" blocks, liquid distribution occurs more frequently than with 6" blocks, as noted above.

However, focusing on a single channel, the flow pattern changes with length. This will be discussed in more detail later which described observations in a single smooth vertical capillary tube.

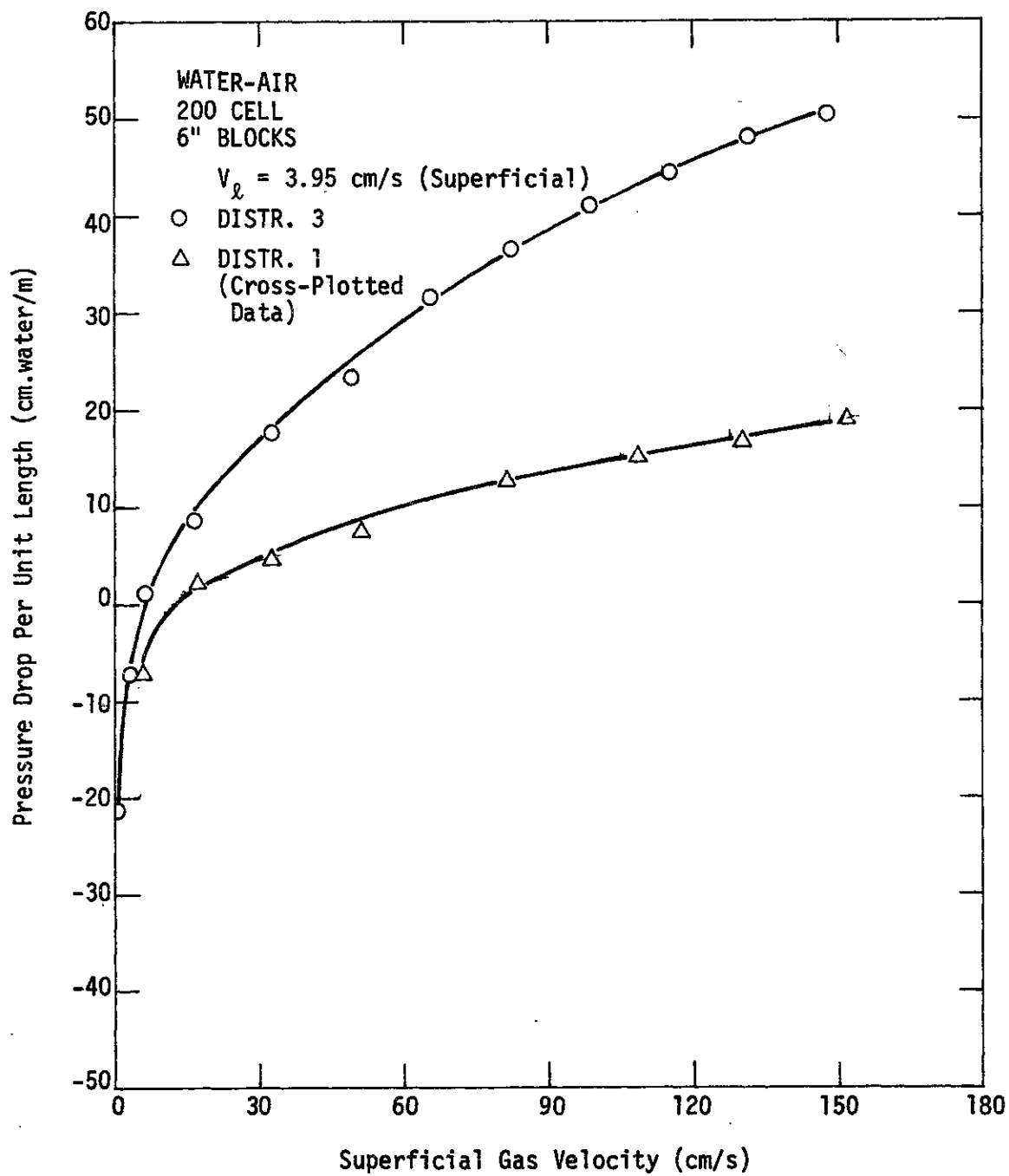


FIGURE 18. COMPARISON OF PRESSURE DROP DATA FOR DISTRIBUTOR 1 AND 3.

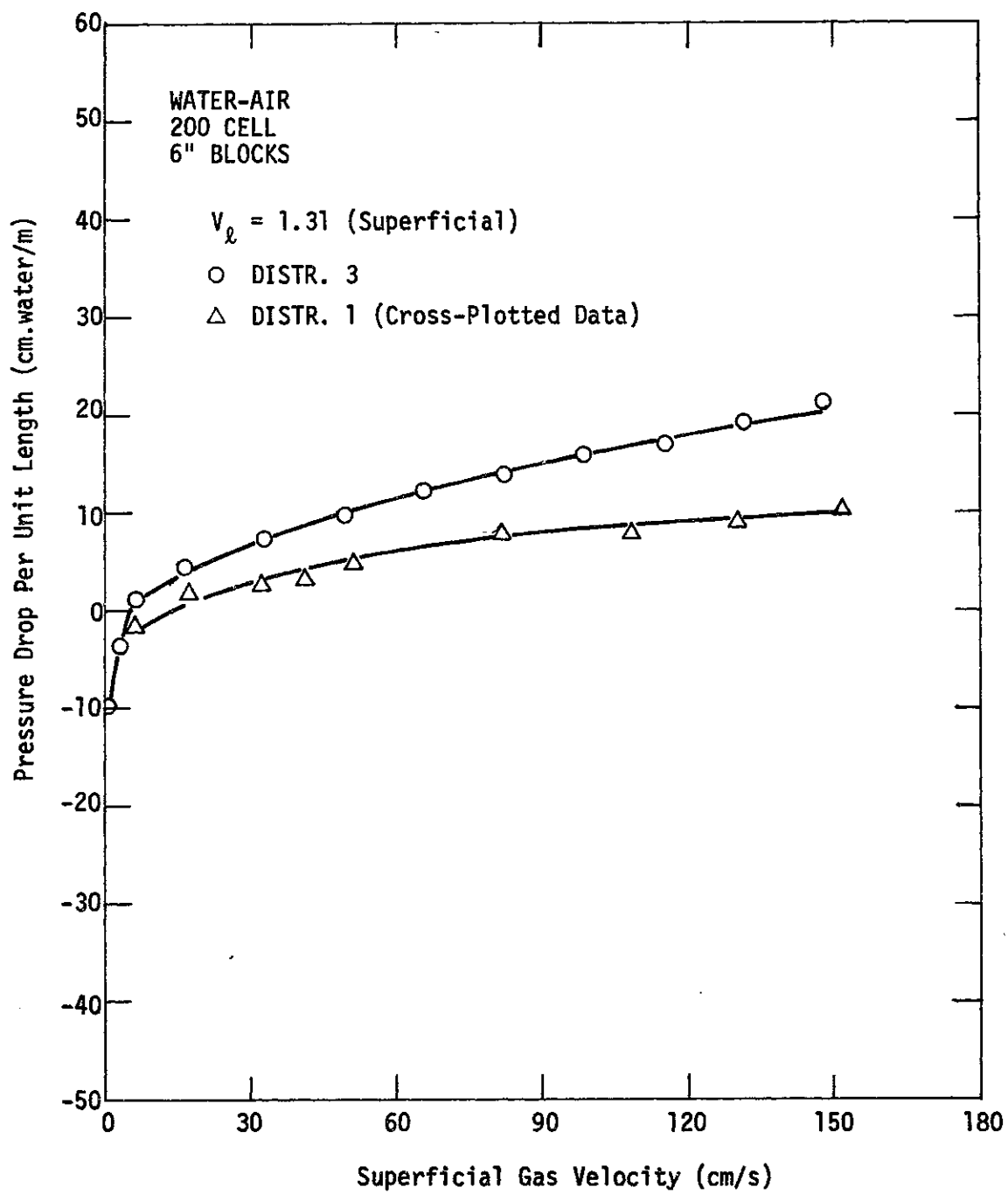


FIGURE 19. COMPARISON OF PRESSURE DROP DATA FOR DISTRIBUTOR 1 AND 3

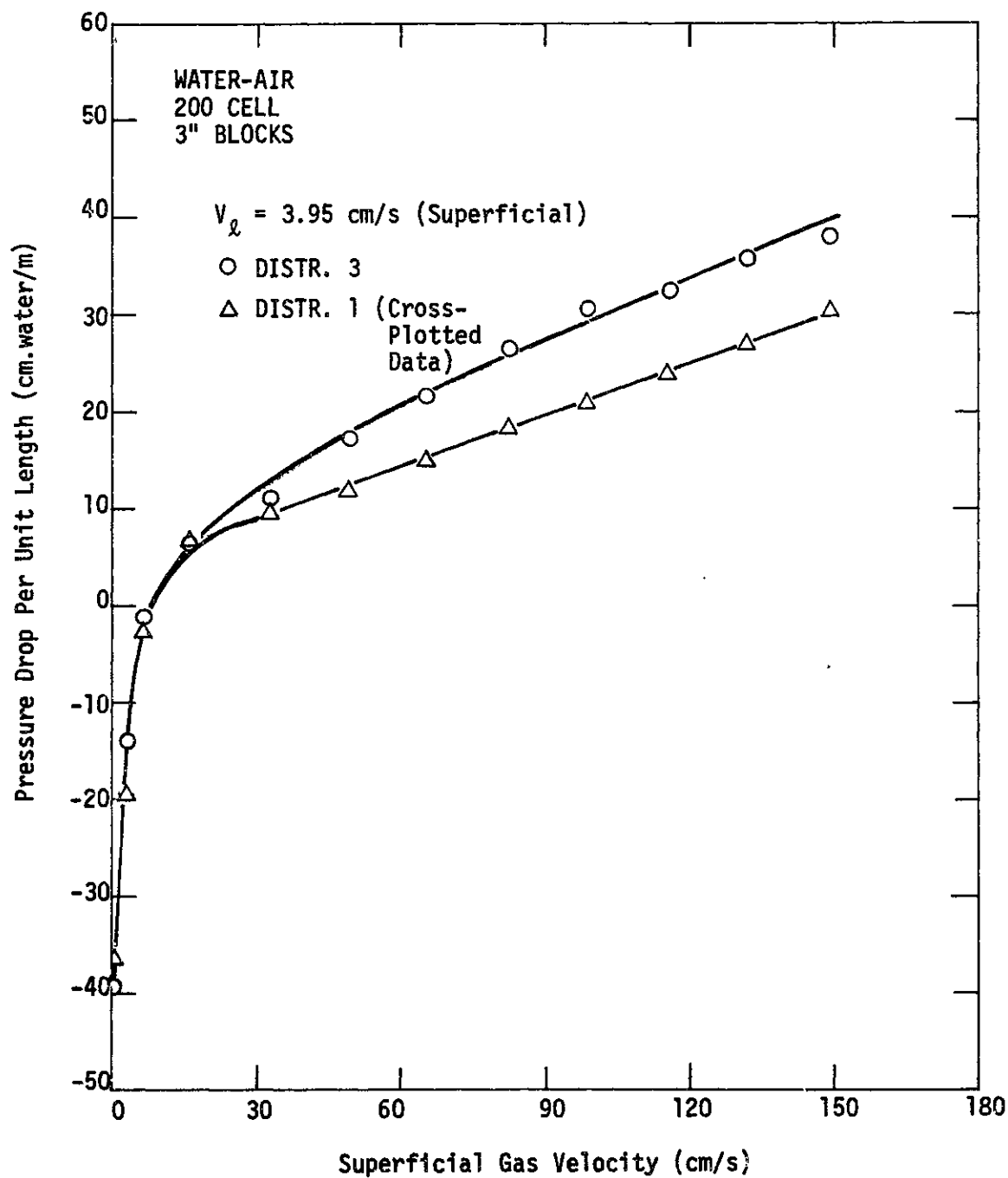


FIGURE 20. COMPARISON OF PRESSURE DROP DATA FOR DISTRIBUTOR 1 AND 3.

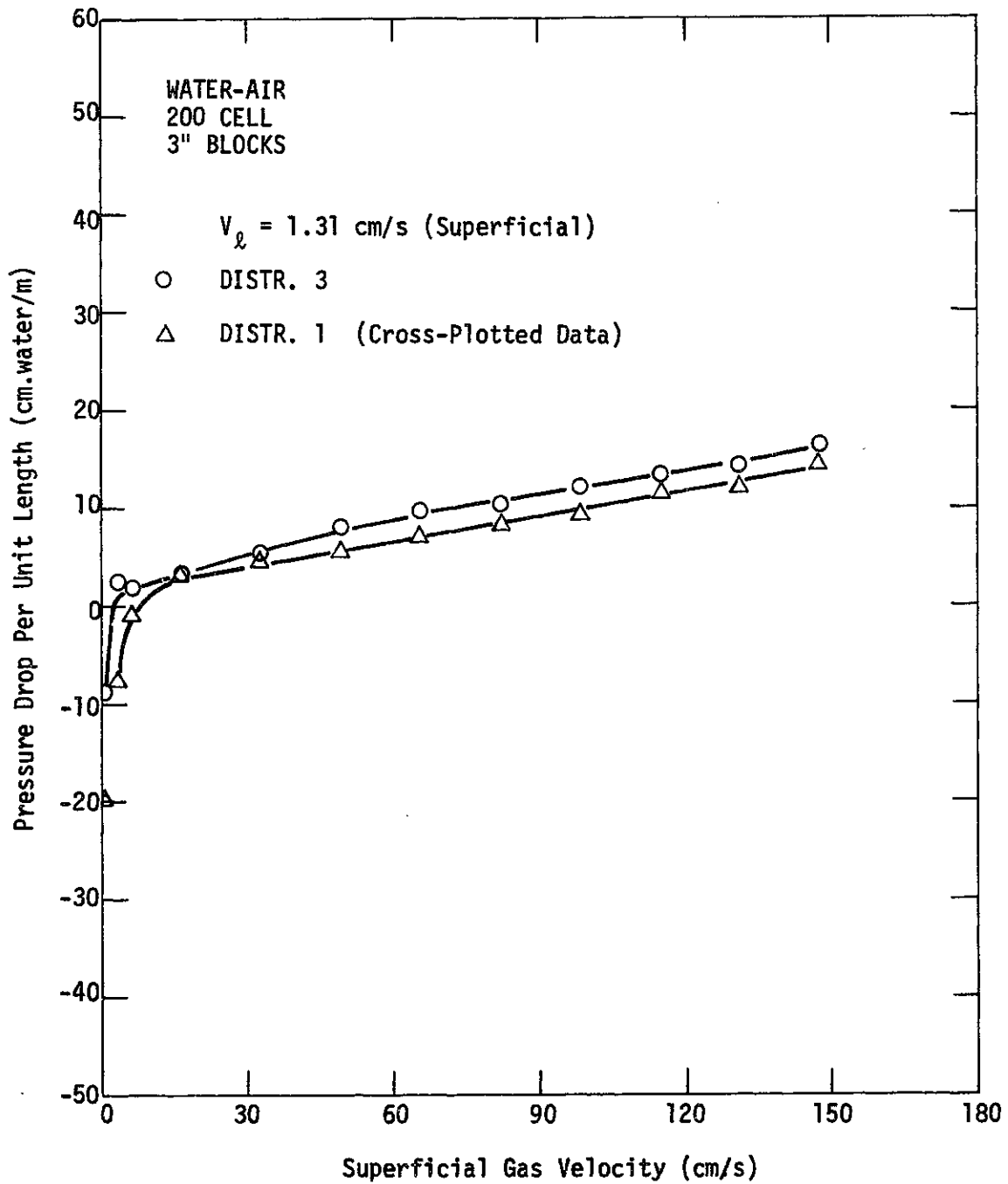


FIGURE 21. COMPARISON OF PRESSURE DROP DATA
FOR DISTRIBUTOR 1 AND 3.

In essence, as bubbles and slugs of liquid follow one another down a tube it is observed that a liquid ring (torus) frequently appears within a bubble, grows in thickness, and finally forms a liquid web across the channel which splits the bubble in two. The appearance of additional slugs would presumably increase the resistance to flow caused by circulation in slugs. It is thus postulated that considerably more bubble break-up occurs in the 6" lengths than in the 3" lengths, accompanied by a higher pressure drop per unit length.

Some additional results of the pressure drop measurements with distributor 1 and 200 cells/in² monoliths for 3" and 6" blocks in a 4 ft column are given in Figures 22 and 23. Here pressure drop per unit length as cm-water/m is plotted against gas superficial linear velocity as cm/sec at constant liquid flow rates. The columns used here were built by the first method and therefore were peripherically sealed with rubber cement. Pressure drop for 3" blocks are much higher than 6" blocks. The apparent reason for this is the redistribution of liquid at the block joints, as discussed above. An orifice effect also may cause some pressure drop at the joints. In randomly stacked monolith blocks, the exits of the passageways are partially closed or restricted by the honeycomb type webs of the next block. These restrictions cause some pressure drop at the joints of the monolith blocks. The total pressure drop created in a reactor or a column by this orifice effect is related to the magnitude of the restriction and number of joints. An orifice effect is not the reason for the difference observed, however, since with a good distributor (distributor 3) a 6" block column gives a higher pressure drop than a 3" one.

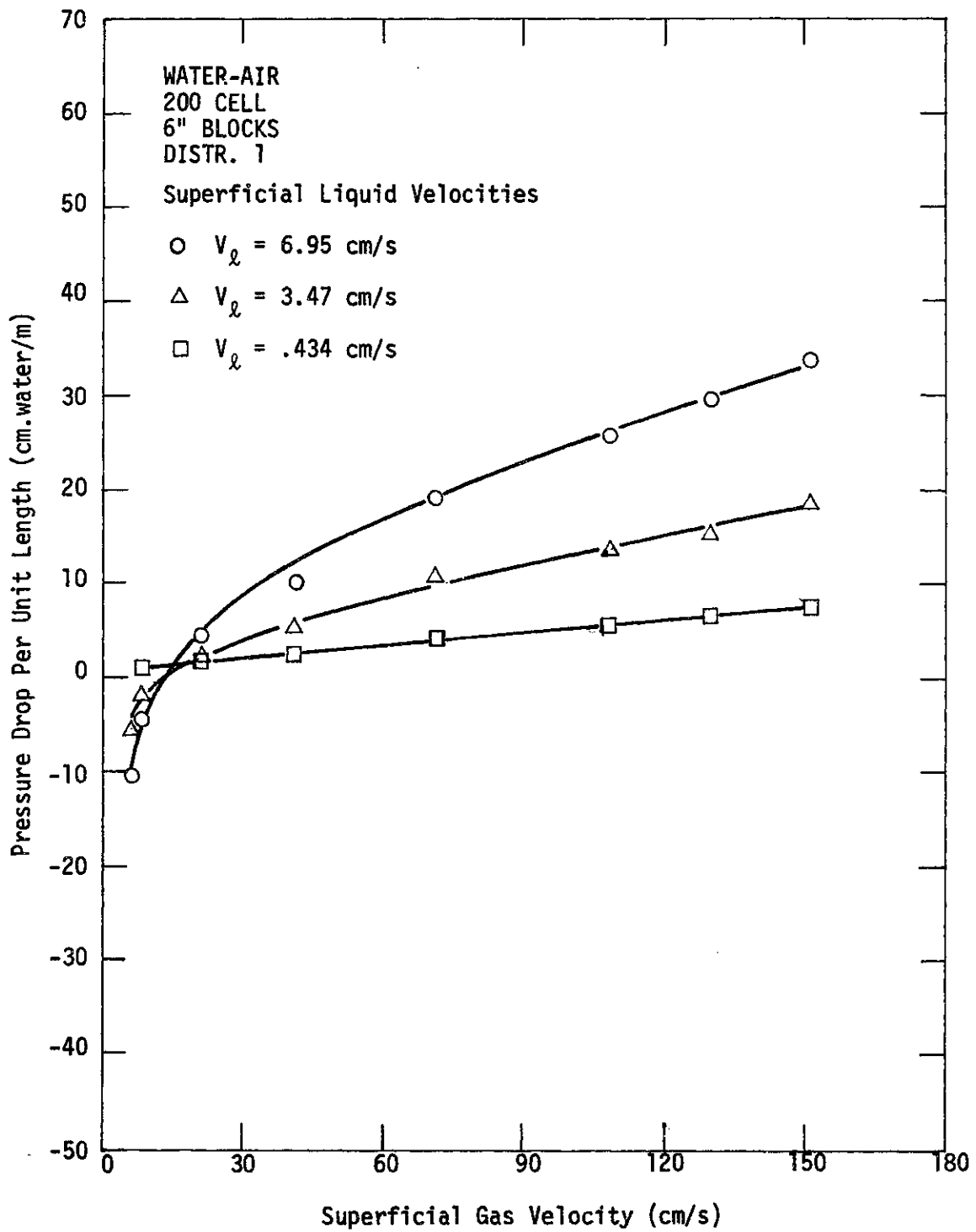


FIGURE 22. PRESSURE DROP FOR DISTRIBUTOR 1

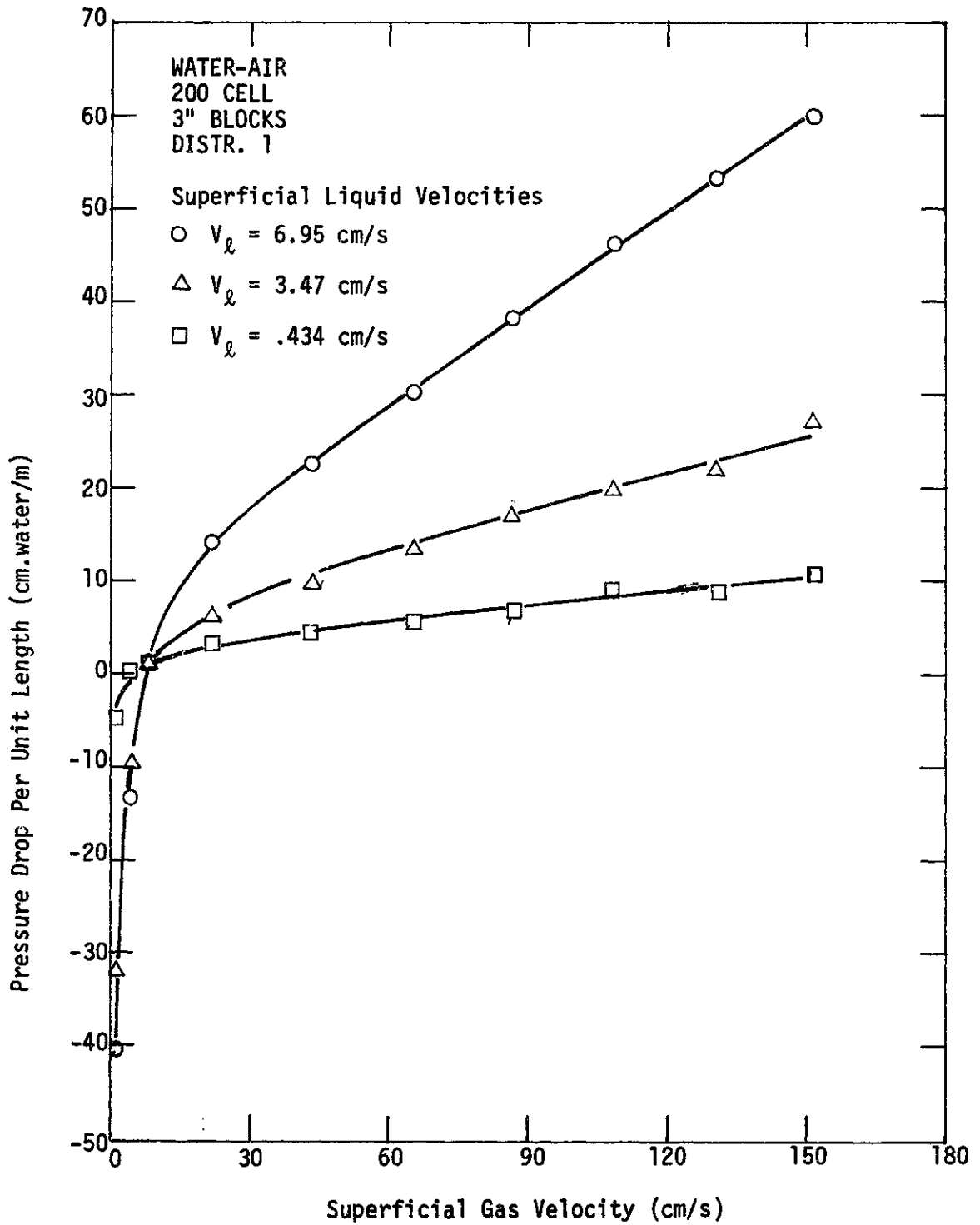


FIGURE 23. PRESSURE DROP FOR DISTRIBUTOR 1

6-II-2

Comparison of Pressure Drop in Capillary Tube and Monolith

In Figure 24 a comparison of the pressure drop for slug flow in a capillary tube and 200 cell, 6" block monoliths in a 4 ft column with distributor 3 is given. Here pressure drop per unit length as cm water/m of column is plotted against interstitial gas velocities as cm/sec at constant liquid flow rates. The capillary tube used had a hydraulic diameter of 0.200914 cm and length of 102 cm. The hydraulic diameter for 200 cells monolith passageways was 0.1528 cm. Pressure drop for both capillary and monolith increases with increasing gas flow rate and the pressure drop curves for both systems follow each other very closely in trend. The higher pressure drops in monoliths are due to smaller hydraulic diameter of monolith passageways. This higher pressure drop in a smaller channel also is an indication of good liquid distribution throughout the monolith channels. A liquid maldistribution or dry channels in a monolith would tend to give much lower pressure drops. Negative pressure drops are encountered in a capillary tube as well as in monoliths. This again is only due to the hydrostatic head of liquid slugs in passageways.

In Figure 25, pressure drop versus liquid superficial velocities are plotted for 200 cells, 3" monoliths, with distributor 3. It is interesting that pressure drops for monoliths follow the same trend seen in pressure drop vs. liquid velocities for capillary tubes.

Some of the pressure drop data for water taken with 200 and 300 cell/in² monoliths in a 4 ft column of 3" or 6" blocks are shown in Figures 26 - 29. Here again pressure drop per unit length as cm water/m is plotted against superficial gas velocities at constant

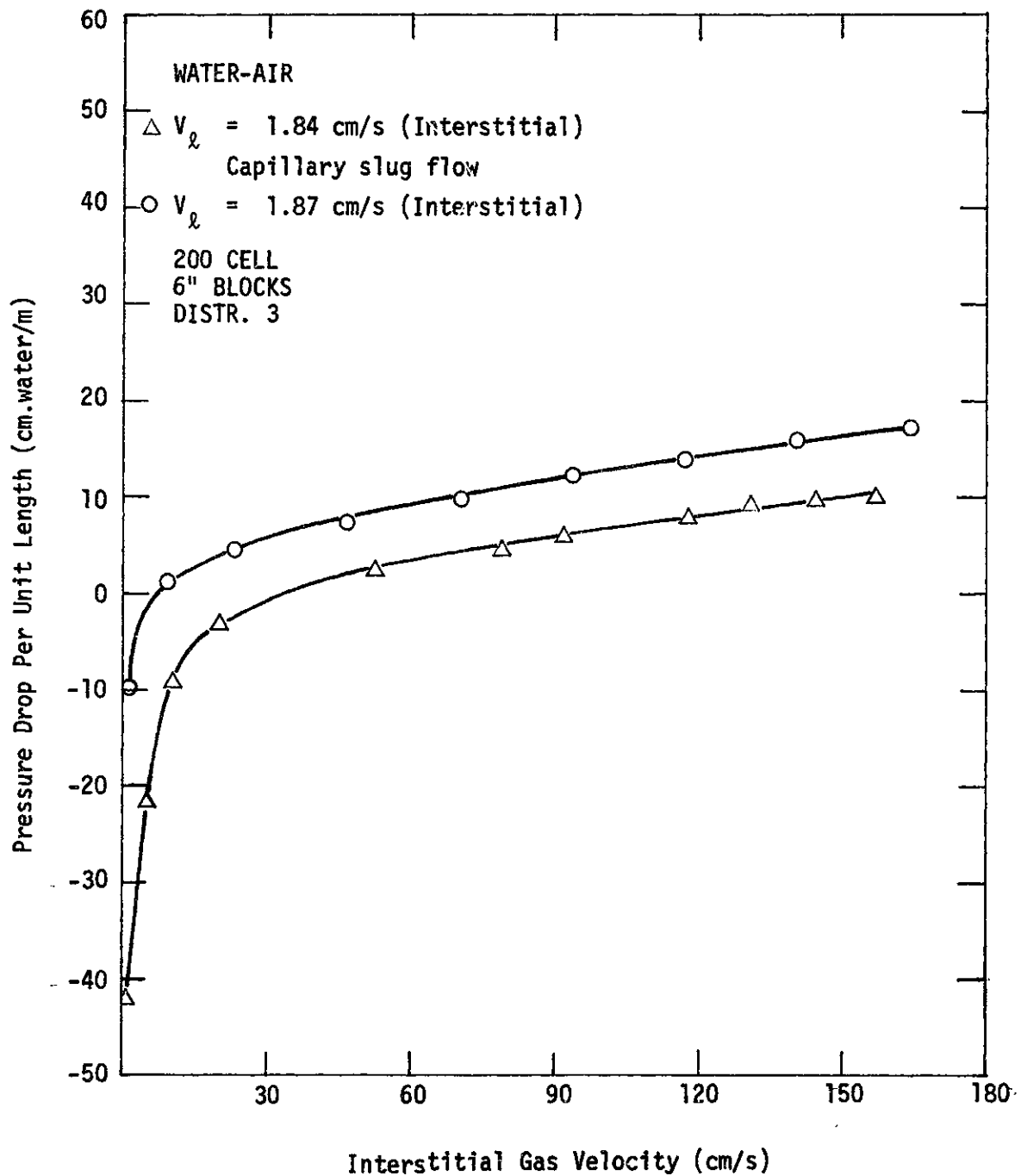


FIGURE 24. COMPARISON OF PRESSURE DROP FOR
CAPILLARY SLUG FLOW AND MONOLITHS

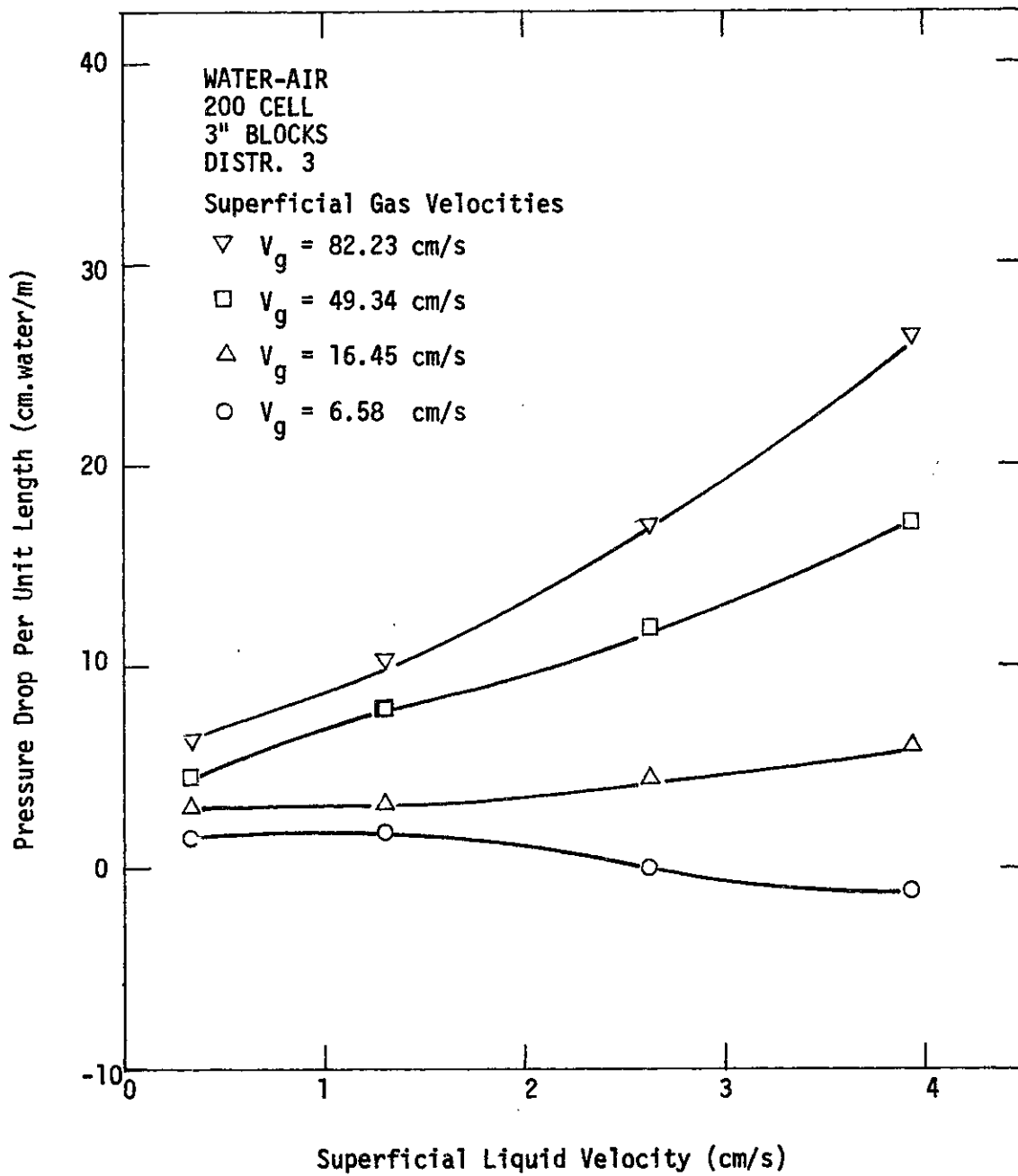


FIGURE 25. PRESSURE DROP vs. LIQUID VELOCITY

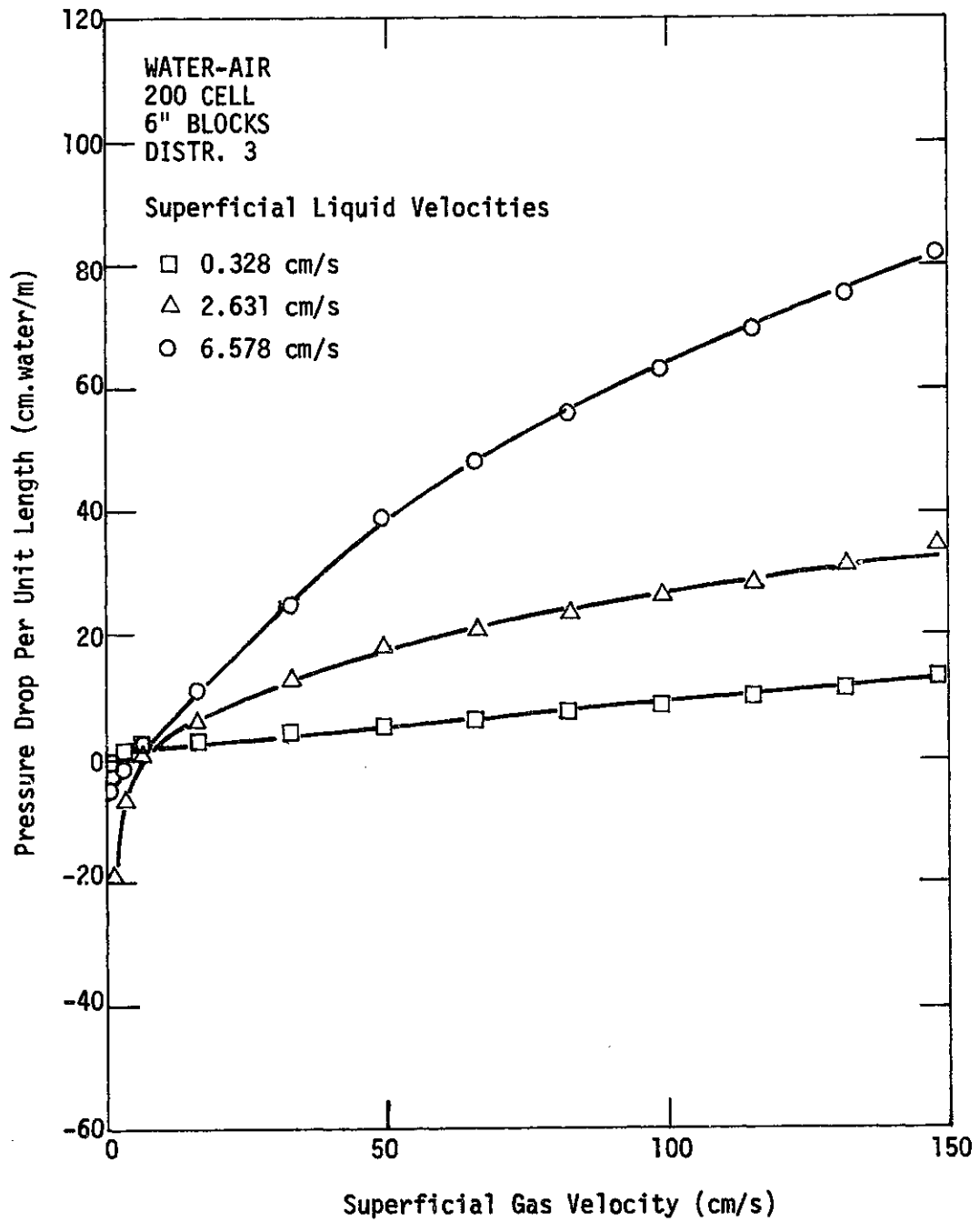


FIGURE 26. PRESSURE DROP

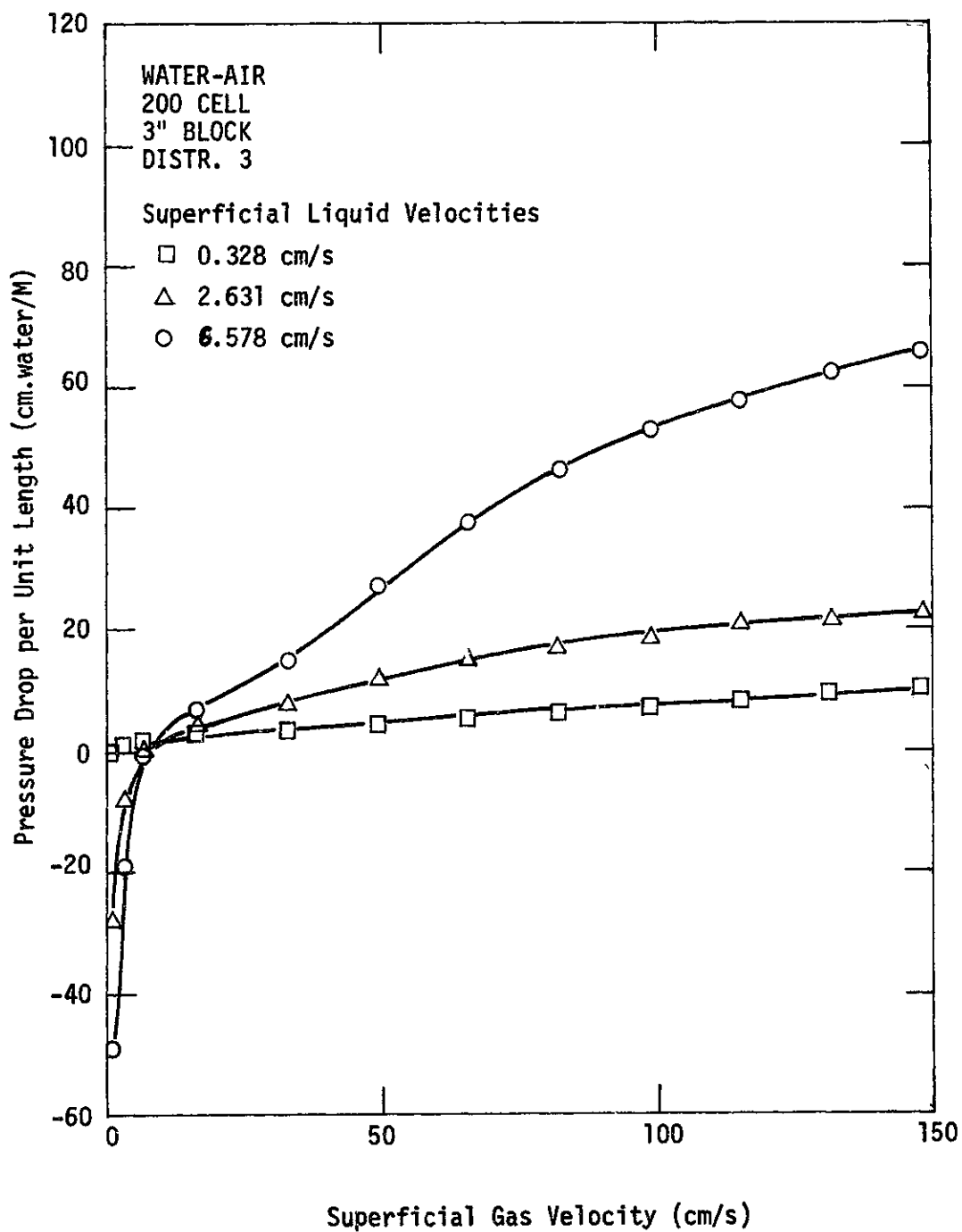


FIGURE 27. PRESSURE DROP

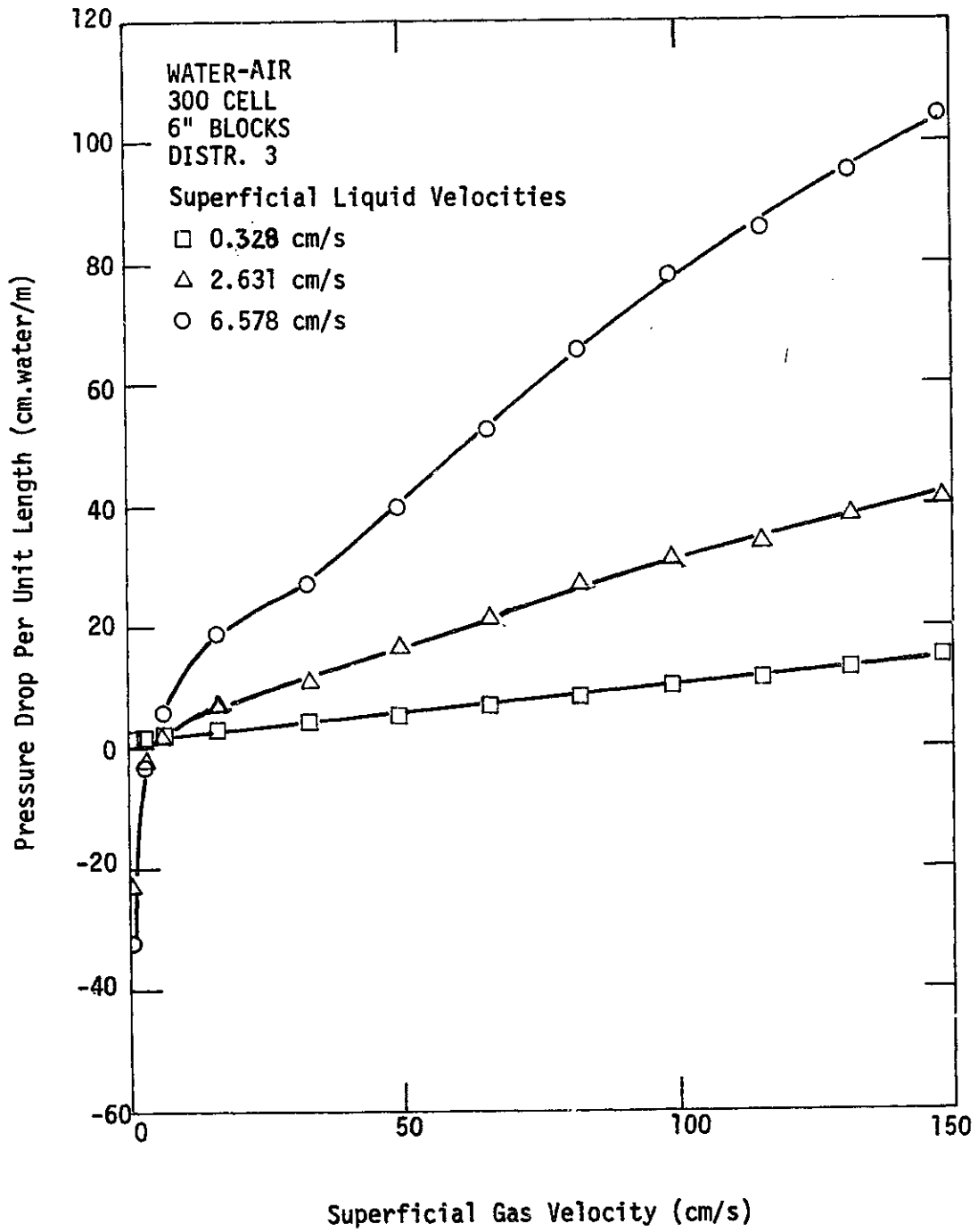


FIGURE 28. PRESSURE DROP

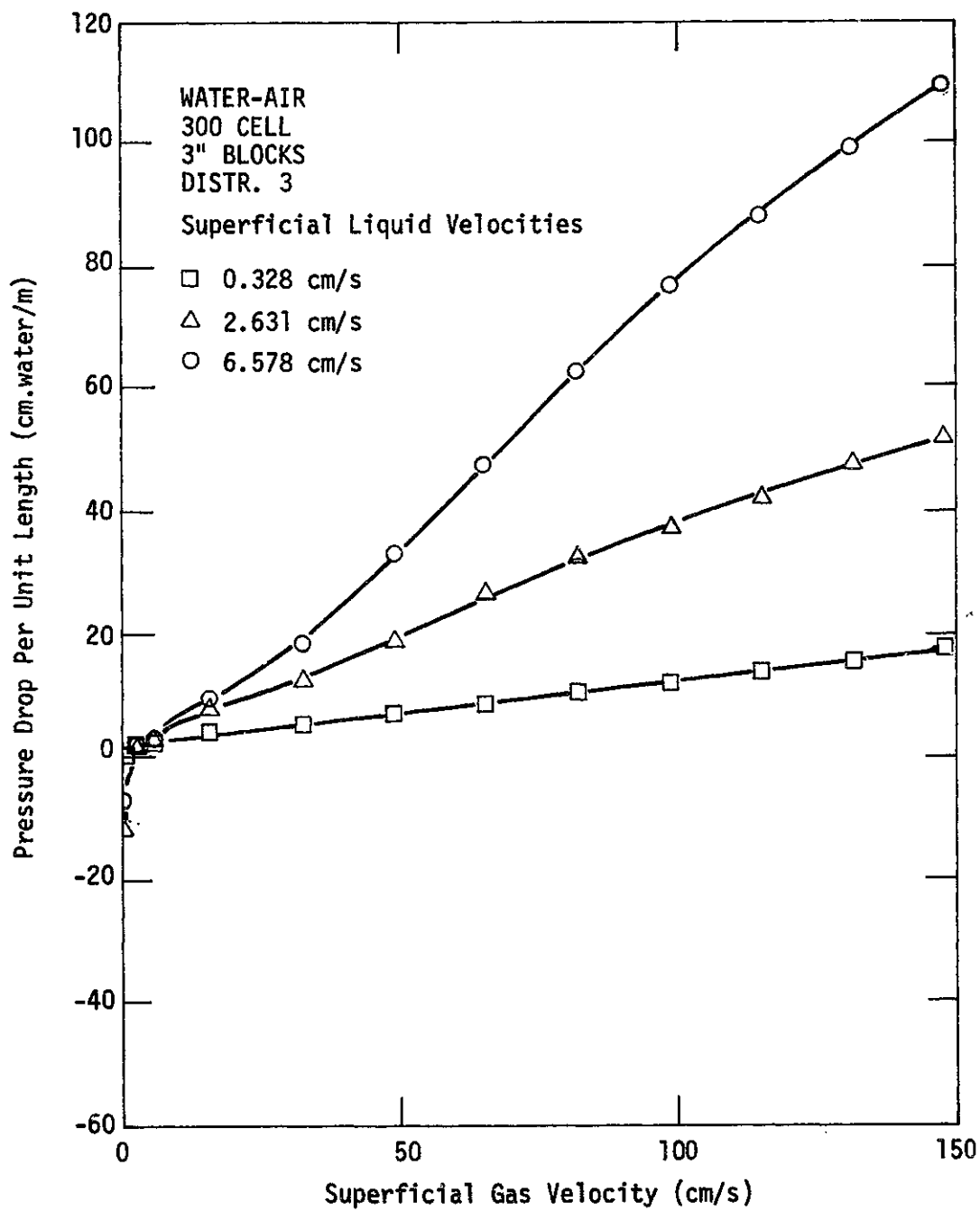


FIGURE 29. PRESSURE DROP

liquid flow rates.

The pressure drop with 200 cell/in² material is slightly higher for 6" blocks than 3" blocks but the opposite is true for 300 cell/in² monoliths. Two competing effects, orifice pressure drop and bubble break up can explain this seeming anomaly. One generally would expect higher pressure drops in 3" blocks due to an orifice effect. However, focusing on a single channel, the flow pattern changes with length. This is observed in two-phase slug flow in the capillaries and it is a similar phenomenon to transition from annular to slug flow described earlier.

In essence, as bubbles and slugs of liquid follow one another down a tube, it is observed that a liquid ring frequently appears within a long cylindrical bubble, which grows in thickness, finally forming a liquid web across the channel which splits the bubble in two. The appearance of additional bubbles and slugs would presumably increase the friction in passageways due to the circulation pattern (Chapt. 6) in liquid slugs and gas bubbles. Since this circulation and energy lost due to it is expected to be higher in magnitude in shorter slugs, it is postulated that considerably more bubble break up occurs in the 6" lengths than in the 3" lengths, accompanied by a higher pressure drop per unit length, with 200 cell material. Both 200 cell/in² and 300 cell/in² monoliths had a measured web wall thickness of .027 cm, but the 300 cell material has a passageway dimension of .107 cm versus .1528 cm for the 200 cell material. Since passageways are smaller in the 300 cell bubbles should reach steady state more quickly than 200 cells and one does not expect very much difference due to bubble break up. Therefore, restrictions

of the channel exits in 300 cell material by the web walls of the next block is greater than with 200 cell blocks and this causes a higher pressure drop across the block joints in 300 cell monolith columns. Indeed if the orifice effect is calculated and subtracted from measured pressure drop for 3" and 6" blocks of 300 cell columns with the equation given in chapter 6, it will be seen that the total of frictional and hydrostatic pressure drop in both systems (presumably hydrostatic pressure drop is the same for 6" and 3" blocks) will be close to each other.

6-II-3

Cyclohexane-Air System

The results of pressure drop measurements with cyclohexane-air for 200 cell, 6" and 3" blocks in a 4 ft reactor are given in Figures 30-31. Here again the pressure drop per unit length versus gas flow rates at constant liquid flow rates is plotted. These relationships follow the same trend as in the case of water-air in 200 cell monoliths. Again for the same reasons, 6" block columns give a higher pressure drop than 3" block columns. Surprisingly, the pressure drops for cyclohexane are close to the pressure drops for water. One might have expected a substantial difference due to 3 times lower surface tension of cyclohexane than water. However, Goldsmith et al. (1962) showed that in capillary slug flow of gas and low viscosity liquids like water, both ends of long cylindrical gas bubbles stay undistorted as semi-spherical caps. Therefore, surface tension does not contribute to pressure drop due to distorted bubble caps but it may play a role in determination of the thickness of liquid film between gas bubbles and the channel wall, and consequently of the pressure drop.

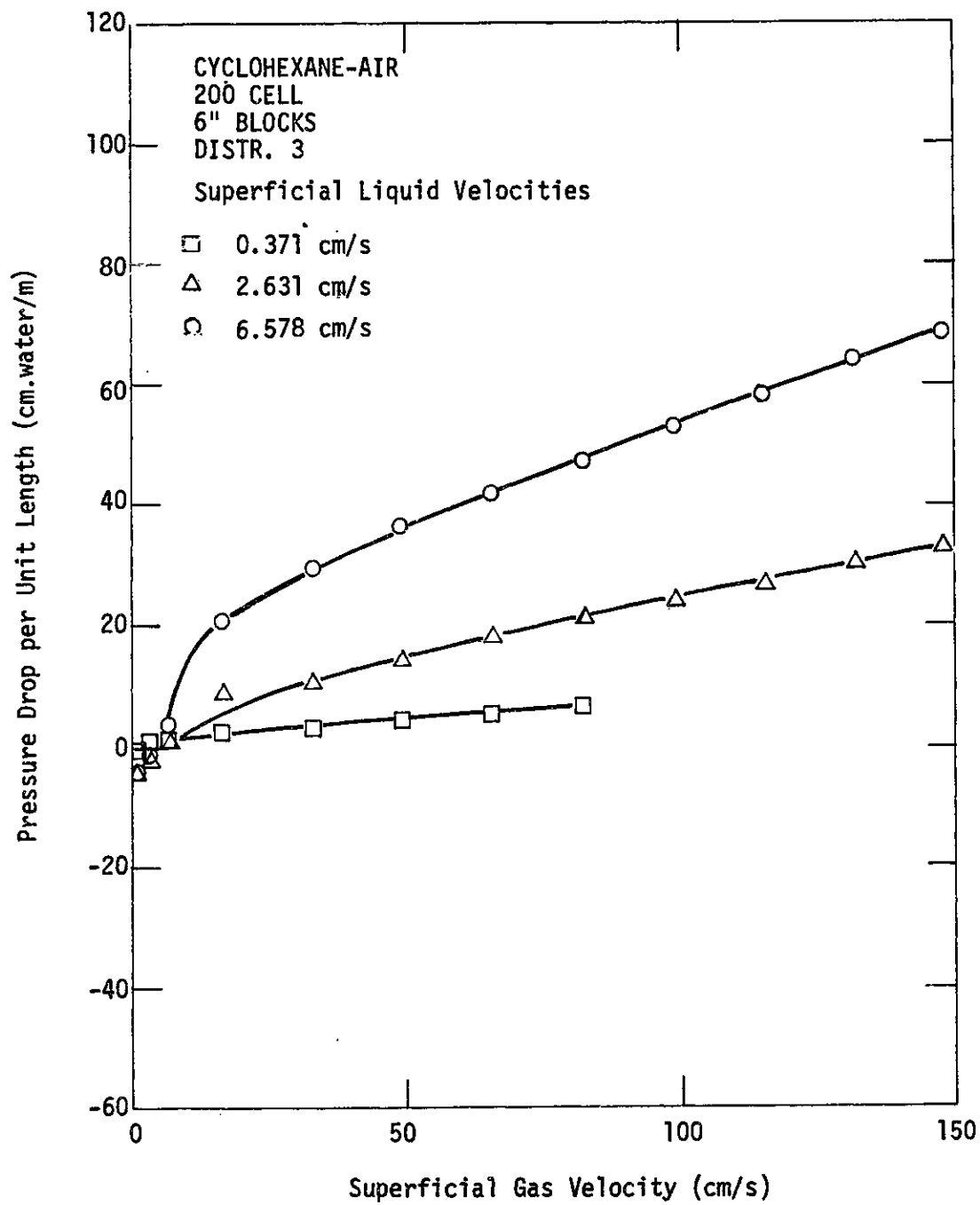


FIGURE 30. PRESSURE DROP

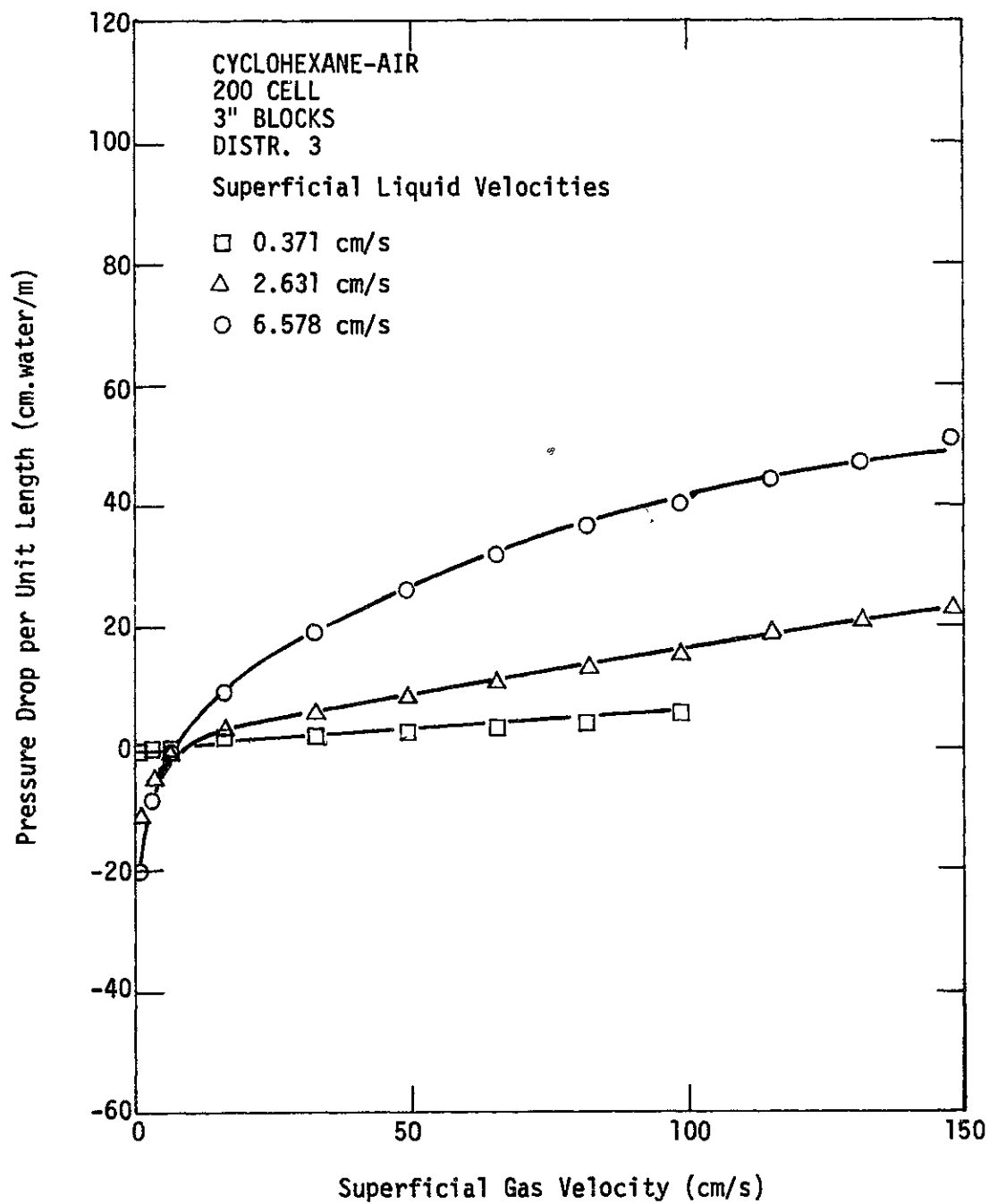


FIGURE 31. PRESSURE DROP

Also, the difference in pressure drop for water and cyclohexane could be very well due to the lower density of cyclohexane than water.

6-II-4

Comparison With Study by Kiser

The 200 cell, 3" block, water-air results with distributor 3 may be compared to a brief study by Kiser (1975) performed on the same type of monolith structure but in a column 4" diameter and 4 ft long consisting of a stack of units each 3" high in Figure 32. The highest liquid flow rate studied by Kiser was 1.24 cm/s but air flow rates of up to 90 cm/s were covered. Kiser's results agree closely with present results at the lowest air and liquid rates but his observed pressure drop was twice that obtained here at the highest combination of liquid and gas. The reason for this could be the combined effect of foaming reported by Kiser and the fact that he used 4" diameter monolith blocks. These monoliths are extrudates and some layers of the channels around their periphery tends to be plugged due to manufacturing imperfections, therefore, causing interstitial velocities higher than calculated. Also, Kiser's distributor was a special Bick spray nozzle which is used to produce a uniform spray but no information is available on the degree of uniformity actually achieved. His study was not intended to be definitive and is cited only to illustrate further the sensitivity of pressure drop and flow pattern in monolith systems to geometrical details.

Some two phase flow pressure drop data in packed beds packed with different size of packings are compared with our data for 200 cell

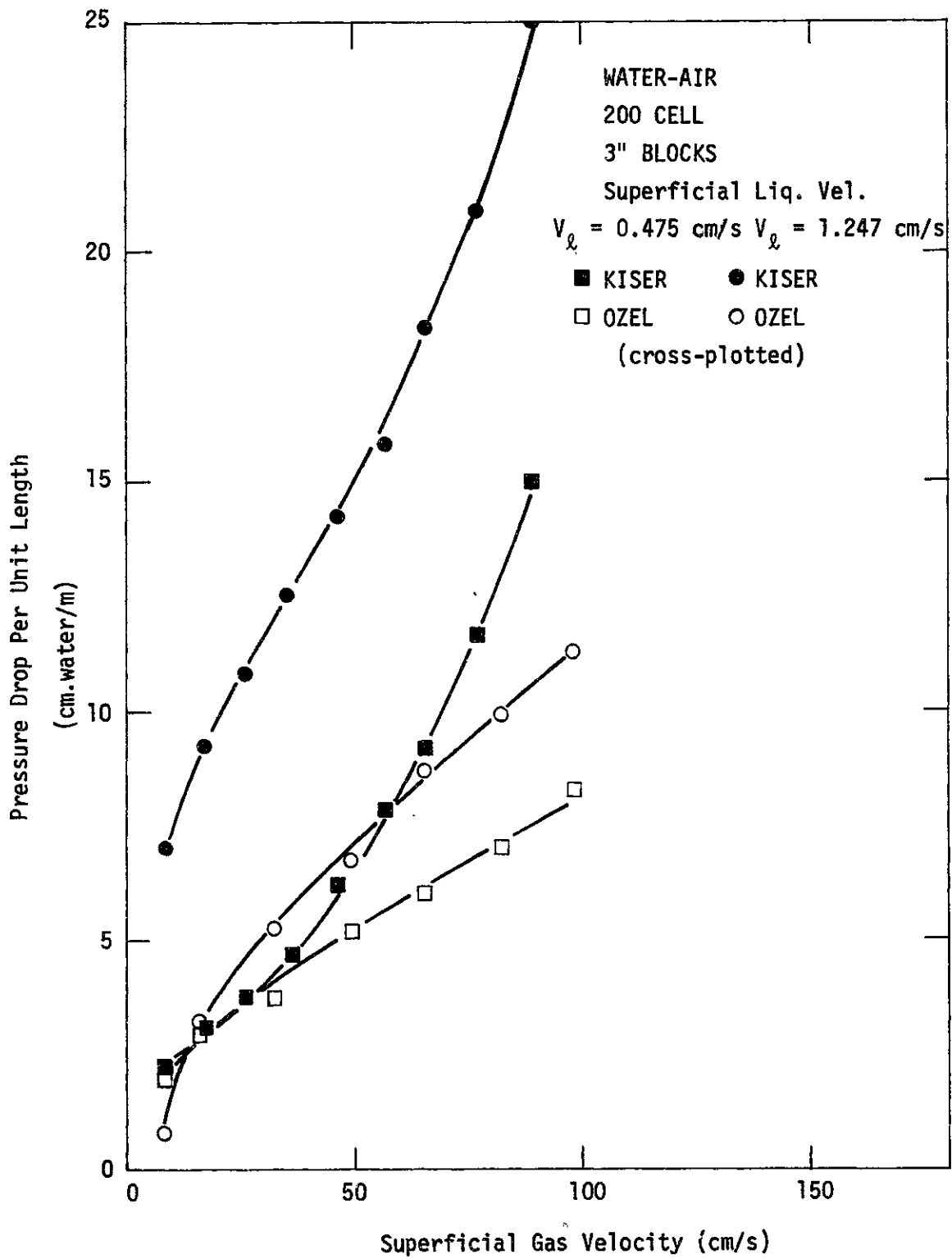


FIGURE 32. COMPARISON OF PRESENT RESULTS AND THOSE OF KISER

monolithic packing in Figure 33. Data for packed beds are taken from the raw data of McIlvried (1956), and M. W. Van Eek (1976). McIlvried's data are with 6 mm and 4 mm glass beads. Van Eeks' data are with 1/8" x 1/8" diameter x height alumina catalytic cylindrical supports. These are commonly-used particle sizes. Monolith data are for 200 cell, 6" long blocks in a 4 ft reactor with distributor system 3. Even larger particles like 6 mm spheres give an order of magnitude higher pressure drop than the monolithic supports, emphasizing one potential advantage of monolith-type packing.

6-II-5

Streamlines in Monolithic Two-Phase Flow

Earlier a sketch of streamlines in two phase capillary flow was presented. A similar type of flow pattern presumably exists in monolithic two phase flow.

A sketch of streamlines is given in Figure 34. This sketch is based on the calculations of blood flow researchers (see Chapter 4) and two phase flow research. Circulation in the liquid slugs and gas bubbles is the most important characteristic of the two phase slug flow in narrow channels. This circulation becomes very important in relatively short cylindrical bubbles and liquid slugs. It increases friction and energy lost due to friction and therefore higher pressure drops results in two phase flow relative to one phase flow. However, it also presumably increases the mass transfer both in bubbles and slugs.

Though the liquid film between the gas bubble and the channel wall causes the liquid phase to lag behind the gas phase, this

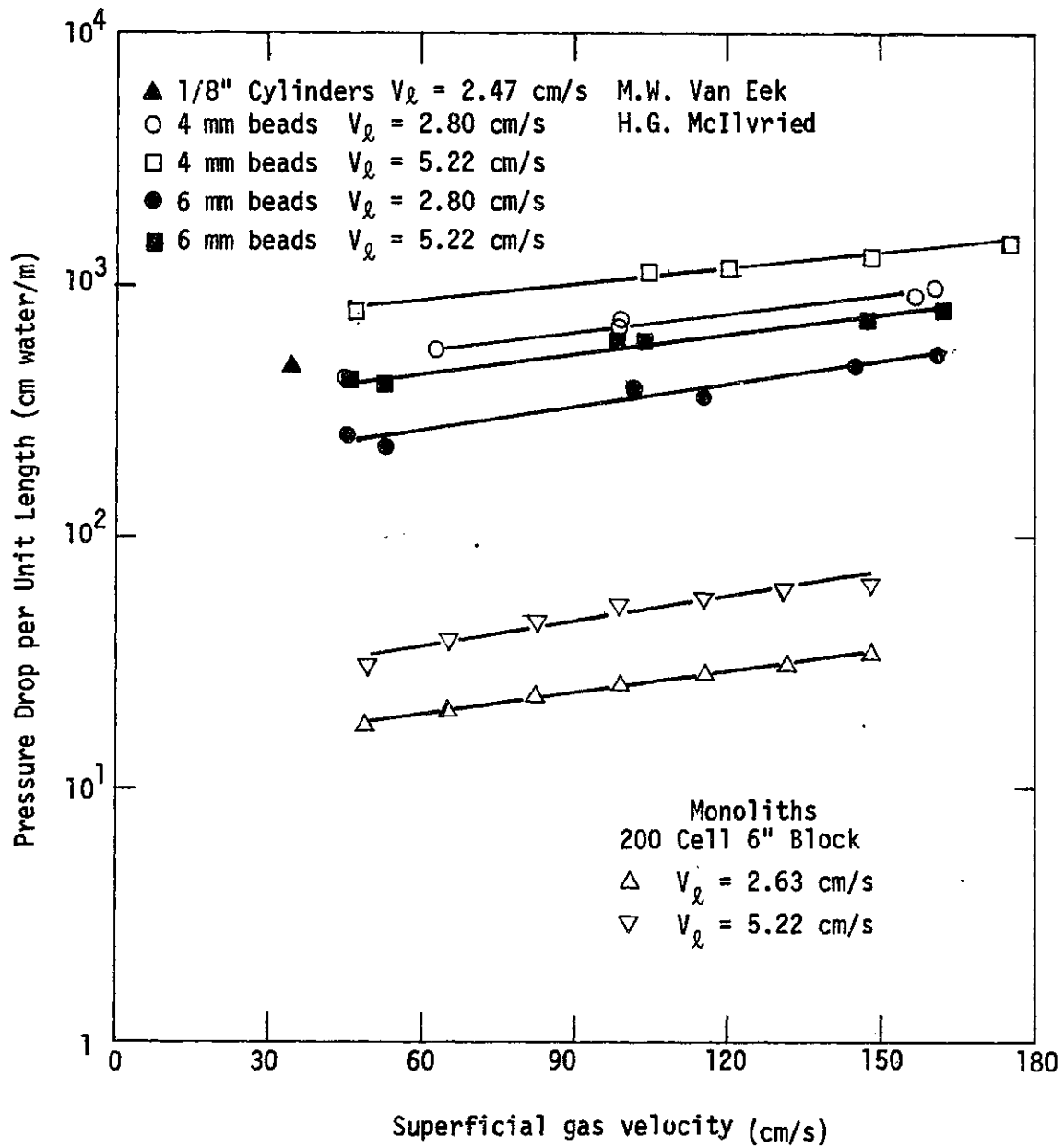


FIGURE 33. COMPARISON OF PRESSURE DROP IN MONOLITHS WITH THOSE IN PACKED BEDS

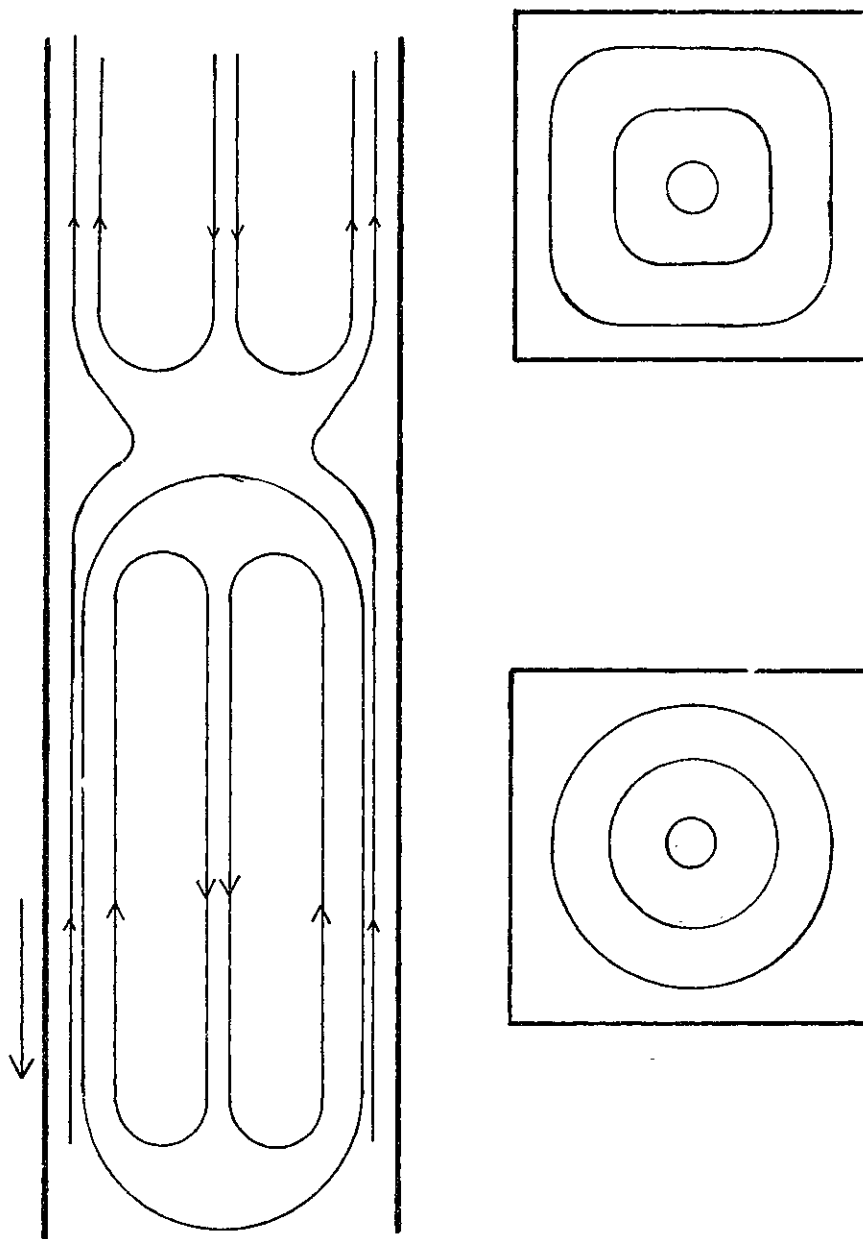


FIGURE 34. STREAMLINES IN MONOLITHIC TWO PHASE FLOW

difference is not expected to be large considering that the film is very thin. Therefore almost ideal plug flow performance is expected in one channel of a monolithic trickle bed reactor. However, bad maldistribution of liquid might cause some variation in the average residence time between different parallel channels.

7 - CORRELATION OF RESULTS

7-I

Calculation of Frictional Pressure Drop From Data

The pressure drop measured is the sum of the frictional pressure drop, the static head and orifice effects.

7-I-1

Orifice Effect

An orifice effect appears here caused by a restriction in the passageway between the exit of one monolith and the entrance to the next, since the two monoliths are not usually aligned. In effect, the exit of one channel is partly obstructed by the walls of the next block, creating an orifice effect.

Using some elementary mathematical considerations, continuity and the Bernoulli equation, the following equations can be derived.

$$V_T = V_L + V_G \quad \text{VII-1}$$

$$A_0 = A^2 - W.A - W(A - W) \quad \text{VII-2}$$

$$V_{or} = V_T \frac{A^2}{A_0} \quad \text{VII-3}$$

$$\Delta P_{\text{orifice}} = N \left(\frac{V_L}{V_T} \rho_L \left(\frac{V_{or}^2 - V_T^2}{2} \right) + \frac{V_G}{V_T} \rho_G \left(\frac{V_{or}^2 - V_T^2}{2} \right) \right) \quad \text{VII-4}$$

Here V_L , V_G , V_T are respectively liquid, gas, total interstitial velocities in cm/sec. V_{or} is the total velocity at the orifice in cm/sec, W is the wall thickness in cm, A is monolith passageway dimension in cm, A_0 is the area at the restriction at orifice in cm^2 ,

N is the number of monolith block joints in the reactor, ρ_L and ρ_G are the liquid and gas densities, respectively, in g/cm^3 .

In the derivation of this equation we assume that gas and liquid move as slugs through the orifice with the same velocity V_T . Then we weighed this pressure drop by liquid and gas volumetric flow rates. The value of (A^2/A_0) is 1.475 for 200 cell/in² monoliths and 1.789 for 300 cell monoliths.

7-I-2

Static Head and Frictional Pressure Drop

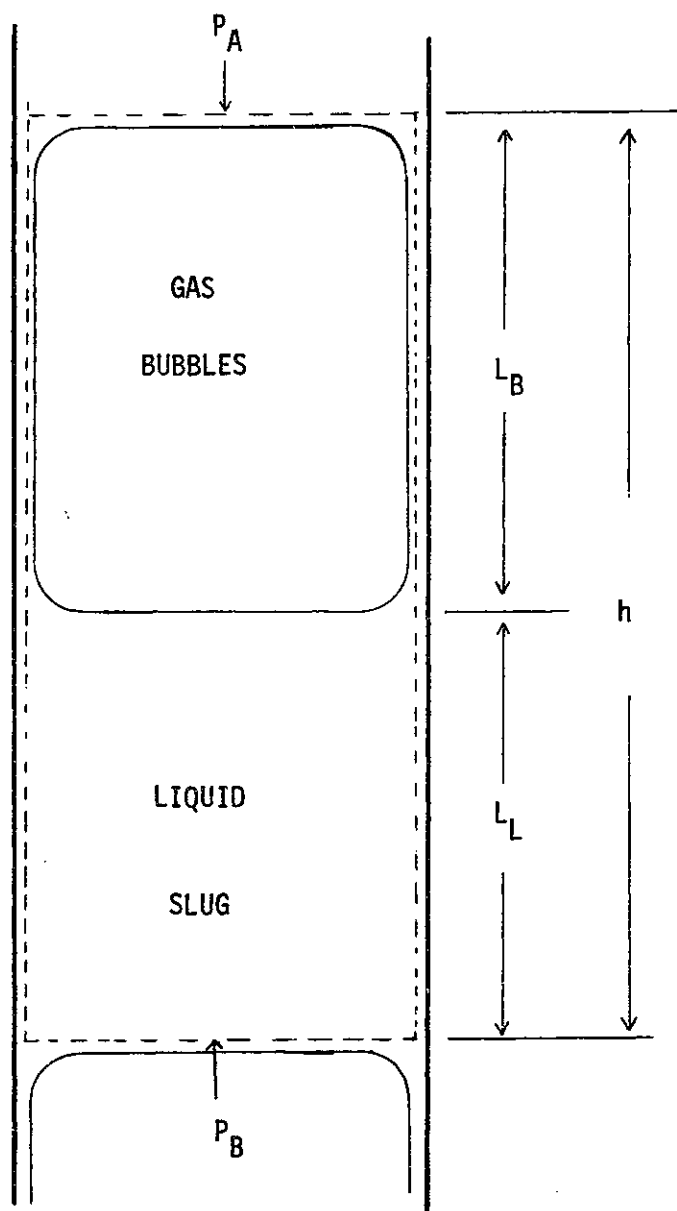
How to calculate the static head in vertical two phase flow is somewhat uncertain. Griffith and Wallis (1961) calculated the static head as the height of liquid slugs, ignoring the weight exerted by cylindrical gas bubbles. Laird et al. (1956) gave the static head by the following equation:

$$\Delta P_{\text{static}} = g\rho(h + \lambda) \quad \text{VII-5}$$

Here h is the height of the liquid slug, λ is the volume of the liquid around the gas bubble, expressed as length of the tube, ρ is the density of liquid, g is the acceleration of gravity. Here the static head of the liquid film around the gas bubble is taken into account. Nicklin et al. (1962) also used this equation for their calculations.

A better understanding of static head can be achieved through a force balance on a control volume in a single monolith channel (Figure 35) as follows:

Weight exerted by mass in control volume + force due to pressure difference - frictional force = 0



CONTROL VOLUME

FIGURE 35

or

$$g(\rho_L V_L + \rho_G V_G) + (P_A - P_B) A^2 - \Delta P_F A^2 = 0 \quad \text{VII-6}$$

Here V_L and V_G are the volume of liquid and gas enclosed in the control volume, P_A and P_B are the pressures at each end of the control volume, A^2 is the cross sectional area of the channels, ΔP_F is the frictional pressure drop. Since the liquid film between the cylindrical gas bubble and the web wall is very thin, its weight can be easily ignored.

$$V_L = A^2 L_L \quad \text{and} \quad V_G = A_B L_G \approx A^2 (h - L_L) \quad \text{VII-7}$$

Here L_L and L_G are the length of liquid slug and the gas bubble respectively, A_B is the cross sectional area of bubbles, h is the height of the control volume. Since $\rho_L \gg \rho_G$ one obtains

$$g \rho_L L_L + P_A - P_B = \Delta P_F \quad \text{VII-8}$$

Here $(P_A - P_B)$ is the measured pressure drop. For the case of monoliths ΔP_F contains the term for the orifice effect of

$$\Delta P_F = \Delta P_{\text{measured}} - \Delta P_{\text{orifice}} + g \rho_L L_L \quad \text{VII-9}$$

Here the static head is equal to

$$\Delta P_{\text{static}} = g \rho_L L_L \quad \text{VII-10}$$

For the total length of reactor L_T can be estimated as $L_R V_L / (V_L + V_G)$ assuming very thin liquid film between gas bubble and web wall. Some values of $\Delta P_{\text{measured}}$, $\Delta P_{\text{orifice}}$, and ΔP_{static} are given in Table 3. For representative flow condition $\Delta P_{\text{orifice}}$ is calculated from Equation (VI-4)p. and P_{static} from Eq. (VI-10), p. . It is seen that over most conditions of interest, the major contribution to pressure drop is the frictional flow term.

7-II

Theoretical Analysis of Data

In two phase monolithic flow, the gas phase moves as long bubbles with a distorted circular cross section. As mentioned earlier, there is a liquid film between the gas bubble and passage-way walls and gas bubbles are separated from each other by liquid slugs. For both the gas and the liquid phase, Navier-Stokes Equations can be written. The Reynold numbers for each phase based on that phase's density, viscosity, superficial velocity and A range up to 160. Therefore, interstitial terms in these equations must be retained. The gravitational term in the gas phase equation can be ignored.

$$V_L \nabla V_L = -\nabla P + \mu_L \nabla^2 V_L + \rho_L g \quad \text{VII-11}$$

$$V_G \nabla V_G = -\nabla P + \mu_G \nabla^2 V_G \quad \text{VII-12}$$

Further, the surface of the bubble and the boundary conditions must be defined. For moving gas-liquid interface in a capillary tube, tangential and normal components of the velocity vector must be the same for both phases on interface or in other words, they must be

TABLE 3

SOME VALUES OF $\Delta P_{\text{measured}}$, $\Delta P_{\text{orifice}}$, ΔP_{static} (Values of ΔP 's given as cm. water/4 ft of column, and velocities are superficial velocities)

		$\Delta P_{\text{measured}}$	$\Delta P_{\text{orifice}}$	ΔP_{static}
WATER-AIR 200 CELL				
$V_L = 1.31$ cm/s	3" BLOCK	12.56	2.17	1.92
	6" BLOCK	17.07	1.01	1.92
$V_L = 3.95$ cm/s	3" BLOCK	32.19	6.39	5.57
	6" BLOCK	44.50	2.98	5.57
C ₆ H ₁₂ -AIR 200 CELL				
$V_L = 1.31$ cm/s	3" BLOCK	8.53	1.73	1.50
	6" BLOCK	14.65	.81	1.50
$V_L = 3.95$ cm/s	3" BLOCK	26.09	5.03	4.35
	6" BLOCK	36.45	2.35	4.35
WATER-AIR 300 CELL				
$V_L = 1.31$ cm/s	3" BLOCK	25.00	5.53	1.92
	6" BLOCK	19.40	2.58	1.92
$V_L = 3.95$ cm/s	3" BLOCK	57.50	16.30	5.58
	6" BLOCK	52.90	7.61	5.58

continuous through the interface, (Levich, 1962). A third boundary condition is the no-slip condition at channel walls. Furthermore, bubble and slug lengths must also be defined. Unfortunately no experimental data exists in literature to be used here.

The bubble surface is defined by two sets of tensor-based differential equations and the preceding boundary conditions. First the normal components of the stress tensor must be continuous across the interface or

$$\tau_{nn}^{(L)} + \tau_{\sigma} = \tau_{nn}^{(G)} \quad (\text{Levich, 1962}) \quad \text{VII-13}$$

Where τ_{σ} is the normal force due to surface tension and is given by the Laplace equation.

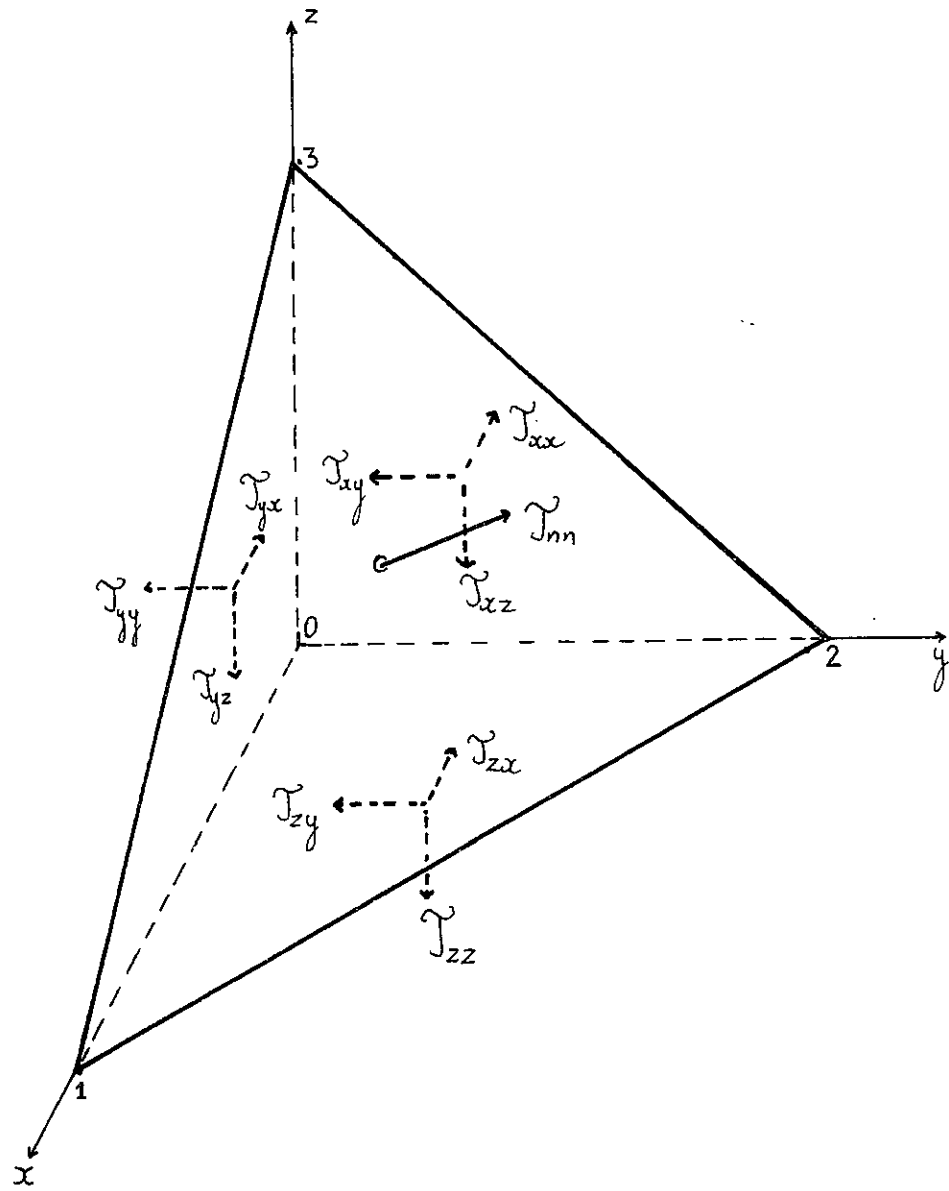
$$\tau_{\sigma} = \sigma \left(\frac{1}{R_1} + \frac{1}{R_2} \right) \quad \text{VII-14}$$

For example, for revolutionary three dimensional surfaces, the radii of curvature R_1 and R_2 are expressed in Cartesian space as

$$R_1 = \frac{[1 + (\partial z / \partial x)^2]}{\partial^2 z / \partial x^2} \quad \text{and} \quad R_2 = z \left(\frac{\partial z}{\partial x} \right) [1 + (\partial z / \partial x)^2]^{1/2} \quad \text{VII-15}$$

Here $z = f(x,y)$ is the equation defining bubble surface.

The normal stress tensor τ_{nn} itself is a function of nine stress tensors. For a better understanding of τ_{nn} consider an infinitesimal tetrahedron of fluid as shown in Figure 36. The normal stress tensor τ_{nn} which is normal to the inclined surface of the tetrahedron will be calculated. Nine stresses on reference planes 0 1 3, 0 1 2, 0 2 3 are as follows:



STRESS TENSORS

FIGURE 36

$$\begin{pmatrix} \tau_{xx} & \tau_{xy} & \tau_{xz} \\ \tau_{yx} & \tau_{yy} & \tau_{yz} \\ \tau_{zx} & \tau_{zy} & \tau_{zz} \end{pmatrix} \quad \text{VII-16}$$

If the directional cosines of the τ_{nn} are ℓ , m , n , these cosines can be utilized to relate areas of the prism faces in the following manner

$$0 \ 2 \ 3 = (123)\ell, \quad 0 \ 1 \ 3 = (123)m, \quad 0 \ 1 \ 2 = (123)n \quad \text{VII-17}$$

using Newtons law of motion and disregarding gravity, one gets

$$\begin{aligned} \tau_{nn} = & \tau_{xx}\ell^2 + \tau_{yy}m^2 + \tau_{zz}n^2 + \tau_{xy}\ell m + \tau_{yx}m\ell \\ & + \tau_{yz}mn + \tau_{zy}nm + \tau_{zx}n\ell + \tau_{xz}\ell n \end{aligned} \quad \text{VII-18}$$

Here, directional cosines of τ_{nn} are also directional cosines of normal of the face 123. Therefore, they can be calculated and related to partial derivatives of $z = f(x,y)$. Landau, et al. (1959). gives the stress tensor components

$$\tau_{ik} = -P\delta_{ik} + \mu \left[\frac{\partial v_i}{\partial x_k} + \frac{\partial v_k}{\partial x_i} \right] \quad \text{VII-19}$$

and $\delta_{ik} = 0$ when $i \neq k$

$\delta_{ik} = 1$ when $i = k$

the second equation defining bubble surface is the continuity of tangential stress component across the interface or

$$\tau_{nt}^{(L)} = \tau_{nt}^{(G)} \quad \text{VII-20}$$

in a similar manner this equation can be expended to its individual terms.

Navier-Stokes equations and some of the boundary conditions are summarized in Table 4.

It is not possible, even with numerical methods, to solve this set of equations. Therefore, one turns to dimensionless analysis as a more promising and more practical approach from the engineering point of view.

7-III

Dimensional Analysis

The frictional pressure drop per unit reactor length can be expressed as a function of the physical properties of the phases, flow rates, surface tension, gravity and the characteristic dimensions of the system. The effect of these variables on pressure drop was discussed qualitatively in the previous chapter.

Mathematically, one may write

$$\frac{\Delta P}{L} = f(\rho_L, \mu_L, \rho_G, \mu_G, V_L, V_G, \sigma, g, A, L_M) \quad \text{VII-21}$$

Using methods described by Langhaar (1951), one finds there are 8 independent variables. Indeed dimensionless analysis gives the following equation:

$$\frac{A\Delta P}{L_R(\rho_L V_L^2)} = f\left(\frac{\rho_L V_L A}{\mu_L}, \frac{\rho_G V_G A}{\mu_G}, \frac{\rho_L V_L^2 A}{\sigma}, \frac{V_L^2}{gA}, \frac{\rho_G}{\rho_L}, \frac{V_G}{V_L}, \frac{L_M}{L_A}\right) \quad \text{VII-22}$$

TABLE 4

EQUATIONS OF FLOW

Navier Stokes Equation

$$V_L \nabla V_L = -\nabla p + \mu_L \nabla^2 V_L + \rho_L g$$

$$V_G \nabla V_G = -\nabla p + \mu_G \nabla^2 V_G$$

Equations defining bubble surface

$$\tau_{nn}^{(L)} + \tau_G = \tau_{nn}^{(G)*} \quad \text{at bubble surface}$$

$$\tau_{nt}^{(L)} = \tau_{nt}^{(G)} \quad \text{at bubble surface}$$

Boundary conditions

$$I \quad v_t^{(L)} = v_t^{(G)} \quad \text{and} \quad v_n^{(L)} = v_n^{(G)}$$

II No slip at web walls

III L_{SLUG} and L_{BUBBLE} is known

* For example where

$$\tau_{nn} = \tau_{xx} n^2 + \tau_{yy} m^2 + \tau_{zz} n^2 + \tau_{xy} 2m + \tau_{yx} m^2 + \tau_{yz} mn + \tau_{zy} nm + \tau_{zx} n^2 + \tau_{xz} n^2$$

$$\text{and } \tau_{ik} = -p \delta_{ik} + \mu \left[\frac{\partial v_i}{\partial x_k} + \frac{\partial v_k}{\partial x_i} \right]$$

$$\delta_{ik} = 0 \quad \text{if } i \neq k, \quad \delta_{ik} = 1 \quad \text{if } i = k$$

Landau, et al. (1959).

Where the left hand side is the Euler number, the ratio of pressure drop force to inertia force. The first term on the right hand side is the Reynolds number based on liquid properties and flow rate and is the ratio of liquid inertia force to friction force due to liquid. The second term is the gas phase Reynolds number and has the same type of definition but expressed for the gas phase. The third group is the Weber number and is the ratio of inertia force due to liquid to surface tension forces. It carries the effect of surface tension. The fourth group is the Froude number and is the ratio of liquid inertia force to gravity of liquid. The last three groups are the characteristic length ratio, velocity ratio and density ratios and their main function is to complete the set of independent dimensionless groups. Here most of the groups, except the gas phase Reynolds number contains the liquid inertia force ($\rho_L V_L^2/A$) rather than gas phase inertia force ($\rho_G V_G^2/A$). $\rho_L V_L^2/A$ are usually more important than $\rho_G V_G^2/A$ in our flow rates; furthermore, in an independent set of dimensionless groups, it does not matter.

The exponents of these groups were determined by multi-linear regression analysis using an IBM 1130 computer scientific subrouting package. A total of 281 (Appendix C - D) data points were available and used, 96 of these were for water in 200 cell monoliths and 96 for water in 360 cell monoliths. Cyclohexane measurements were represented by 89 data points in 200 cell material. Data were distributed over a gas superficial velocity range of 20-150 cm/s and liquid superficial velocity range of 0.3-7 cm/s. The results of this analysis are given in Table 5.

TABLE 5

Variable	Mean	Standard Deviation	Correlation Coefficient	Regression Coefficient	Computed T Value
LOG(V_G/V_L)	1.51820	.464202	.927001	-2.71303	-1.93487
LOG (WE)	-1.49097	.876410	-.919389	1.19959	1.12980
LOG (FR)	-0.99070	.851970	-.971457	-1.97026	-5.12414
LOG (RE _L)	1.63236	.436022	-.894568	-2.50859	-7.43856
LOG (RE _G)	2.04482	.213600	.146330	3.18098	2.26852
LOG(L _M /A)	1.90065	.167918	.024775	0.435348	15.7955
LOG(ρ_g/ρ_L)	-2.88533	.050291	.010368	-6.00354	-1.69147
Dependent					
LOG (EU)	.38473	.580895			

Intercept. -16.219

Multiple Correlation Coefficient .99338

Analysis of Variance for the Regression

Source of Variation	Degrees of Freedom	Sum of Squares	Mean Squares	F Value
Attributable to regression	7	93.2375	13.31964	2919.05
Deviation from regression	273	1.24569	0.00456	
Total	280	94.4832		

TABLE 5 (Continued)

EQUATION

$$EU = 10^{-16.219} \frac{V_G}{V_L}^{-2.71303} WE^{1.19959} FR^{-1.97026} RE_L^{-2.50859} RE_G^{3.18098} \frac{L_M}{A}^{0.435348} \frac{\rho_G}{\rho_L}^{-6.00354}$$

The partial correlation coefficient shows the relation between dependent and the independent variables. It takes values between -1 and 1. Its absolute value should be higher than a critical value which is dependent on the degrees of freedom and the confidence interval. For 273 degrees of freedom and 95% confidence interval, the value of the critical correlation coefficient is calculated as 0.118 (Owen, 1962). For (L_M/A) and (ρ_G / ρ_G) actual value of coefficient is less than the critical one for 95% confidence interval, meaning the lower confidence intervals for these three variables.

t values may be used also as a test for the contribution of each variable. A t value lower than the critical t value specified for that particular number of degrees of freedom and confidence interval, means that the regression coefficient or the exponent of the variable is not significantly different than zero for the chosen significance level. For 95% confidence level and 273 degrees of freedom, critical t value is 0.1960 (Crow, Davis, Maxfield, 1960). t values were found to be lower for Weber number, (V_G/V_L) and (ρ_G/ρ_L) than critical values for 95% confidence level. But for 90% confidence interval, only Weber number's t value was lower than the critical t value of 1.645.

The multiple correlation coefficient is higher than its critical value of 0.2214 for 95% confidence limit and 273 degrees of freedom. This test is equivalent to the F test and both show for values higher than critical ones that the variance accounted for regression is smaller than could be reasonably expected for any practical significance level, if all the true partial regression coefficients were zero. As one expects, F value is higher than its critical value of

1.94 for 95% confidence level.

Although the equation finally developed has some statistical drawbacks, it is the equation calculated from dimensional analysis. 79% of the data points fall within $\pm 20\%$ deviation interval and average deviation of all the data points is 13 percent. The lack of statistical significance for (ρ_G/ρ_L) is most probably due to small changes in its value.

If one assumes (ρ_G/ρ_L) is constant and eliminates it and then applies the regression analysis, results obtained are shown in Table 6. In this case, critical t values and partial correlation coefficient stay the same in limits of accuracy for 95% confidence level. Multiple correlation coefficient's critical value calculated to be .21 (Owen 1962).

The partial correlation coefficient for (L_M/A) given in Table 6 is lower than the critical value, meaning that much lower confidence levels. Multiple correlation coefficient, F value ($F_{\text{critical}} = 2.01$) and t values of each variable are higher than their corresponding critical values for 95% confidence interval and 274 degrees of freedom. The average deviation of data is again $\pm 13\%$ and the equation expresses 81% of the data within ± 20 percent. Statistically, correlation is somewhat improved and at the same time its accuracy retained. This equation only can be used for cases involving liquid phases with densities between water and cyclohexane and gas phases with densities close to atmospheric air density.

If one eliminates the (L_M/A) and (ρ_G/ρ_L) from the original equation, statistically excellent correlation coefficients, t and F values yields, but average deviation of data is ± 18 percent from

TABLE 6

Variable	Mean	Standard Deviation	Correlation Coefficient	Regression Coefficient	Computed T Value
LOG(V _G /V _L)	1.51820	.464202	.927001	-4.817	-6.98966
LOG (WE)	-1.49097	.876410	-.919389	-0.589005	-6.19286
LOG (FR)	-0.99070	.851970	-.971457	-1.33526	-15.2360
LOG (RE _L)	1.63236	.436022	-.894568	-2.3034	-6.87776
LOG (RE _G)	2.04482	.213600	.146330	5.28034	7.66137
LOG (L _M /A)	1.90065	.167918	0.024775	0.434036	14.8052

Dependent		
LOG (EU)	.38473	.580895

Intercept -2.36543

Multiple Correlation Coefficient .99338

Analysis of Variance for the Regression

Source of Variation	Degrees of Freedom	Sum of Squares	Mean Squares	F Value
Attributable to regression	6	93.06752	15.51125	3002.15
Deviation from regression	274	1.41568	0.00516	
Total	280	94.48320		

EQUATION: $EU = 10^{-2.36543} \frac{V_G}{V_L}^{-4.817} WE^{-0.589005} FR^{-1.33526} RE_L^{-2.3034} RE_G^{5.28034} \frac{L_M}{A}^{0.434036}$

TABLE 7

Variable	Mean	Standard Deviation	Correlation Coefficient	Regression Coefficient	Computed T Value
LOG(V _G /V _L)	1.51820	.464202	.92701	-2.15988	-2.35167
LOG (WE)	-1.49097	.876410	-.919389	-0.276337	-2.15863
LOG (FR)	-0.9907	.851970	-.971457	-0.901950	-7.90963
LOG (RE _L)	1.63236	.436022	-.894568	-1.13466	-2.52548
LOG (RE _G)	2.04482	.213600	.146330	2.62149	2.85408
Dep ndent					
LOG (EU)	.38473	.580895			

Intercept -1.15001

Multiple Correlation Coefficient .98556

Analysis of Variance For the Regression

Source of Variation	Degrees of Freedom	Sum of Squares	Mean Squares	F Value
Attributable to Regression	5	91.77543	18.35508	1864.14
Deviation From Regression	275	2.70776	0.00984	
Total	280	94.48320		

EQUATION: $EU = 10^{-1.15001} \frac{V_G}{V_L}^{-2.15988} WE^{-0.276337} FR^{-0.901950} RE_L^{-1.13466} RE_G^{2.62149}$

the resulted equation and this equation expresses only 63% of the data within $\pm 20\%$ limits (Table 7). Furthermore, this equation does not contain all the independent groups given by dimensional analysis.

After all is said and done, however, one cannot really recommend the use of these empirical equations for several reasons. First, the uncertainty in the value of ΔP_{or} causes a corresponding uncertainty in ΔP_f . Secondly, the use of power functions may not be the best form of correlation. Thirdly, the large number of adjustable parameters available permits reasonably good fitting of the data in any event.

8 - CONCLUSIONS

Conclusions

1. The comparison of pressure drop measurements using different liquid distributors showed that the pressure drop is extremely sensitive to the degree of uniformity of the initial distribution of liquid. A distributor design, termed here distributor No. 3, seemed to perform very well.
2. A study of two phase flow in a single capillary showed that a slug flow regime may exist in monoliths under the flow conditions considered, and that the pressure drop behavior is very sensitive to the type of flow regime encountered.
3. Comparison of measured pressure drops in monoliths with those encountered with conventional catalyst supports showed much lower pressure drops for monoliths.
4. An orifice effect caused by the discontinuity between adjacent monolith blocks may make a significant contribution to the pressure drop, depending on flow conditions.
5. For a fixed total length of stacked monolith blocks, the pressure drop is a function of the length of individual blocks. This is in part an orifice effect (see Section 6) but also may reflect redistribution of gas and liquid.
6. Since some uncertainties remain about the details of the flow pattern it was not attempted to solve the equations of flow for this system.
7. Provided that good initial liquid and gas distribution can be obtained, stacked monolith beds have the potential advantage over conventional packings of (a) providing low pressure drop, (b) allowing

deep beds to be constructed without intermediate supports, (c) minimizing radial dispersion and liquid flow to the wall, (d) permitting higher effectiveness factors under some circumstances.

9 - RECOMMENDATIONS

1. Mass transfer studies are needed to evaluate the effectiveness of gas and liquid contacting with the solid.
2. The degree of axial dispersion as a function of flow parameters needs to be determined.
3. The degree of radial dispersion as a function of vertical distance and of distributor design is important to know.

10-1 APPENDIX A

Ratios of Superficial Areas for Spherical and
Monolith Packing and Void Fractions

If there are n pellets in a cylindrical reactor with a volume of R^2h , then the superficial area for the spherical pellets is expressed as

$$\frac{4nr^2}{R^2h} \quad (A1)$$

Since void fraction θ is given as 37.5% by McGreary(1961)

$$1 - \theta = 0.625 = \frac{4}{3} \cdot \frac{n\pi r^3}{\pi R^2 h} = \frac{4}{3} \cdot \frac{nr^3}{R^2 h} \quad (A2)$$

and placing (A2) in (A1) we get

$$\text{Superficial area for spherical pellets} = \frac{1.875}{r} \quad (A3)$$

For monolith packing with hole dimensions of ℓ , wall thickness of a , and m number of holes per unit area,

$$\text{Superficial area} = \frac{4\ell h m \pi R^2}{\pi R^2 h} = 4m\ell \quad (A4)$$

We can also write that for a square monolith,

$$1 - 2a\sqrt{m} \cdot \ell = m\ell^2 \quad (A5)$$

From Eq. (A5),

$$\ell = \sqrt{\frac{1 - 2a\sqrt{m}}{m}} \quad (\text{A6})$$

Placing (A6) in (A4),

$$\text{Superficial area for monolith} = 4\sqrt{m(1-2a\sqrt{m})} \quad (\text{A7})$$

So the ratio of superficial areas for monoliths versus that for spheres

$$Q = \frac{\text{monolith}}{\text{spherical}} = \frac{2\sqrt{m(1-2a\sqrt{m})}}{1.875} d \quad (\text{A8 or 1})$$

The following equation is for void fractions in monoliths:

$$\theta = \frac{\pi R^2(1 - 2a\sqrt{m})h}{\pi R^2 h} = m\ell^2 = (1 - 2a\sqrt{m}) \quad (\text{A9})$$

APPENDIX B

Pressure Drop Data With Capillary Tubes

Liquid Phase: Water

Gas Phase: Air

Temperature: 18°C**

Tube Length: 102 cm

Tube I.D.: $.200914 \pm 2.54 \times 10^{-4}$ cm

I. DATA WITH LIQUID DISTRIBUTOR A

V_G (cm/s)	V_L (cm/s)	ΔP cm.water/M	ΔL (cm/s)	ΔP cm.water/M
1.05	.078	0	.26	.017
5.27	.078	0.07	.26	.07
10.51	.078	0.15	.26	0.15
15.71	.078	0.22	.26	0.24
21.03	.078	0.31	.26	0.31
26.28	.078	0.39	.26	0.44
41.00	.078	0.78	.26	0.82
52.57	.078	0.94	.26	0.99
65.71	.078	1.19	.26	1.24
78.85	.078	1.45	.26	1.51
91.99	.078	1.67	.26	1.78
105.14	.078	1.89	.26	2.03
118.28	.078	2.13	.26	2.26
131.42	.078	2.33	.26	2.52
144.57	.078	2.60	.26	2.77

DATA WITH LIQUID DISTRIBUTOR A (Cont'd)

V_G (cm/s)	V_L cm/s	ΔP cm.water/M	ΔL cm/s	ΔP cm.water/M
157.71	.078	2.8	.26	3.00
1.05	.52	-.03	.788	-.03
5.27	.52	.05	.788	.05
10.51	.52	.12	.788	.14
15.71	.52	.22	.788	.20
21.03	.52	.31	.788	.31
26.28	.52	.44	.788	.44
41.00	.52	.80	.788	.83
52.57	.52	.99	.788	1.00
65.71	.52	1.24	.788	1.29
78.85	.52	1.50	.788	1.57
91.99	.52	1.75	.788	1.80
105.14	.52	2.01	.788	2.09
118.28	.52	2.28	.788	2.35
131.42	.52	2.52	.788	2.62
144.57	.52	2.78	.788	2.89
157.71	.52	3.01	.788	3.13
1.05	1.05	-.033	1.31	-.05
5.27	1.05	.03	1.31	0.03
10.51	1.05	.15	1.31	0.15
15.71	1.05	.2	1.31	0.19
21.03	1.05	.31	1.31	0.31
26.28	1.05	.44	1.31	0.43
41.00	1.05	.82	1.31	0.73

DATA WITH LIQUID DISTRIBUTOR A (Cont'd)

V_G (cm/s)	V_L cm/s	ΔP cm.water/M	ΔL cm/s	ΔP cm.water/M
52.57	1.05	1.03	1.31	1.07
65.71	1.05	1.33	1.31	1.40
78.85	1.05	1.57	1.31	1.68
91.99	1.05	1.91	1.31	1.99
105.14	1.05	2.16	1.31	2.31
118.28	1.05	2.47	1.31	2.64
131.42	1.05	2.69	1.31	2.89
144.57	1.05	3.00	1.31	3.25
157.71	1.05	3.27	1.31	3.39
1.05	1.58	-.09	1.84	Unstable
5.27	1.58	0	1.84	Slug
10.51	1.58	.14	1.84	Flow
15.71	1.58	.19	1.84	"
21.03	1.58	.29	1.84	"
26.28	1.58	.44	1.84	"
41.00	1.58	.87	1.84	"
52.57	1.58	1.11	1.84	"
65.71	1.58	1.41	1.84	"
78.85	1.58	1.75	1.84	"
91.99	1.58	2.03	1.84	"
105.14	1.58	2.32	1.84	"
118.28	1.58	2.59	1.84	"
131.42	1.58	2.91	1.84	Slug
144.57	1.58	3.23	1.84	Flow
157.71	1.58	3.50	1.84	

II. DATA WITH LIQUID DISTRIBUTOR B

V_G (cm/s)	V_L cm/s	ΔP cm.water/M	ΔL cm/s	ΔP cm.water/M
1.05	.078	-4.39	.26	-11.22
5.27	.078	-.98	.26	-3.22
10.51	.078	—	.26	-1.27
15.71	.078	.45	.26	-0.68
21.03	.078	.45	.26	-0.39
26.28	.078	.45	.26	0.16
41.00	.078	1.08*	.26	1.00
52.57	.078	1.68*	.26	2.35
65.71	.078	1.87*	.26	—
78.85	.078	2.02*	.26	— *
91.99	.078	1.89*	.26	2.02*
105.14	.078	2.10*	.26	2.19*
118.28	.078	2.27*	.26	2.35*
131.42	.078	2.44*	.26	2.78*
144.57	.078	2.86*	.26	2.86*
157.71	.078	3.12*	.26	3.12*
1.05	.52	-18.24	.788	-26.34
5.27	.52	-5.85	.788	-9.56
10.51	.52	-2.24	.788	-5.56
15.71	.52	-1.85	.788	-3.22
21.03	.52	-0.97	.788	-1.85
26.28	.52	-0.135	.788	-0.41
41.00	.52	1.31	.788	1.00
52.57	.52	1.85	.788	1.47

DATA WITH LIQUID DISTRIBUTOR B (Cont'd)

V_G (cm/s)	V_L cm/s	ΔP cm.water/M	ΔL cm/s	ΔP cm.water/M
65.71	.52	2.02	.788	2.10
78.85	.52	2.19	.788	2.52
91.99	.52	2.35*	.788	2.78
105.14	.52	2.61*	.788	2.95
118.28	.52	2.86*	.788	3.29
131.42	.52	3.12*	.788	4.05*
144.57	.52	3.37*	.788	4.56*
157.71	.52	3.54*	.788	4.90*
1.05	1.05	-29.56	1.31	-35.3
5.27	1.05	-11.90	1.31	-13.36
10.51	1.05	-5.56	1.31	-5.95
15.71	1.05	-4.58	1.31	-4.0
21.03	1.05	-2.63	1.31	-1.95
26.28	1.05	-0.39	1.31	-0.48
41.00	1.05	1.00	1.31	1.00
52.57	1.05	1.51	1.31	1.68
65.71	1.05	2.35	1.31	2.69
78.85	1.05	2.86	1.31	3.71
91.99	1.05	3.88	1.31	4.73
105.14	1.05	4.22	1.31	5.74
118.28	1.05	5.06	1.31	6.93
131.42	1.05	5.74	1.31	7.61
144.57	1.05	6.59	1.31	8.45
157.71	1.05	7.09	1.31	8.96

DATA WITH LIQUID DISTRIBUTOR B (Cont'd)

V_G (cm/s)	V_L cm/s	ΔP cm.water/M	ΔL cm/s	ΔP cm.water/M
1.05	1.58	-39.7	1.84	-42.10
5.27	1.58	-18.34	1.84	-21.50
10.51	1.58	-	1.84	-8.09
15.77	1.58	-5.74	1.84	-7.60
21.03	1.58	-3.5	1.84	-3.40
26.28	1.58	-1.07	1.84	-.78
41.00	1.58	.49	1.84	.80
51.57	1.58	1.42	1.84	2.44
65.71	1.58	2.78	1.84	3.20
78.85	1.58	4.05	1.84	4.56
91.99	1.58	5.49	1.84	5.74
105.14	1.58	6.76	1.84	6.67
118.28	1.58	8.45	1.84	7.94
131.42	1.58	8.79	1.84	9.13
144.57	1.58	9.47	1.84	9.64
157.71	1.58	9.41	1.84	10.15
1.05	2.10	-45.60	2.63	-50.10
5.27	2.10	-21.00	2.63	-24.40
10.51	2.10	-12.00	2.63	-14.10
15.77	2.10	-7.80	2.63	-9.20
21.03	2.10	-4.48	2.63	-4.97
26.28	2.10	-2.24	2.63	-2.44
41.00	2.10	1.00	2.63	1.42
51.57	2.10	2.18	2.63	2.69

DATA WITH LIQUID DISTRIBUTOR B (Cont'd)

V_G (cm/s)	V_L cm/s	ΔP cm.water/M	ΔL cm/s	ΔP cm.water/M
65.71	2.10	3.62	2.63	4.52
78.85	2.10	4.90	2.63	5.81
91.99	2.10	6.42	2.63	7.44
105.14	2.10	7.60	2.63	8.96
118.28	2.10	8.45	2.63	9.98
131.42	2.10	9.30	2.63	10.82
144.57	2.10	10.48	2.63	11.84
157.71	2.10	11.16	2.63	12.35

* Annular Flow Regime

** Physical Properties of both phases can be found in (Lange, 1967)

APPENDIX C

PRESSURE DROP DATA WITH 200 CELL/IN² MONOLITHS⁺

C-I. DATA WITH DISTRIBUTOR 1

Distributor: Distributor 1

Liquid Phase: Water

Gas Phase: Air

Column Length: 4 ft

Block Length: 6 in

Temperature: 20°C

V_G (cm/s)	V_L (cm/s)	ΔP cm,water/4 ft	V_L (cm/s)	ΔP cm,water/4 ft
6.51	.434	—	1.737	-3.1
8.68	.434	1.49	1.737	-1.1
10.85	.434	1.65	1.737	0.36
13.02	.434	1.79	1.737	1.27
15.20	.434	1.93	1.737	1.72
17.36	.434	2.07	1.737	2.10
19.54	.434	2.19	1.737	2.55
21.70	.434	2.27	1.737	2.78
23.88	.434	2.36	1.737	3.19
26.04	.434	2.45	1.737	3.49
28.22	.434	2.59	1.737	3.84

⁺Velocities reported in this appendix are superficial velocities.

DATA WITH DISTRIBUTOR 1 (Cont'd)

V_G (cm/s)	V_L cm/s	ΔP cm.water/4 ft	V_L cm/s	ΔP cm.water/4 ft
30.39	.434	2.67	1.737	4.08
32.56	.434	2.80	1.737	4.36
34.73	.434	2.90	1.737	4.69
36.91	.434	3.00	1.737	4.88
39.07	.434	3.14	1.737	5.14
41.25	.434	3.25	1.737	5.45
51.23	.434	3.80	1.737	7.22
61.47	.434	4.56	1.737	8.35
71.72	.434	5.22	1.737	9.43
81.96	.434	5.92	1.737	10.61
92.20	.434	7.08	1.737	11.65
108.54	.434	7.10	1.737	11.00
130.24	.434	8.10	1.737	12.10
151.96	.434	9.40	1.737	14.10
173.67	.434	10.80	1.737	15.8
195.37	.434	12.00	1.737	17.5
6.51	3.47	-6.50	5.21	-12.2
8.68	3.47	-2.10	5.21	-4.6
10.85	3.47	0	5.21	-1.40
13.02	3.47	1.53	5.21	1.15
15.20	3.47	1.91	5.21	2.12
17.36	3.47	2.27	5.21	3.00
19.54	3.47	2.71	5.21	3.75

DATA WITH DISTRIBUTOR 1 (Cont'd)

V_G (cm/s)	V_L cm/s	ΔP cm.water/4 ft	V_L cm/s	ΔP cm.water/4 ft
21.70	3.47	2.95	5.21	4.10
23.88	3.47	3.28	5.21	4.70
26.04	3.47	3.72	5.21	5.31
28.22	3.47	4.09	5.21	5.95
30.39	3.47	4.39	5.21	6.53
32.56	3.47	5.05	5.21	7.22
34.73	3.47	5.57	5.21	7.65
36.91	3.47	6.00	5.21	8.35
39.07	3.47	6.25	5.21	8.70
41.25	3.47	6.60	5.21	9.31
51.23	3.47	8.70	5.21	12.26
61.47	3.47	10.40	5.21	14.55
71.72	3.47	13.12	5.21	16.77
81.96	3.47	15.10	5.21	19.03
92.20	3.47	16.94	5.21	22.20
108.54	3.47	16.60	5.21	24.00
130.24	3.47	19.00	5.21	27.20
151.96	3.47	22.70	5.21	30.50
173.67	3.47	25.90	5.21	34.50
195.37	3.47	29.00	5.21	39.50
6.51	6.95	-12.5	8.68	-14.4
8.68	6.95	-5.4	8.68	-6.5
10.85	6.95	-1.3	8.68	-0.7

DATA WITH DISTRIBUTOR 1 (Cont'd)

V_G (cm/s)	V_L cm/s	ΔP cm.water/4 ft	V_L cm/s	ΔP cm.water/4 ft
13.02	6.95	1.4	8.68	2.15
15.20	6.95	2.79	8.68	3.83
17.36	6.95	3.97	8.68	5.31
19.54	6.95	4.96	8.68	6.82
21.70	6.95	5.48	8.68	7.48
23.88	6.95	6.35	8.68	8.52
26.04	6.95	6.87	8.68	9.56
28.22	6.95	7.74	8.68	10.61
30.39	6.95	8.61	8.68	11.39
32.56	6.95	9.39	8.68	12.78
34.73	6.95	10.35	8.68	13.73
36.91	6.95	10.95	8.68	14.70
39.07	6.95	11.73	8.68	15.29
41.25	6.95	12.52	8.68	16.50
51.23	6.95	16.16	8.68	20.07
61.47	6.95	19.40	8.68	24.00
71.72	6.95	23.20	8.68	27.4
81.96	6.95	26.50	8.68	31.00
92.20	6.95	29.40	8.68	35.20
108.54	6.95	31.50	8.68	40.50
130.24	6.95	36.50	8.68	47.10
151.96	6.95	41.50	8.68	53.00
173.67	6.95	46.00	8.68	59.00
195.37	6.95	50.50	8.68	65.50

Distributor: Distributor 1

Liquid Phase: Water

Gas Phase: Air

Column Length: 4 ft

Block Length: 3 in

Temperature: 20°C*

V_G (cm/s)	V_L (cm/s)	ΔP cm.water/4 ft	V_L (cm/s)	ΔP cm.water/4 ft
1.30	.434	-5.7	1.737	-26
4.34	.434	.21	1.737	-7.2
8.68	.434	1.75	1.737	.23
21.71	.434	3.87	1.737	6.53
43.41	.434	5.30	1.737	9.43
65.13	.434	6.91	1.737	12.38
86.82	.434	8.25	1.737	14.73
108.54	.434	9.86	1.737	17.07
130.24	.434	11.34	1.737	19.40
151.96	.434	12.82	1.737	22.80
173.67	.434	14.53	1.737	24.60
195.37	.434	16.41	1.737	27.30
1.30	3.47	-39.3	5.21	-47.00
4.34	3.47	-11.70	5.21	-14.50
8.68	3.47	1.22	5.21	1.01
21.71	3.47	7.52	5.21	12.47
43.41	3.47	11.86	5.21	20.00

V_G (cm/s)	V_L cm/s	ΔP cm.water/4 ft	V_L cm/s	ΔP cm.water/4 ft
65.13	3.47	16.29	5.21	26.00
86.82	3.47	20.80	5.21	32.50
108.54	3.47	24.00	5.21	39.50
130.24	3.47	28.20	5.21	45.20
151.96	3.47	33.00	5.21	51.80
173.67	3.47	37.6	5.21	59.00
195.37	3.47	43.0	5.21	63.50
1.30	6.95	-49.5	8.68	-50.20
4.34	6.95	-16.4	8.68	-17.00
8.68	6.95	1.61	8.68	3.50
21.71	6.95	17.20	8.68	24.00
43.41	6.95	27.50	8.68	38.00
65.13	6.95	37.00	8.68	50.00
86.82	6.95	46.50	8.68	60.00
108.54	6.95	56.50	8.68	70.00
130.24	6.95	65.00	8.68	79.00
151.96	6.95	73.00	8.68	90.00
173.67	6.95	79.00	8.68	96.50
195.37	6.95	86.50	8.68	104.00

C-II

DATA WITH DISTRIBUTOR 3

Distributor: Distributor 3

Liquid Phase: Water

Gas Phase: Air

Column Length: 4 ft

Block Length: 6 in

Temperature: 21°C*

V_G (cm/s)	V_L (cm/s)	ΔP cm.water/4 ft	V_L (cm/s)	ΔP cm.water/4 ft
.987	.329	-1.0	1.316	-11.7
3.29	.329	1.5	1.316	-4.2
6.58	.329	2.0	1.316	1.5
16.45	.329	3.5	1.316	5.5
32.89	.329	5.1	1.316	9.0
49.34	.329	6.0	1.316	12.0
65.78	.329	7.5	1.316	15.0
82.23	.329	9.1	1.316	17.1
98.67	.329	10.5	1.316	19.5
115.12	.329	12.0	1.316	21.0
131.57	.329	13.8	1.316	23.5
148.01	.329	15.9	1.316	26.1
.987	2.631	-23.0	3.947	-26.0
3.29	2.631	-8.0	3.947	-9.0
6.58	2.631	0.6	3.947	1.4
16.45	2.631	7.5	3.947	10.5
32.89	2.631	15.5	3.947	21.5
49.34	2.631	22.0	3.947	31.5
65.78	2.631	25.2	3.947	38.5

V_G (cm/s)	V_L cm/s	ΔP cm.water/4 ft	V_L cm/s	ΔP cm.water/4 ft
82.23	2.631	28.5	3.947	44.5
98.67	2.631	32.0	3.947	50.0
115.12	2.631	34.5	3.947	54.0
131.57	2.631	38.0	3.947	58.5
148.01	2.631	42.0	3.947	61.5
.987	5.262	-6.6	6.578	-6.6
3.29	5.262	-5.5	6.578	-2.3
6.58	5.262	2.4	6.578	2.5
16.45	5.262	10.5	6.578	13.0
32.89	5.262	24.1	6.578	29.5
49.34	5.262	38.8	6.578	46.9
65.78	5.262	49.1	6.578	58
82.23	5.262	56.2	6.578	67.6
98.67	5.262	63.1	6.578	76.5
115.12	5.262	69.4	6.578	84.1
131.57	5.262	76.2	6.578	91.5
148.01	5.262	80.5	6.578	99.2

Distributor: Distributor 3

Liquid Phase: Water

Gas Phase: Air

Column Length: 4 ft

Block Length: 3 in

Temperature: 23°C

V_G (cm/s)	V_L (cm/s)	ΔP cm.water/4 ft	V_L (cm/s)	ΔP cm.water/4 ft
.987	.329	0	1.316	-10.7
3.29	.329	1.1	1.316	-3.0
6.58	.329	1.8	1.316	2.2
16.45	.329	3.7	1.316	4.1
32.89	.329	4.4	1.316	6.7
49.34	.329	5.6	1.316	9.8
65.78	.329	6.7	1.316	11.2
82.23	.329	7.8	1.316	12.6
98.67	.329	9.0	1.316	14.6
115.12	.329	10.2	1.316	16.3
131.57	.329	11.4	1.316	17.6
148.01	.329	12.6	1.316	19.7
.987	2.631	-34.0	3.947	-48.0
3.29	2.631	-9.6	3.947	-17.1
6.58	2.631	0.0	3.947	-1.5
16.45	2.631	5.4	3.947	7.3
32.89	2.631	9.5	3.947	13.5
79.34	2.631	14.5	3.947	20.9
65.78	2.631	17.6	3.947	27.3
82.23	2.631	20.8	3.947	32.2

V_G (cm/s)	V_L cm/s	ΔP cm.water/4 ft	V_L cm/s	ΔP cm.water/4 ft
98.67	2.631	22.6	3.947	37.2
115.12	2.631	25.5	3.947	39.6
131.57	2.631	26.0	3.947	43.5
148.01	2.631	27.6	3.947	46.3
.987	5.262	-55.5	6.578	-59.8
3.29	5.262	-20.4	6.578	-23.0
6.58	5.262	-2.3	6.578	-.8
16.45	5.262	7.4	6.578	8.4
32.89	5.262	16.0	6.578	18.2
49.34	5.262	29.0	6.578	33.3
65.78	5.262	38.3	6.578	46.0
82.23	5.262	45.3	6.578	56.4
98.67	5.262	50.7	6.578	64.1
115.12	5.262	56.0	6.578	70.3
131.57	5.262	58.5	6.578	76.0
148.01	5.262	62.5	6.578	79.8

C-II

Distributor: Distributor 3
 Liquid Phase: Cyclohexane
 Gas Phase: Air
 Column Length: 4 ft
 Block Length: 6 in
 Temperature: 20.5°C*

V_G (cm/s)	V_L (cm/s)	ΔP cm.water/4 ft	V_L (cm/s)	ΔP cm.water/4 ft
.987	.371	-0.7	1.316	-4.1
3.29	.371	0.8	1.316	-1.8
6.58	.371	1.3	1.316	1.0
16.45	.371	2.7	1.316	4.5
32.89	.371	3.8	1.316	6.8
49.34	.371	5.2	1.316	9.4
65.78	.371	6.3	1.316	12.0
82.23	.371	7.8	1.316	14.6
98.67	.371	8.9	1.316	16.0
115.12	.371	-	1.316	18.4
131.57	.371	-	1.316	20.7
148.01	.371	-	1.316	22.7
.987	2.631	-5.5	3.947	-4.9
3.29	2.631	-3.3	3.947	-3.0
6.58	2.631	1.0	3.947	1.5

16.45	2.631	11.0	3.947	17.2
32.89	2.631	13.2	3.947	20.5
49.34	2.631	17.8	3.947	26.2
65.78	2.631	21.9	3.947	31.0
82.23	2.631	25.9	3.947	36.5
98.67	2.631	29.3	3.947	41.1
115.12	2.631	32.6	3.947	46.2
131.57	2.631	36.6	3.947	51.5
148.01	2.631	40.2	3.947	56.7
.987	5.262	-4.8	6.578	-5.3
3.29	5.262	-2.5	6.578	-2.1
6.58	5.262	3.1	6.578	4.4
16.45	5.262	23.7	6.578	25.0
32.89	5.262	27.5	6.578	35.5
49.34	5.262	34.8	6.578	44.0
65.78	5.262	41.0	6.578	50.7
82.23	5.262	47.3	6.578	57.3
98.67	5.262	52.7	6.578	64.0
115.12	5.262	57.9	6.578	70.5
131.57	5.262	64.4	6.578	77.5
148.01	5.262	70.0	6.578	83.0

Distributor: Distributor 3

Liquid Phase: Cyclohexane

Gas Phase: Air

Column Length: 4 ft

Block Length: 3 in

Temperature: 21.5°C*

V_G (cm/s)	V_L (cm/s)	ΔP cm.water/4 ft	V_L (cm/s)	ΔP cm.water/4 ft
.987	.371	-0.4	1.316	-3.2
3.29	.371	0.2	1.316	-1.4
6.58	.371	0.4	1.316	0.3
16.45	.371	2.4	1.316	3.5
32.89	.371	2.7	1.316	4.5
49.34	.371	3.6	1.316	5.6
65.78	.371	4.4	1.316	7.6
82.23	.371	5.4	1.316	8.6
98.67	.371	7.1	1.316	10.4
115.12	.371	-	1.316	11.8
131.57	.371	-	1.316	13.6
148.01	.371	-	1.316	14.8
.987	2.631	-13.0	3.947	-17.0
3.29	2.631	-5.3	3.947	-8.0
6.58	2.631	-0.7	3.947	-1.0
16.45	2.631	3.9	3.947	5.5
32.89	2.631	7.5	3.947	12.1

49.34	2.631	10.6	3.947	17.6
65.78	2.631	13.7	3.947	22.2
82.23	2.631	16.4	3.947	26.1
98.67	2.631	19.0	3.947	30.0
115.12	2.631	23.0	3.947	33.3
131.57	2.631	25.4	3.947	36.7
148.01	2.631	28.0	3.947	40.2
.987	5.262	-16.0	6.578	-25.0
3.29	5.262	-9.0	6.578	-11.0
6.58	5.262	-0.5	6.578	-0.5
16.45	5.262	7.5	6.578	11.0
32.89	5.262	16.9	6.578	23.2
49.34	5.262	24.4	6.578	31.4
65.78	5.262	30.2	6.578	38.5
82.23	5.262	35.1	6.578	44.2
98.67	5.262	38.7	6.578	48.6
115.12	5.262	43.1	6.578	53.7
131.57	5.262	46.7	6.578	57.0
148.01	5.262	51.4	6.578	61.8

* Physical properties of both phases can be found in Lange (1967).

APPENDIX D

Pressure Drop Data With 300 Cell/in² Monoliths[†]

Distributor: Distributor 3

Liquid Phase: Water

Gas Phase: Air

Column Length: 4 ft.

Block Length: 3 in.

Temperature: 7°C*

V_G (cm/s)	$(V_L$ cm/s	ΔP cm.water/4 ft)	$(V_L$ cm/s	ΔP cm.water/4ft)
.987	.329	.5	1.316	-8.1
3.29	.329	2.3	1.316	1.7
6.58	.329	2.8	1.316	2.4
16.45	.329	4.7	1.316	6.3
32.89	.329	6.7	1.316	11.2
49.34	.329	8.8	1.316	15.5
65.78	.329	10.5	1.316	21.0
82.23	.329	12.8	1.316	25.0
98.67	.329	14.8	1.316	28.0
115.12	.329	16.9	1.316	31.0
131.57	.329	19.1	1.316	34.5
148.01	.329	21.8	1.316	38.0
.987	2.631	-14.4	3.947	-4.5
3.29	2.631	2.0	3.947	2.3
6.58	2.631	3.5	3.947	3.6
16.45	2.631	9.5	3.947	10.0
32.89	2.631	15.3	3.947	19.0
49.34	2.631	23.0	3.947	31.0

Continued

[†] Actual count of CELLS/in² was 360 and velocities reported in this appendix are superficial velocities

Continued from previous pages

115.12	.329	16.9	1.316	31.0
131.57	.329	19.1	1.316	34.5
148.01	.329	21.8	1.316	38.0
.987	2.631	-14.4	3.947	-4.5
3.29	2.631	2.0	3.947	2.3
6.58	2.631	3.5	3.947	3.6
16.45	2.631	9.5	3.947	10.0
32.89	2.631	15.3	3.947	19.0
49.34	2.631	23.0	3.947	31.0
65.78	2.631	33.0	3.947	42.0
82.23	2.631	40.0	3.947	57.5
98.67	2.631	45.7	3.947	67.4
115.12	2.631	51.5	3.947	77.0
131.57	2.631	58.5	3.947	84.5
148.01	2.631	63.5	3.947	90.7
.987	5.262	-12.0	6.578	-8.5
3.29	5.262	2.6	6.578	2.7
6.58	5.262	4.4	6.578	4.2
16.45	5.262	9.5	6.578	11.8
32.89	5.262	20.5	6.578	22.5
49.34	5.262	37.0	6.578	40.5
65.78	5.262	54.7	6.578	58.3
82.23	5.262	69.5	6.578	77.0
98.67	5.262	83.5	6.578	94.0
115.12	5.262	96.8	6.578	108.0
131.57	5.262	102.5	6.578	121.0
148.01	5.262	110.7	6.578	133.5

Distributor: Distributor 3

Liquid Phase: Water

Gas Phase: Air

Column Length: 4 ft.

Block Length: 6 in.

Temperature: 10°C*

V_G cm/s	$\left(\begin{array}{l} V_L \\ \text{cm/s} \end{array} \right)$	ΔP cm.water/4 ft)	$\left(\begin{array}{l} V_L \\ \text{cm/s} \end{array} \right)$	ΔP cm.water/4 ft)
.987	.329	2.0	1.316	-14.8
3.29	.329	2.3	1.316	--.6
6.58	.329	2.5	1.316	2.6
16.45	.329	3.9	1.316	5.6
32.89	.329	5.2	1.316	8.8
49.34	.329	6.7	1.316	12.6
65.78	.329	8.5	1.316	15.9
82.23	.329	10.2	1.316	19.4
98.67	.329	12.4	1.316	22.0
115.12	.329	14.0	1.316	23.7
131.57	.329	16.0	1.316	26.2
148.01	.329	18.0	1.316	29.0
.987	2.631	-27.6	3.947	-40.3
3.29	2.631	-2.4	3.947	-9.5
6.58	2.631	2.4	3.947	4.3
16.45	2.631	8.8	3.947	14.7
32.89	2.631	13.4	3.947	25.4
49.34	2.631	20	3.947	36.7
65.78	2.631	26	3.947	45.3
82.23	2.631	32.6	3.947	52.9
98.67	2.631	37.8	3.947	58.6
115.12	2.631	41.3	3.947	65.6
131.57	2.631	46.4	3.947	69.3

Continued

Continued from previous pages

148.01	2.631	49.4	3.947	73.5
.987	5.262	-42.0	6.578	-30.7
3.29	5.262	-8.2	6.578	-4.0
6.58	5.262	3.8	6.578	7.1
16.45	5.262	16.4	6.578	22.9
32.89	5.262	26.5	6.578	32.7
49.34	5.262	38.5	6.578	48.0
65.78	5.262	53.0	6.578	64.0
82.23	5.262	66.0	6.578	79.5
98.67	5.262	76.7	6.578	94.5
115.12	5.262	86.2	6.578	104.0
131.57	5.262	94.3	6.578	115.4
148.01	5.262	99.0	6.578	126.0

*Physical properties of both phases can be found in (Lange, 1967)

NOMENCLATURE

- A = Dimension of square passageway (cm)
 A_B = Cross-sectional area of long cylindrical gas bubble (cm^2)
 A_O = Cross-sectional area at restricted passageway exits (cm^2)
 EU = Euler number defined as $\Delta P/(\rho V^2 L)$
 FR = Froude number defined as $V^2/(gA)$
 g = Acceleration of gravity (cm/s^2)
 h = Height (cm)
 l = Directional cosine
 L = Length (cm)
 m = Directional cosine
 n = Directional cosine
 N = Number of block joints
 P = Pressure (dyne/cm^2)
 RE = Reynolds number defined as $V\rho A/\mu$
 V = Interstitial velocity, if not specified otherwise (cm/s)
 V_{or} = Interstitial velocity at block exits (cm/s)
 V_T = Velocity defined as $(V_L + V_G)$ (cm/s)
 W = Web wall thickness (cm/s)
 WE = Weber number defined as $\rho V^2 A/\sigma$

Greek

- ΔP = Pressure drop (dyne/cm^2)
 μ = Dynamic viscosity (poise)
 V = Volume (cm^3)
 ρ = Density (g/cm^3)
 σ = Surface tension (dyne/cm)
 τ = Stress tensor component

Subscripts

- F = Related to friction
- g,G = Gas phase
- l,L = Liquid phase
- M = Related to monolith block
- R = Related to reactor of column
- n = Normal
- t = Tangential

LITERATURE CITATIONS

- Aroesty, J., and J. F. Gross, "Convection and Diffusion in the Microcirculation" Microvascular Research 2, 247 (1970).
- Crow, E.L., F.A. Davis and M.W. Maxfield, "Statistics Manual," Dover Publications, Inc., New York, N.Y. (1960).
- Fairbrother, F. and A.E. Stubbs, "Studies in Electro-Endosmosis," J. Chem. Soc. 1,527 (1935).
- Fitz-Gerald, J.M., "Mechanics of red-cell motion through very narrow capillaries," Proc. Roy. Soc. Lond. B 174, 193 (1969).
- Fitz-Gerald, J.M., "Plasma motions in narrow capillary flow," J. Fluid Mech. 51, 463 (1972).
- Goldsmith, H.L., and S.G. Mason, "The Movement of single large bubbles in closed vertical tubes," 14, 42 (1962).
- Griffith, P., and G.B. Wallis, "Two-Phase Slug Flow," Tans. Am. Soc. Mech. Engrs. 83C, 307 (1961).
- Kiser, K.M., Private Communication, Stanford University, Stanford, California (1975).

- Laird, A.D.K., and A. Chisolm, "Pressure and Forces Along Cylindrical Bubbles in a Vertical Tube," Ind. Eng. Chem., 48, 1361 (1956).
- Landau, L.D. and L.M. Lifshitz, "Fluid Mechanics," Addison-Wesley, Reading, Mass., 1959.
- Lange, N.A., Handbook of Chemistry, 10th ed., McGraw-Hill, New York, 1967.
- Levich, V.G., Physicochemical Hydrodynamics, Prentice-Hall, New Jersey, 1962.
- Lew, H. and Y. Fung, "Plug effect of Erythrocytes in capillary blood vessels," Biophysical Journal 10, 80 (1970).
- Lockhart, R.W., and R.C. Martinelli, "Proposed Correlation of Data for Isothermal Two-Phase, Two-Component Flow in Pipes," Chem. Eng. Progr., 45 (1), 39 (1949).
- McGreary, R.K., "Mechanical Packing of Spherical Particles," J. Am. Ceram. Soc., 44, 513 (1961).
- McIlvried, H.G., Ph.D. Thesis, Carnegie Inst. of Tech., Penn. (1956).
- Nicklin, D.J., J.O. Wilkes, and J.F. Davidson, "Two-Phase Flow in Vertical Tubes," Trans. Inst. Chem. Engrs., 40, 61 (1962).
- Owen, D.B., "Handbook of Statistical Tables," Addison-Wesley, Reading, Mass., (1962).

Satterfield, C.N., A.A. Pelossof, and T.K. Sherwood, "Mass Transfer Limitations in a Trickle-Bed Reactor," AICHE J., 15, 226 (1969).

Satterfield, C.N., Mass Transfer in Heterogeneous Catalysis, M.I.T. Press, Cambridge, Mass. (1970).

Satterfield, C.N., "Trickle bed reactors," AICHE J., 21, 209 (1975).

Suo, M., "Two Phase Flow in Capillary Tubes," Sc.D. Thesis, Mech. Eng. Department, M.I.T., Cambridge, Mass. (1963).

Taylor, G.I., "Deposition of a viscous fluid on the wall of a tube," J. Fluid Mech., 10, 161 (1961).

Van Eek, M.W., Private Communication, M.I.T., Mass. (1975).

BIOGRAPHY OF AUTHOR

Fahri Özel was born on November 15, 1947 in Nevşehir, Turkey. He attended Kurtulus Lisesi and Atatürk Lisesi, both in Ankara, for his high school education. In 1965 he graduated from Atatürk Lisesi and won NATO undergraduate and graduate scholarships. In the same year he entered the School of Science at Ankara University from where he was awarded the degrees of B.S. and M.S. in Chemical Engineering in June 1970. He entered M.I.T. in January 1971 and was awarded the degree of Master of Science in Chemical Engineering in January 1973. He held several teaching and research assistantships. Currently he is the manager of the Chemical Engineering computing facilities.

Mr. Özel is a member of the Society of Sigma Xi.

He is the co-author of one scientific paper.